High-Accuracy Partially- and Fully-Coherent Wavefront Propagation Calculations for Storage Ring and FEL Sources

O. Chubar, NSLS-II, BNL

“Software for Optical Simulations” Workshop
Trieste, Italy, October 3 - 7, 2016

U.S. DEPARTMENT OF ENERGY

BROOKHAVEN NATIONAL LABORATORY
BROOKHAVEN SCIENCE ASSOCIATES

Outline

- Basics of Synchrotron Radiation (SR) calculation
- Basics of radiation Wavefront Propagation using Fourier Optics and compatible methods
- SR calculation examples; comparison with experiments
- Examples of Partially-Coherent SR propagation calculations for beamlines in Low-Emittance storage rings
- Example of Time-/Frequency-dependent Wavefront Propagation calculation for X-FEL applications
- Summary and comments

Emission by a Relativistic Charged Particle in Free Space: Retarded Potentials Approach

$$\vec{A} = e\int_{-\infty}^{+\infty}\vec{\beta}_e R^{-1}\delta(\tau - t + R/c)d\tau, \quad \varphi = e\int_{-\infty}^{+\infty} R^{-1}\delta(\tau - t + R/c)d\tau$$

(Gaussian CGS)

$$\Downarrow \quad \delta(t') = (1/2\pi)\int_{-\infty}^{+\infty}\exp(i\omega t')d\omega$$

$$\vec{A} = \frac{e}{2\pi}\int_{-\infty}^{+\infty}\exp(-i\omega t)d\omega\int_{-\infty}^{+\infty}\vec{\beta}_e R^{-1}\exp[i\omega(\tau + R/c)]d\tau$$

$$\varphi = \frac{e}{2\pi}\int_{-\infty}^{+\infty}\exp(-i\omega t)d\omega\int_{-\infty}^{+\infty} R^{-1}\exp[i\omega(\tau + R/c)]d\tau$$

Ternov used this approach to derive far-field SR expressions

$$\vec{E} = -\frac{1}{c}\frac{\partial\vec{A}}{\partial t} - \nabla\varphi = \frac{ie}{2\pi c}\int_{-\infty}^{+\infty}\omega\cdot\exp(-i\omega t)d\omega\int_{-\infty}^{+\infty}[\vec{\beta}_e - [1 + ic/(\omega R)]\cdot\vec{n}]R^{-1}\exp[i\omega(\tau + R/c)]d\tau$$

$$\Downarrow \quad \vec{E}_\omega \equiv \int_{-\infty}^{+\infty}\vec{E}\exp(i\omega t)dt$$

Exact expression, valid in the Near Field:

$$\vec{E}_\omega = iec^{-1}\omega\int_{-\infty}^{+\infty}[\vec{\beta}_e - [1 + ic/(\omega R)]\cdot\vec{n}]R^{-1}\exp[i\omega(\tau + R/c)]d\tau \qquad (\surd)$$

The equivalence of (√) to the well-known expression of Jackson can be shown by integration by parts

$$\vec{E}_\omega = ec^{-1}\int_{-\infty}^{+\infty}\frac{\vec{n}\times[(\vec{n} - \vec{\beta}_e)\times\dot{\vec{\beta}}_e] + cR^{-1}\gamma^{-2}(\vec{n} - \vec{\beta}_e)}{R\cdot(1 - \vec{n}\cdot\vec{\beta}_e)^2}\cdot\exp[i\omega(\tau + R/c)]d\tau$$

Emission by a Relativistic Charged Particle Efficient Computation

Exact expression obtained from Retarded Potentials:

$$\vec{E}_{\omega} = iec^{-1}\omega \int_{-\infty}^{+\infty} [\vec{\beta}_e - [1 + ic/(\omega R)] \cdot \vec{n}] R^{-1} \exp[i\omega(\tau + R/c)] d\tau$$

Phase expansion valid in the Near Field:

$$\omega \cdot (\tau + R/c) \approx \Phi_0 + \frac{\pi}{\lambda} \left[s\gamma^{-2} + \int_0^s |\vec{\beta}_{e\perp}|^2 \, d\tilde{s} \;\; + \;\; \frac{(x - x_e)^2 + (y - y_e)^2}{z - s} \right]$$

Particle dynamics in external magnetic field:

$$\vec{r}_e = \vec{r}_e(s, \vec{r}_{e0}, \vec{\beta}_{e0}); \;\; \vec{\beta}_e \approx d\vec{r}_e / ds$$

Asymptotic expansion of the radiation integral (to accelerate computation):

$$\int_{-\infty}^{+\infty} F \exp(i\Phi) ds = \int_{s_1}^{s_2} F \exp(i\Phi) ds + \int_{-\infty}^{s_1} F \exp(i\Phi) ds + \int_{s_2}^{+\infty} F \exp(i\Phi) ds$$

$$\int_{-\infty}^{s_1} F \exp(i\Phi) ds + \int_{s_2}^{+\infty} F \exp(i\Phi) ds \approx \left[\left(\frac{F}{i\Phi'} + \frac{F'\Phi' - F\Phi''}{\Phi'^3} + \ldots \right) \exp(i\Phi) \right]_{s_2}^{s_1}$$

Temporally-Incoherent and Coherent Spontaneous Emission by Many Electrons

Electron Dynamics:

$$\begin{pmatrix} x_e \\ y_e \\ z_e \\ \beta_{xe} \\ \beta_{ye} \\ \delta\gamma_e \end{pmatrix} = \mathbf{A}(\tau) \begin{pmatrix} x_{e0} \\ y_{e0} \\ z_{e0} \\ x'_{e0} \\ y'_{e0} \\ \delta\gamma_{e0} \end{pmatrix} + \mathbf{B}(\tau)$$

← Initial Conditions

Spectral **Photon Flux per unit Surface** emitted by the **whole Electron Beam**:

$$\frac{dN_{ph}}{dt dS (d\omega/\omega)} = \frac{c^2 \alpha I}{4\pi^2 e^3} \left\langle \left| \vec{E}_\omega \right|^2 \right\rangle$$

"Incoherent" SR

$$\left\langle \left| \vec{E}_\omega \right|^2 \right\rangle = \int \left| \vec{E}_{\omega 0}(\vec{r}; x_{e0}, y_{e0}, z_{e0}, x'_{e0}, y'_{e0}, \delta\gamma_{e0}) \right|^2 f(x_{e0}, y_{e0}, z_{e0}, x'_{e0}, y'_{e0}, \delta\gamma_{e0}) dx_{e0} dy_{e0} dz_{e0} dx'_{e0} dy'_{e0} d\delta\gamma_{e0} +$$

$$+ (N_e - 1) \left| \int \vec{E}_{\omega 0}(\vec{r}; x_{e0}, y_{e0}, z_{e0}, x'_{e0}, y'_{e0}, \delta\gamma_{e0}) f(x_{e0}, y_{e0}, z_{e0}, x'_{e0}, y'_{e0}, \delta\gamma_{e0}) dx_{e0} dy_{e0} dz_{e0} dx'_{e0} dy'_{e0} d\delta\gamma_{e0} \right|^2$$

Coherent SR

Common Approximation for CSR: **"Thin" Electron Beam**: $\left\langle \left| \vec{E}_\omega \right|^2 \right\rangle_{CSR} \approx N_e \left| \int_{-\infty}^{\infty} \tilde{f}(z_{e0}) \exp(ikz_{e0}) dz_{e0} \right|^2 \left| \vec{E}_{\omega 1} \right|^2$

For Gaussian Longitudinal Bunch Profile: $\left\langle \left| \vec{E}_\omega \right|^2 \right\rangle_{CSR} \approx N_e \exp(-k^2 \sigma_b^2) \left| \vec{E}_{\omega 1} \right|^2$

If $f(x_{e0}, y_{e0}, z_{e0}, x'_{e0}, y'_{e0}, \delta\gamma_{e0})$ is Gaussian, 6-fold integration over electron phase space can be done analytically for the (Mutual) Intensity of Incoherent SR and for the Electric Field of CSR

Self-Amplified Spontaneous Emission Described by Paraxial FEL Equations

Approximation of Slowly Varying Amplitude of Radiation Field

Particles' dynamics in undulator and radiation fields (averaged over many periods):

$$\frac{d\theta}{dz} = k_u - k_r \frac{1 + p_\perp^2 + a_u^2 - 2a_r a_u \cos(\theta + \phi_r)}{2\gamma^2}$$

$$\frac{d\gamma}{dz} = -\frac{k_r f_c a_r a_u}{\gamma} \sin(\theta + \phi_r)$$

$$\frac{d\vec{p}_\perp}{dz} = -\frac{1}{2\gamma} \frac{\partial a_u^2}{\partial \vec{r}_\perp} + \mathbf{k}_{foc} \vec{r}_\perp$$

$$\frac{d\vec{r}_\perp}{dz} = \frac{\vec{p}_\perp}{\gamma}$$

W.B.Colson
J.B.Murphy
C.Pellegrini
E.Saldin
E.Bessonov
et. al.

Paraxial wave equation with current:

$$\left[2ik_r \frac{\partial}{\partial z} + \nabla_\perp^2 \right] a_r \exp(i\phi_r) = -\frac{e\varepsilon_0 I f_c a_u}{mc} \left\langle \frac{\exp(-i\theta)}{\gamma} \right\rangle$$

Solving this system gives Electric Field at the FEL exit for one "Slice": $E_{slice}\big|_{z=z_{exit}} \sim a_r \exp(i\phi_r)\big|_{z=z_{exit}}$

Loop on "Slices" (copying Electric Field to a next slice from previous slice, starting from back)

Popular TD 3D FEL computer code: **GENESIS** (S.Reiche)

One run provides Time-Domain Electric Field in transverse plane at FEL exit: $E(x, y, z_{exit}, t)$

Electric Field in **Frequency** domain: $\vec{\tilde{E}}(\vec{r},\omega) \equiv \int_{-\infty}^{\infty} \vec{E}(\vec{r},t) \exp(i\omega t)\, dt$

Wavefront Propagation in the Case of Full Transverse Coherence

Kirchhoff Integral Theorem applied to Spontaneous Emission by One Electron

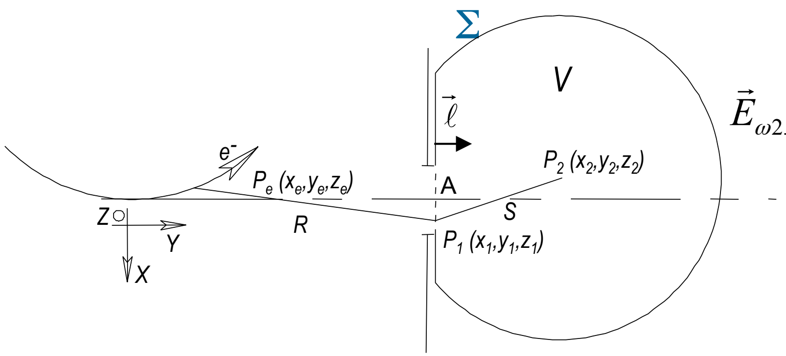

$$\vec{E}_{\omega 2\perp}(P_2) \approx \frac{k^2 e}{4\pi}\int_{-\infty}^{+\infty} d\tau \iint_{A} \frac{\vec{\beta}_{e\perp} - \vec{n}_{\perp}}{RS} \exp[ik(c\tau + R + S)] \cdot (\vec{\ell}\cdot\vec{n}_{p_e p_1} + \vec{\ell}\cdot\vec{n}_{p_1 p_2}) d\Sigma$$

Valid at large observation angles;
Is applicable to complicated cases of diffraction inside vacuum chamber

Huygens-Fresnel Principle

$$\vec{E}_{\omega 2\perp}(P_2) \approx \frac{k}{4\pi i}\iint_{A} \vec{E}_{\omega 1\perp}(P_1)\frac{\exp(ikS)}{S}(\vec{\ell}\cdot\tilde{\vec{n}} + \vec{\ell}\cdot\vec{n}_{p_1 p_2}) d\Sigma$$

Fourier Optics

Free Space:
(between parallel planes perpendicular to optical axis)

$$\vec{E}_{\omega 2\perp}(x_2, y_2) \approx \frac{k}{2\pi i L}\iint \vec{E}_{\omega 1\perp}(x_1, y_1)\exp[ik[L^2 + (x_2 - x_1)^2 + (y_2 - y_1)^2]^{1/2}] dx_1 dy_1$$

Assumption of small angles

"**Thin**" Optical Element:

$$\vec{E}_{\omega 2\perp}(x, y) \approx \mathbf{T}(x, y, \omega)\, \vec{E}_{\omega 1\perp}(x, y)$$

"**Thick**" Optical Element:
(propagation from transverse plane before the element to a transverse plane just after it)

$$\vec{E}_{\omega 2\perp}(x_2, y_2) \approx \mathbf{G}(x_2, y_2, \omega)\exp[ik\Lambda(x_2, y_2, k)]\, \vec{E}_{\omega 1\perp}(x_1(x_2, y_2), y_1(x_2, y_2))$$

"Economic" and Numerically Stable Version of the Free-Space Fourier-Optics Propagator

Huygens-Fresnel Principle:
(paraxial approximation)

$$\vec{E}_{\omega 2\perp}(x_2, y_2) \approx \frac{k}{2\pi i L}\iint \vec{E}_{\omega 1\perp}(x_1, y_1)\exp[ik[L^2 + (x_2 - x_1)^2 + (y_2 - y_1)^2]^{1/2}]dx_1 dy_1$$

Analytical Treatment of **Quadratic Phase Term**:

Before Propagation:

$$\vec{E}_{\omega 1\perp}(x_1, y_1) = \vec{F}_{\omega 1}(x_1, y_1)\exp\left[ik\frac{(x_1 - x_0)^2}{2R_x} + ik\frac{(y_1 - y_0)^2}{2R_y}\right]$$

After Propagation:

$$\vec{E}_{\omega 2\perp}(x_2, y_2) \approx \frac{k}{2\pi i L}\exp(ikL)\iint_{\Sigma}\vec{F}_{\omega 1}(x_1, y_1)\exp\left[ik\frac{(x_1 - x_0)^2}{2R_x} + ik\frac{(y_1 - y_0)^2}{2R_y} + ik\frac{(x_2 - x_1)^2 + (y_2 - y_1)^2}{2L}\right]dx_1 dy_1$$

$$= \frac{k}{2\pi i L}\exp\left[ikL + ik\frac{(x_2 - x_0)^2}{2(R_x + L)} + ik\frac{(y_2 - y_0)^2}{2(R_y + L)}\right]\times$$

$$\times\iint_{\Sigma}\vec{F}_{\omega 1}(x_1, y_1)\exp\left[ik\frac{R_x + L}{2R_x L}\left(x_1 - \frac{R_x x_2 + L x_0}{R_x + L}\right)^2 + ik\frac{R_y + L}{2R_y L}\left(y_1 - \frac{R_y y_2 + L y_0}{R_y + L}\right)^2\right]dx_1 dy_1$$

$$= \vec{F}_{\omega 2}(x_2, y_2)\exp\left[ik\frac{(x_2 - x_0)^2}{2(R_x + L)} + ik\frac{(y_2 - y_0)^2}{2(R_y + L)}\right]$$

An Approach to High-Accuracy Partially-Coherent Emission and Wavefront Propagation Simulations

Averaging (over **phase-space volume** occupied by **e-beam**) of the **intensity** (or mutual intensity, or mathematical brightness) obtained from **electric field emitted by an electron** and **propagated** through an optical system:

$$I_\omega(x,y) = \int I_{\omega 1}(x,y;x_e,y_e,z_e,x'_e,y'_e,\delta\gamma_e)\, f(x_e,y_e,z_e,x'_e,y'_e,\delta\gamma_e)\, dx_e dy_e dz_e dx'_e dy'_e d\delta\gamma_e$$

$$I_{\omega 1}(x,y;x_e,y_e,z_e,x'_e,y'_e,\delta\gamma_e) = \left|\mathbf{E}_{\omega 1\perp}(x,y;x_e,y_e,z_e,x'_e,y'_e,\delta\gamma_e)\right|^2$$

$$M_{\omega 1}(x,y,\tilde{x},\tilde{y};x_e,y_e,z_e,x'_e,y'_e,\delta\gamma_e) = \mathbf{E}_{\omega 1\perp}(x,y;\ x_e,y_e,z_e,x'_e,y'_e,\delta\gamma_e)\mathbf{E}^*_{\omega 1\perp}(\tilde{x},\tilde{y};\ x_e,y_e,z_e,x'_e,y'_e,\delta\gamma_e)$$

$$B_{\omega 1}(x,y,\theta_{\mathrm{x}},\theta_{\mathrm{y}};x_e,y_e,z_e,x'_e,y'_e,\delta\gamma_e) \sim \mathbf{E}_{\omega 1\perp}(x,y;\ x_e,y_e,z_e,x'_e,y'_e,\delta\gamma_e)\int \mathbf{E}^*_{\omega 1\perp}(\tilde{x},\tilde{y};\ x_e,y_e,z_e,x'_e,y'_e,\delta\gamma_e)\exp\left[i\frac{\omega}{c}(\theta_{\mathrm{x}}\tilde{x}+\theta_{\mathrm{y}}\tilde{y})\right]d\tilde{x}d\tilde{y}$$

This method is **general** and **accurate**. For the most part, it is already implemented in SRW code. However, it can be **CPU-intensive**, requiring **parallel calculations** on a multi-core server or a small cluster. Several approaches are considered for increasing the efficiency, including use of low-discrepancy sequences (collaboration with R. Lindberg, K.-J. Kim, X. Shi, ANL), “improved Monte-Carlo” type techniques, as well as “coherent mode decomposition”.

NOTE: the **smaller** the **e-beam emittance** (the higher the radiation coherence) – the **faster** is the **convergence** of simulations with this general method.

NOTE: **convolution** can be valid in some cases, such as pure projection geometry, focusing by a thin lens, diffraction at one slit, etc.

$$I_\omega(x,y) \approx \int \tilde{I}_{\omega 1}(x-\tilde{x}_e, y-\tilde{y}_e)\tilde{f}(\tilde{x}_e,\tilde{y}_e)\, d\tilde{x}_e d\tilde{y}_e$$

If convolution is valid, the **calculations can be accelerated** dramatically. The validity of the convolution relation can be easily verified numerically.

All calculations presented below were done with "Synchrotron Radiation Workshop" code

First work on Wavefront Propagation applied to SR beamlines (PHASE code): J. Bahrdt, Appl. Opt. 36 (19) 4367 (1997)

- First official version of SRW was developed at ESRF in 1997-98 (written in C++, interfaced to IGOR Pro); compiled versions are distributed from: http://www.esrf.eu/Accelerators/Groups/InsertionDevices/Software/SRW
- SRW was released to Open Source in 2012 under BSD type license. To make the release possible, permissions were obtained from all previously contributed Institutes: ESRF, European XFEL, SOLEIL, DIAMOND, BNL, and from US DOE

The main Open Source repository, containing all C/C++ sources, C API, all interfaces and project development files, is on GitHub: https://github.com/ochubar/SRW

- SRW for Python (2.7.x and 3.x, 32- and 64-bit) cross-platform versions were released in 2012
- SRW development is partially supported by US DOE SBIR Program (BNL acts as subcontractor of RadiaSoft LLC, headed by D. Bruhwiler)

Single-Electron (Fully Transversely-Coherent) UR Intensity Distributions, “in Far Field” and “at Source”

UR “Single-Electron” Intensity and “Multi-Electron” Flux

E-Beam Energy: 3 GeV
Current: 0.5 A
Undulator Period: 20 mm

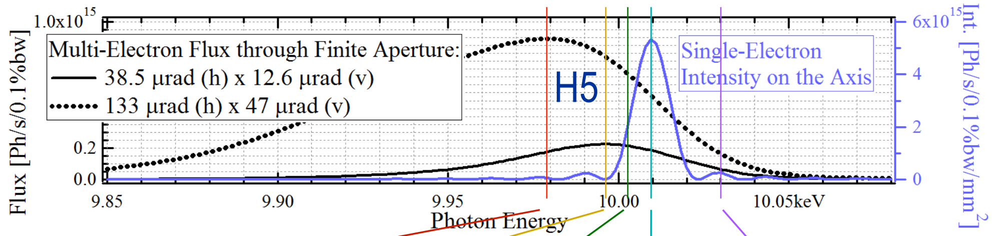

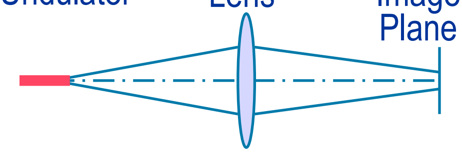

Intensity Distributions at 30 m from Undulator Center

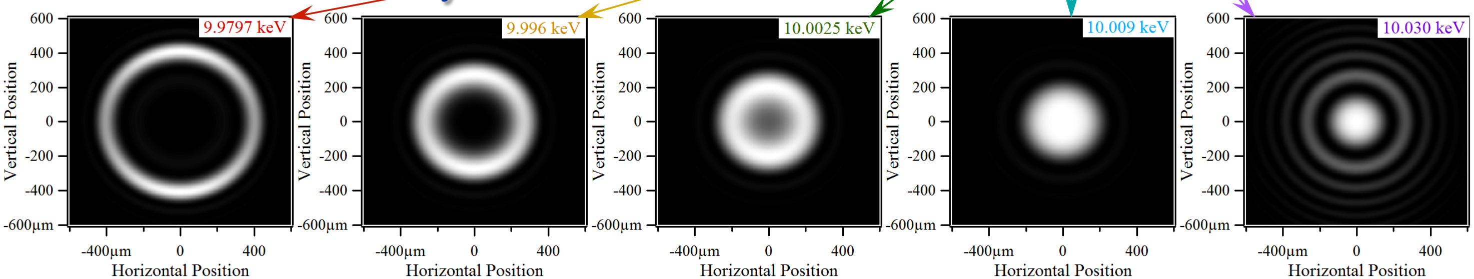

Vertical Cuts (x = 0)

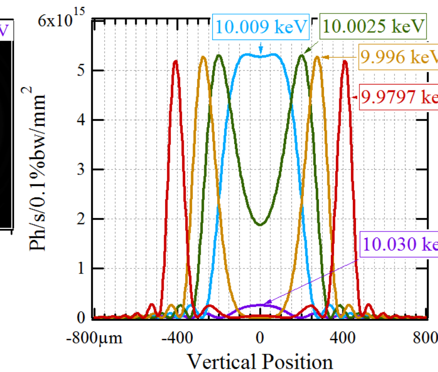

Intensity Distributions in 1:1 Image Plane

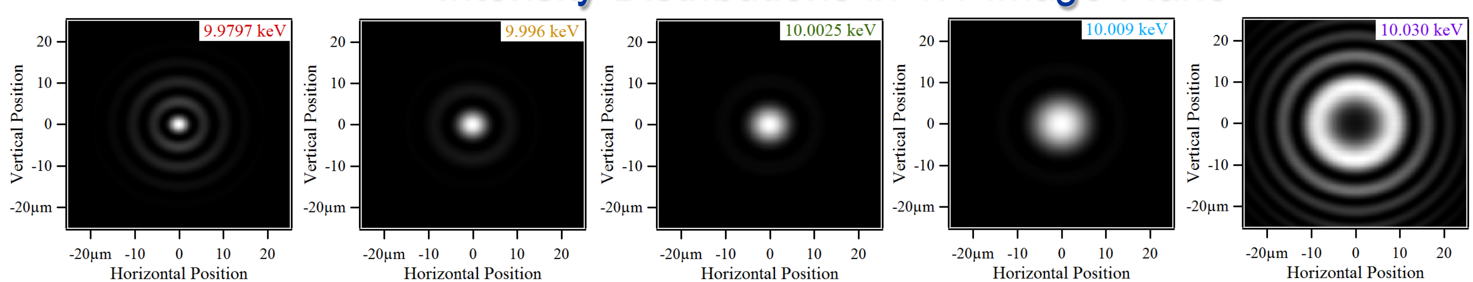

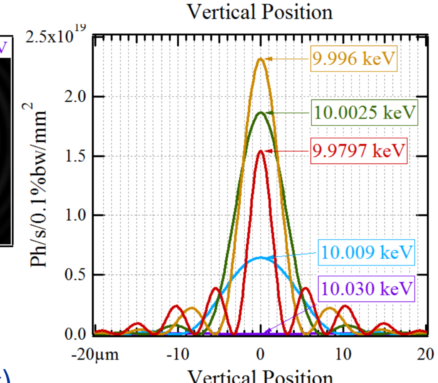

“Phase-Space Volume” Estimation for Vertical Plane

(RMS sizes/divergences calculated for the portions of intensity distributions containing 95% of flux)

$\sigma_y \sigma_y' \approx 7.7 \dfrac{\lambda}{4\pi}$ $\quad 3.3 \dfrac{\lambda}{4\pi}$ $\quad 1.9 \dfrac{\lambda}{4\pi}$ $\quad 1.5 \dfrac{\lambda}{4\pi}$ $\quad 9.2 \dfrac{\lambda}{4\pi}$

"Phase Correction" for Coherent Radiation

"Real Wave Front" + "Phase Correction" = "Spherical Wave Front"

$$E_{out}(x,y) = T(x,y)E_{in}(x,y) = A(x,y)\exp[i\pi(x^2+y^2)/(\lambda R)]$$

$$T(x,y) = \exp[i\Phi_{cor}(x,y)]$$

$$\Downarrow$$

$$\Phi_{cor}(x,y) = \arg[\exp[i\pi(x^2+y^2)/(\lambda R) + i\Phi_0]/E_{in}(x,y)]$$

Testing Efficiency of Phase Corrections

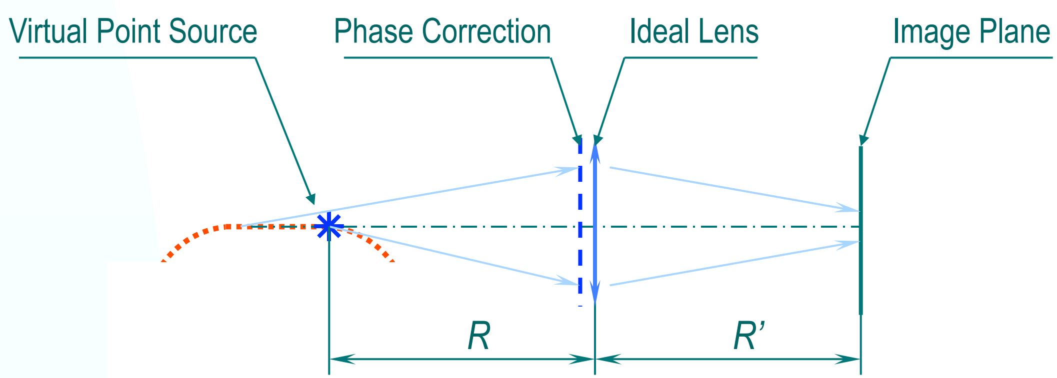

Phase Corrections for Single-Electron UR (I)

Planar undulator, odd harmonics

E = 6 GeV; *K* = 2.2; 38 x 42 mm; ε = 2.36 keV (~ fundamental)

1 : 1 imaging; 30 m from middle of Undulator to Thin Lens & Phase Correction

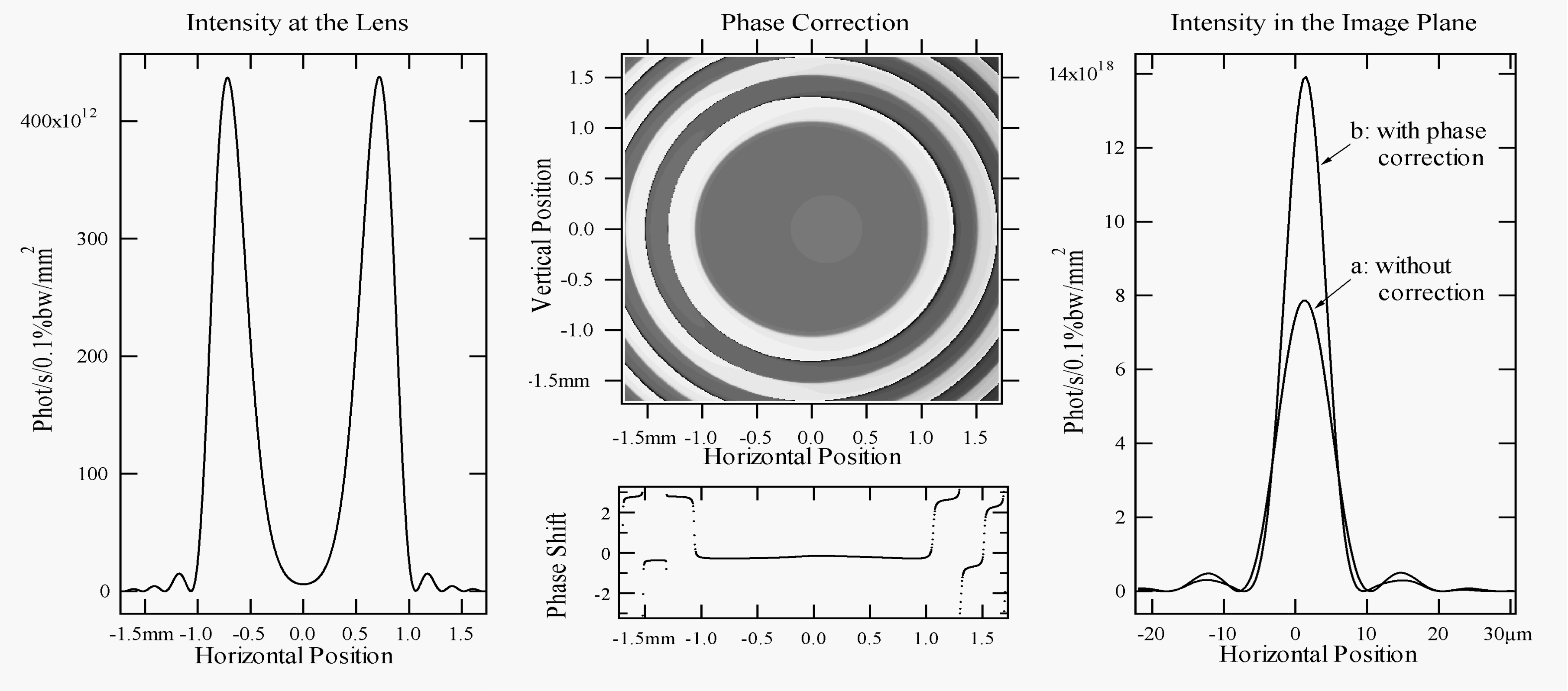

O. Chubar, P. Elleaume, A. Snigirev, NIMA 435 (1999) 495 - 508

Phase Corrections for Single-Electron UR (II)

Planar undulator, even harmonics

E = 6 GeV; *K* = 2.2; 38 x 42 mm; ε = 4.775 keV (2-nd harmonic)

1 : 1 imaging; 30 m from middle of Undulator to Thin Lens & Phase Correction

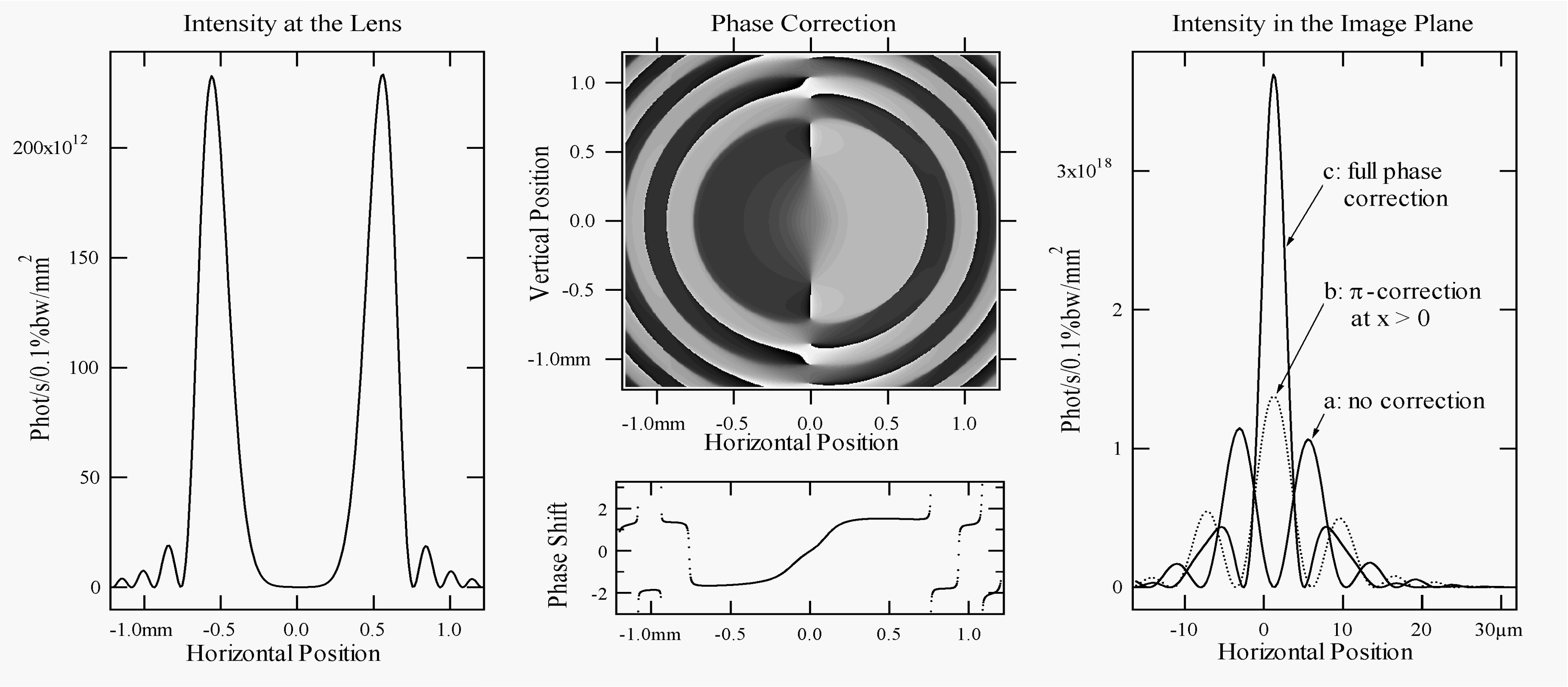

Phase Corrections for Single-Electron UR (III)

Helical undulator, harmonics n > 1

E = 6 GeV; $B_{x\ max} = B_{z\ max}$ = 0.3 T; 28 x 52 mm; ε = 4.20 keV (2^{-nd} harmonic)

1 : 1 imaging; 30 m from middle of Undulator to Thin Lens & Phase Correction

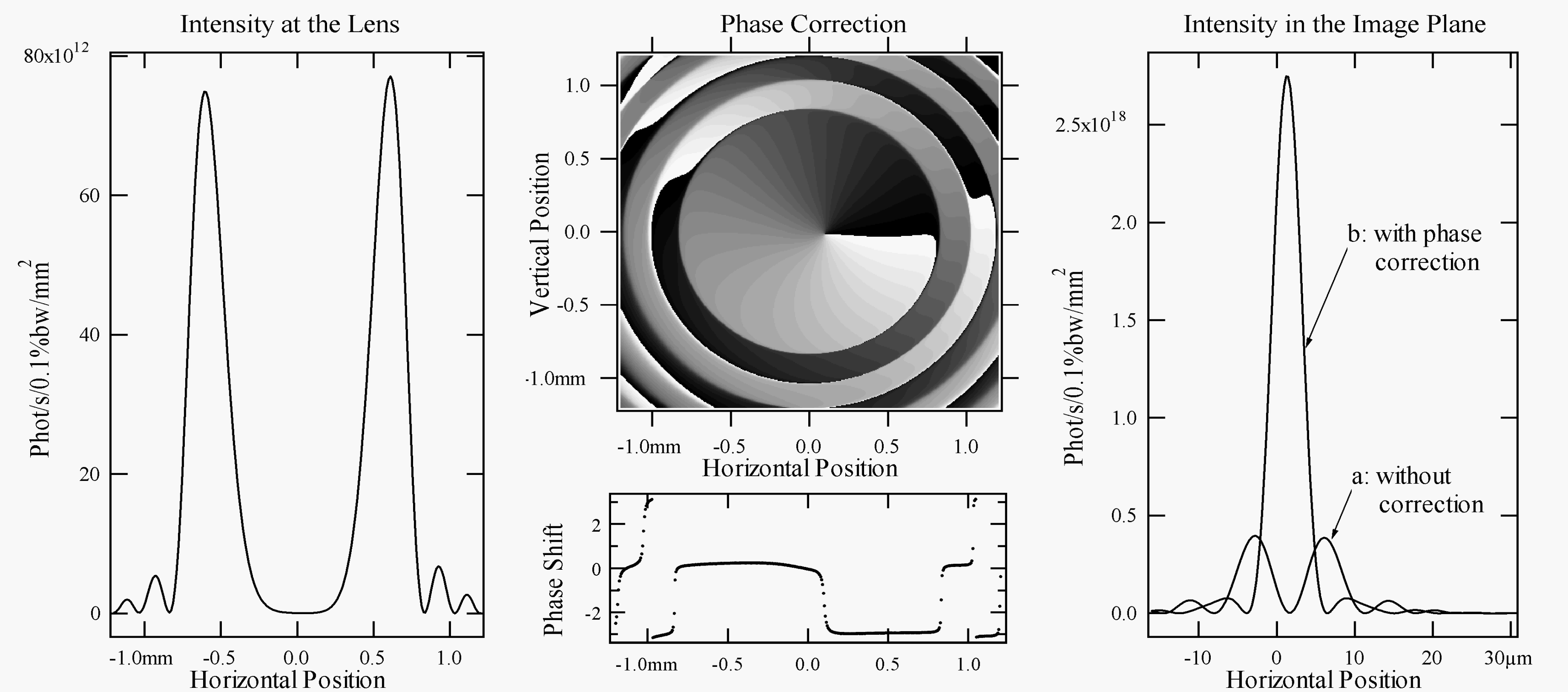

O. Chubar, P. Elleaume, A. Snigirev, NIMA 435 (1999) 495 - 508

S. Sasaki, I. McNulty, PRL 100, 124801 (2008) interpreted of this effect – azimuthal phase dependence – as “Orbital Angular Momentum”; several other publications followed.

Phase Corrections for Bending Magnet SR

E = 2.5 GeV
B = 1.6 T
ε = 40 eV
5 m from source

Intensity at the Lens | Phase Correction

Horizontal Polarization

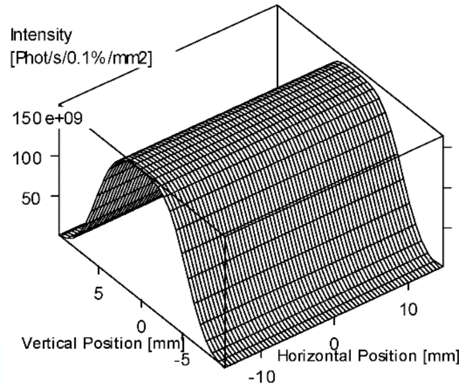

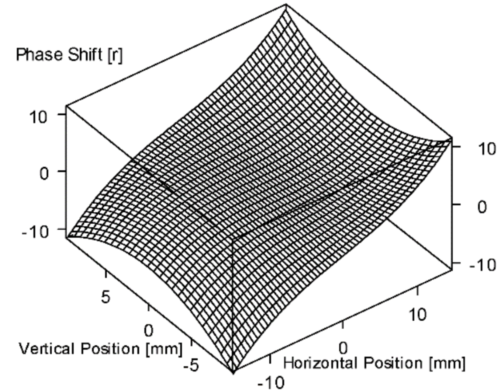

Vertical Polarization

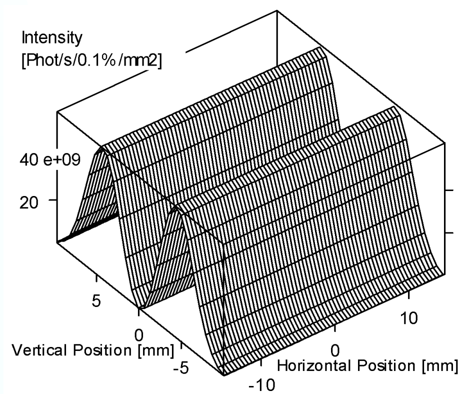

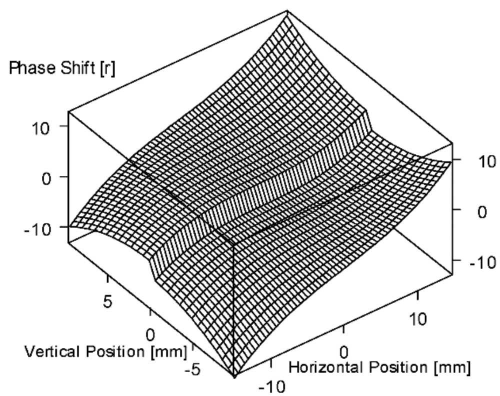

Analytical Approximation:

$$\Phi_{cor\ BM\ hor} \approx -(\pi/\lambda)\rho\theta_x(\gamma^{-2} + \theta_x^2/3 + \theta_y^2)$$

$$\Phi_{cor\ BM\ vert} = \Phi_{cor\ BM\ hor} + \pi\eta(\theta_y)$$

O. Chubar, P. Elleaume, A. Snigirev, NIMA 435 (1999) 495 - 508

Phase Corrections for Bending Magnet SR

Intensity in the Image Plane

E = 2.5 GeV; B = 1.56 T; ε = 40 eV; 1 : 1 imaging; 5 m from “Source Point” to Thin Lens

Horizontal Polarization

Without Phase Correction

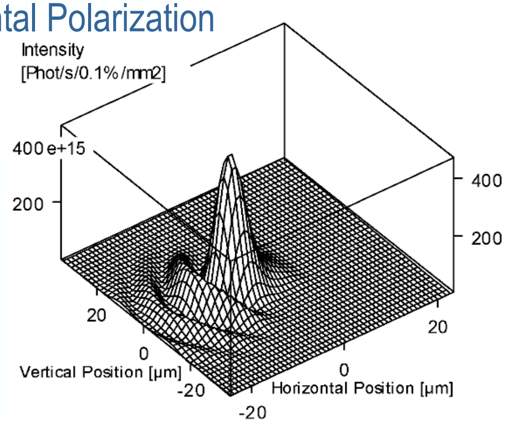

With Phase Correction

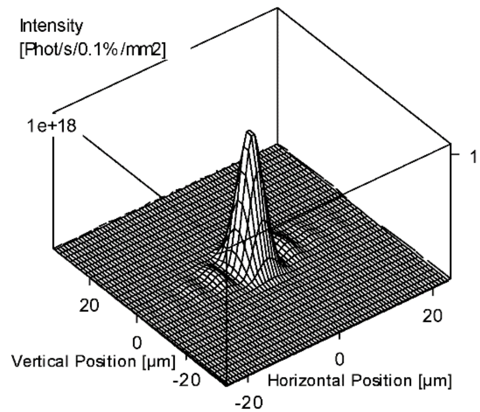

Horizontal Intensity Cut

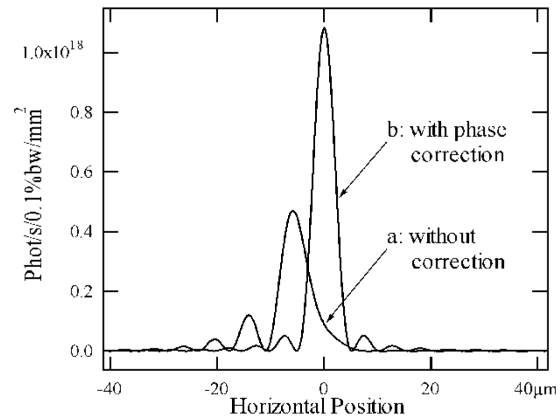

Vertical Polarization

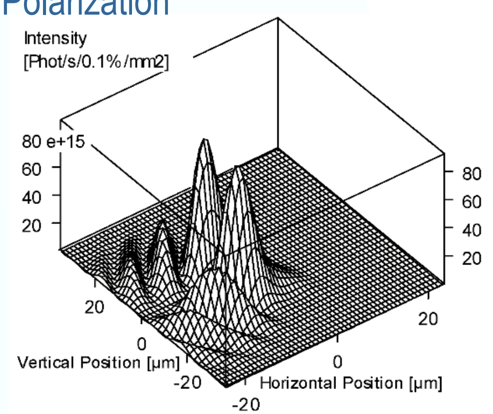

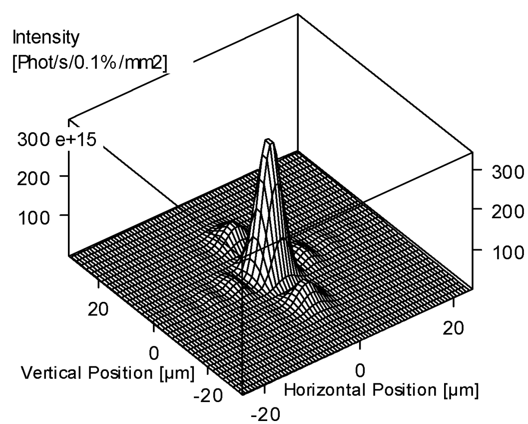

Vertical Intensity Cut

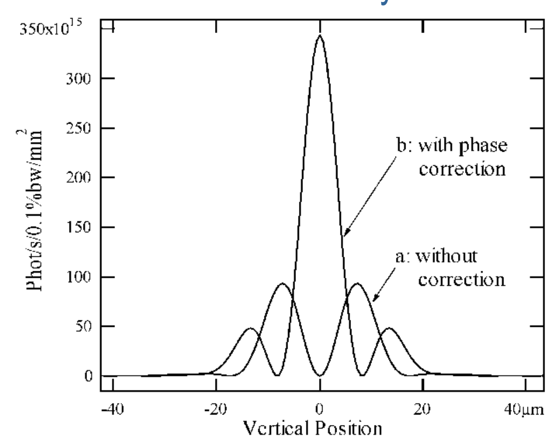

O. Chubar, P. Elleaume, A. Snigirev, NIMA 435 (1999) 495 - 508

Determining Electron Beam Size from Focused Visible Bending Magnet SR

Measurements at MAX-II

Å. Andersson, M. Eriksson, O. Chubar, 1996

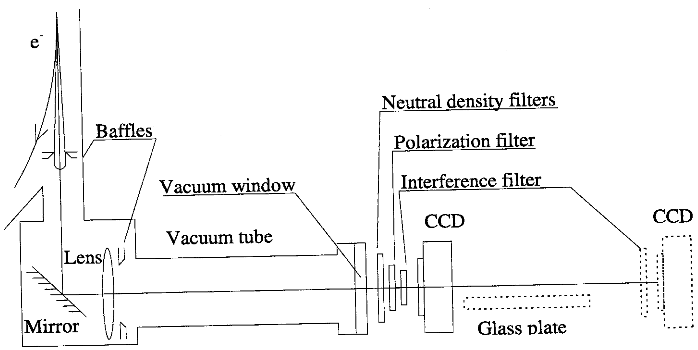

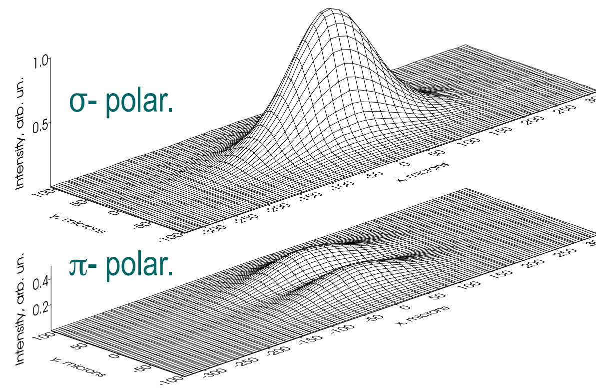

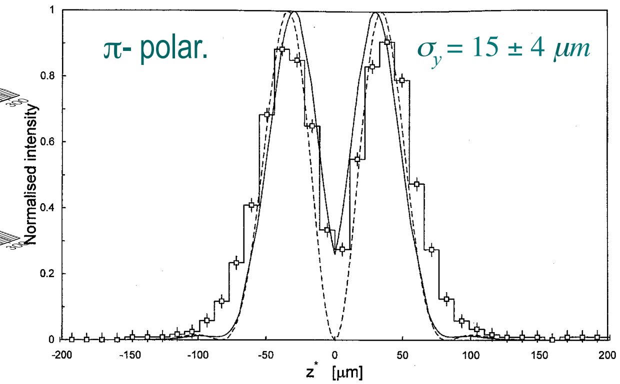

Measurements at MAX-IV

J. Breunlin, Å.Andersson, 2015

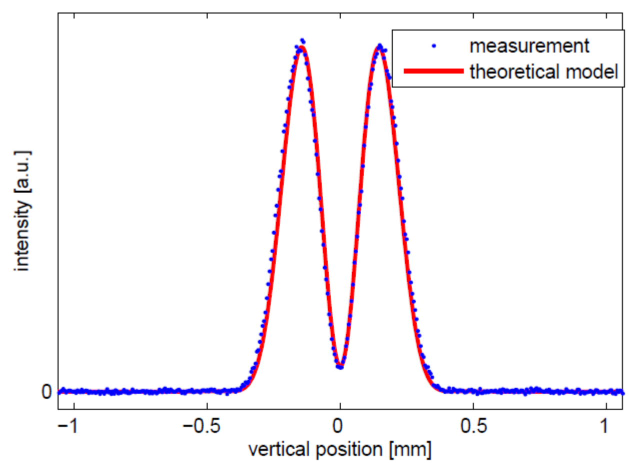

Figure 3: Vertical profile of imaged π-polarized SR at 488 nm wavelength. Measurement (blue dots) and SRW calculation (red lines). The vertical beam size is 11.5 μm.

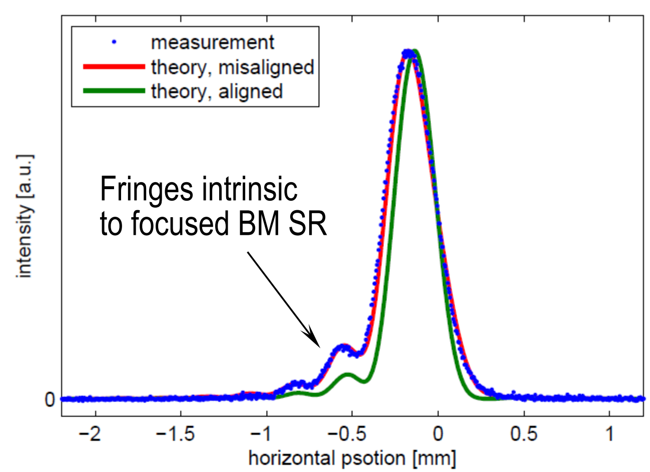

Figure 7: Horizontal profiles of σ-polarized SR at 930 nm for 8.2 mrad horizontal opening angle. The horizontal beam size is 24.5 μm.

Calculated UR Intensity Distributions from Finite-Emittance Electron Beam, “in Far Field” and “at Source”

IVU20-3m Spectral Flux

through 100 μrad (H) x 50 μrad (V) Aperture
at K~1.5 providing H5 peak at ~10 keV

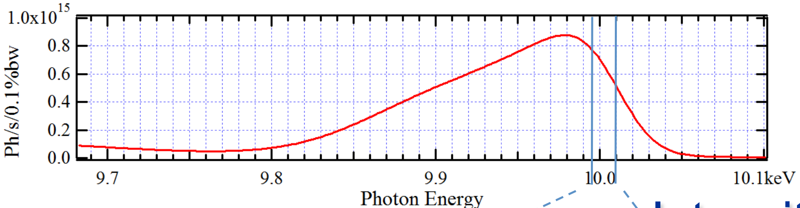

Electron Beam (NSLS-II):

Hor. Emittance: 0.9 nm
Vert. Emittance: 8 pm
Energy Spread: 8.9×10^{-4}
Current: 0.5 A
Low-Beta Straight

Test Optical Scheme

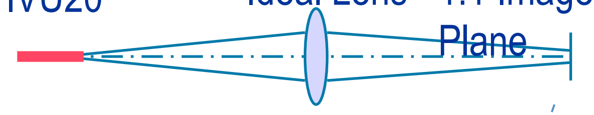

Intensity Distributions at ~10 keV

At 30 m from Undulator

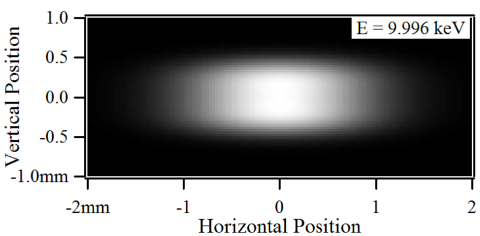

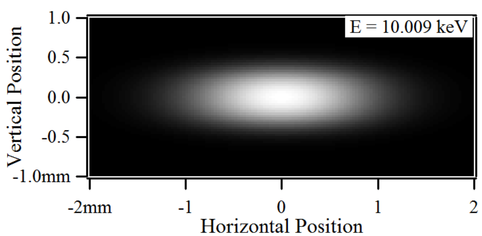

In 1:1 Image Plane

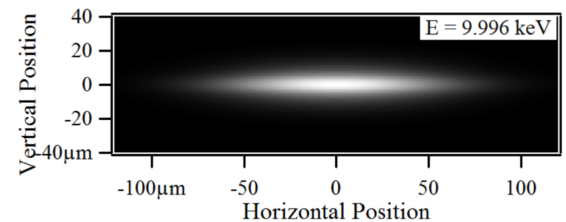

Horizontal Cuts (y = 0)

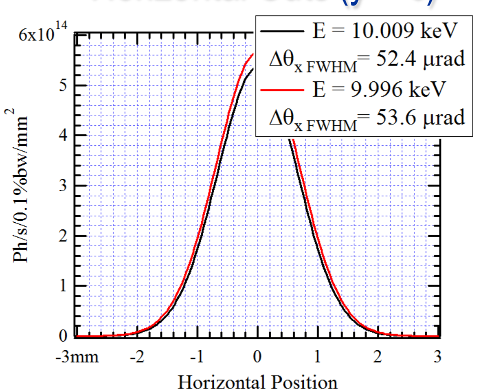

Vertical Cuts (x = 0)

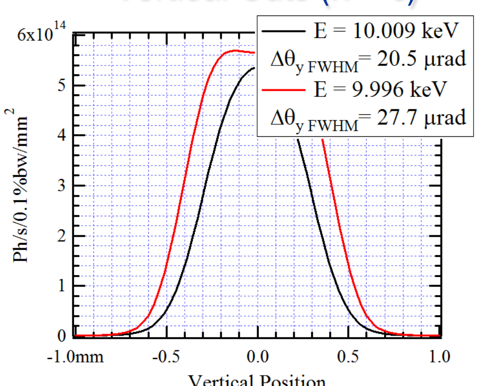

Horizontal Cuts (y = 0)

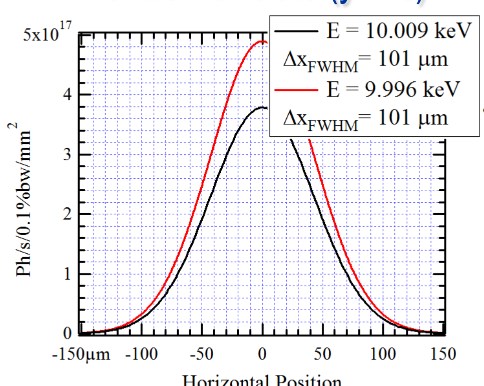

Vertical Cuts (x = 0)

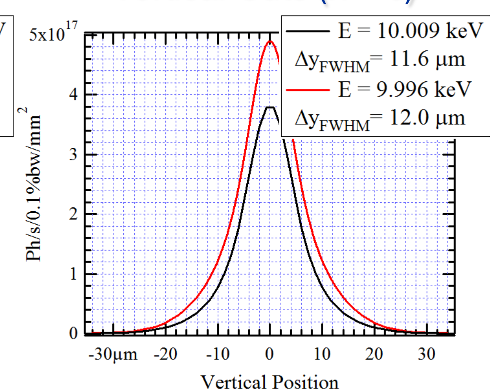

$$\sigma_x \sigma_x' \approx \mathbf{97} \frac{\lambda}{4\pi}; \quad \sigma_y \sigma_y' \approx \mathbf{5.7} \frac{\lambda}{4\pi}$$

…very far from Coherent Gaussian Beam !

On-Axis "Gap Spectrum" and Intensity Distributions of Radiation from IVU20 at HXN Beamline (I)

On-Axis Gap Spectrum at ~8.0 keV Photon Energy (5th Harmonic)

Undulator: λ_u= 20 mm, L_u = 3 m
Low-Beta Straight Section of NSLS-II:
β_x= 1.84 m (σ_x'= 22 μrad at ε_x= 0.9 nm)
β_y= 1.17 m (σ_y'= 2.6 μrad at ε_y= 8 pm)

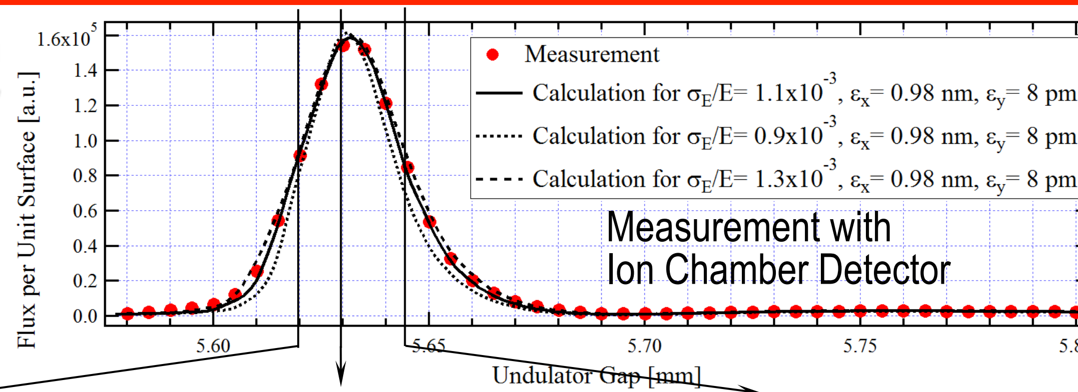

Intensity Distributions at 5th Harmonic at Different Undulator Gaps at 30.4 m

Vertical Cuts (x = 0)

Gap: 5.62 mm

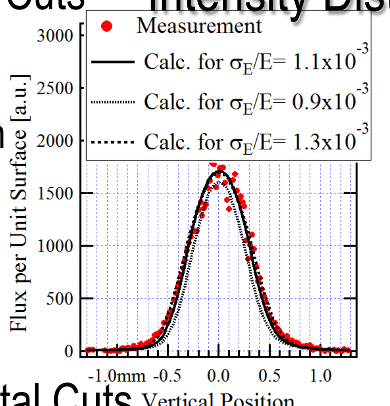

Gap: 5.63 mm

Measurements with Imaging Detector (Scintillator + Lens +CCD)

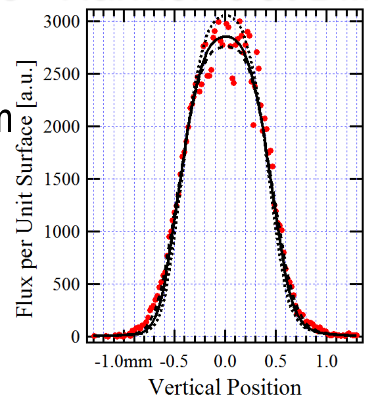

Gap: 5.645 mm

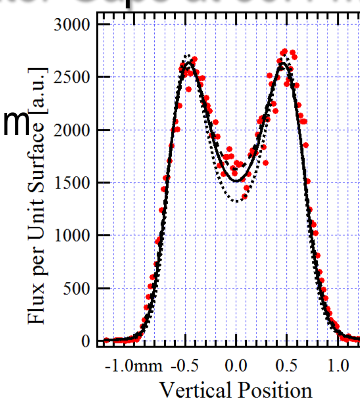

Horizontal Cuts (y = 0)

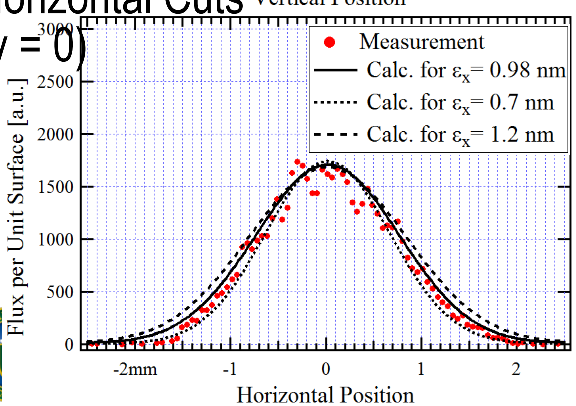

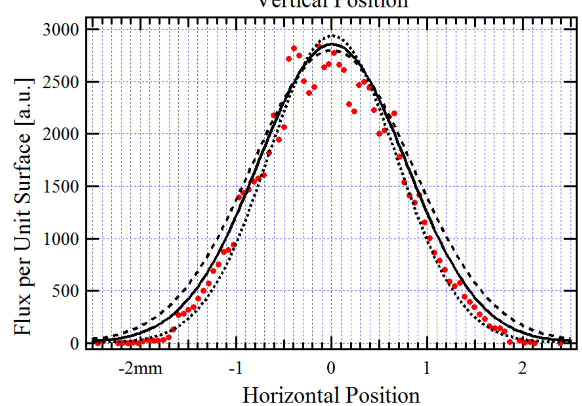

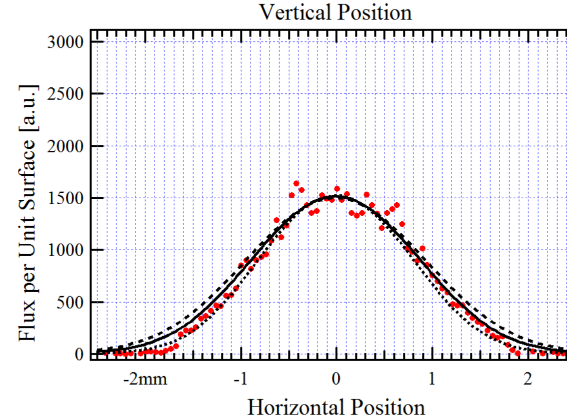

On-Axis "Gap Spectrum" and Intensity Distributions of Radiation from IVU20 at HXN Beamline (II)

On-Axis Gap Spectrum at ~8.0 keV Photon Energy (5^{th} Harmonic)

Undulator: λ_u= 20 mm, L_u = 3 m

Low-Beta Straight Section of NSLS-II:

β_x= 1.84 m (σ_x'= 22 μrad at ε_x= 0.9 nm)

β_y= 1.17 m (σ_y'= 2.6 μrad at ε_y= 8 pm)

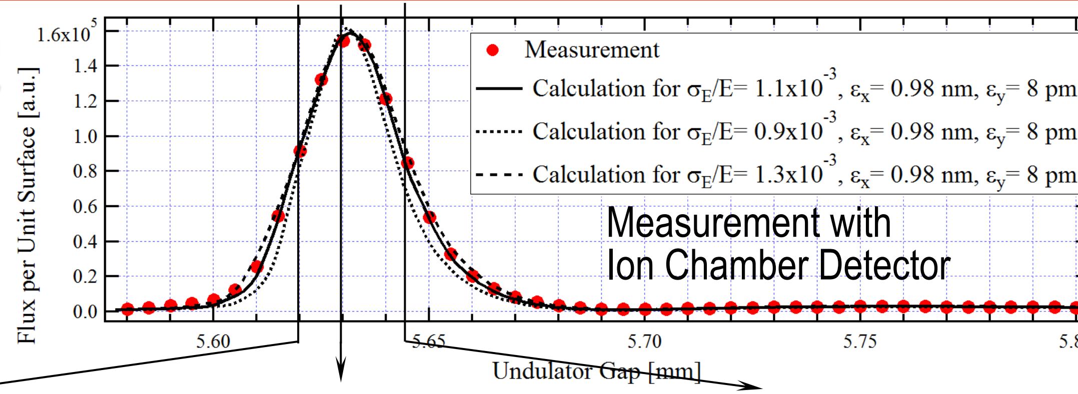

Intensity Distributions at 5^{th} Harmonic at Different Undulator Gaps at 30.4 m

Measurements after Monochromator (Scintillator Screen + Lens +CCD)

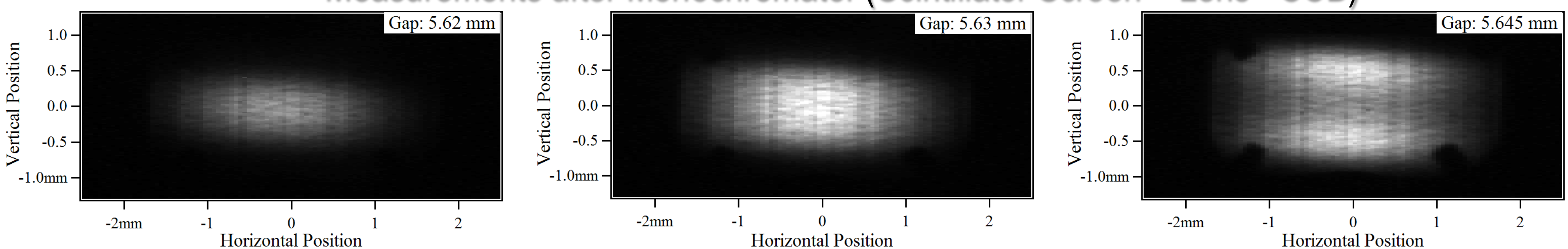

Calculations (SRW)

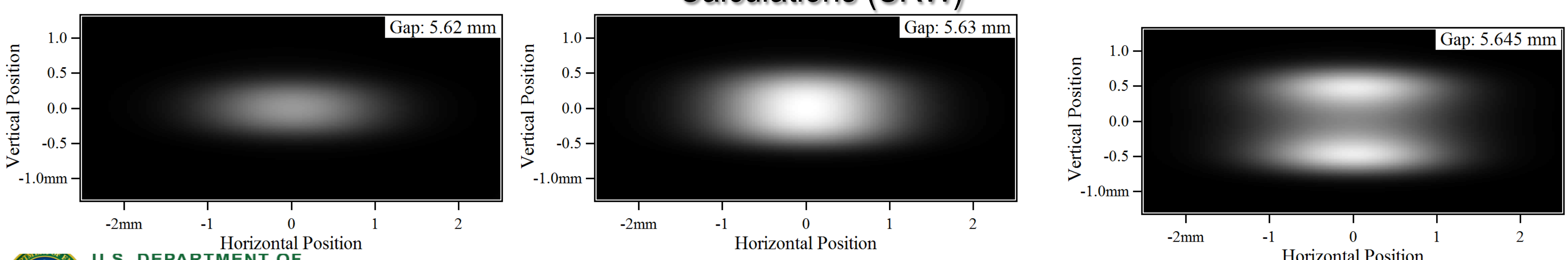

IVU20 (HXN) On-Axis "Gap Spectra" with Damping Wiggler Gaps "Open" and "Closed"

$E_{ph} \approx 8.0$ keV
5^{th} UR Harm.

Low-Beta Straight Section of NSLS-II
β_x= 1.84 m
β_y= 1.17 m

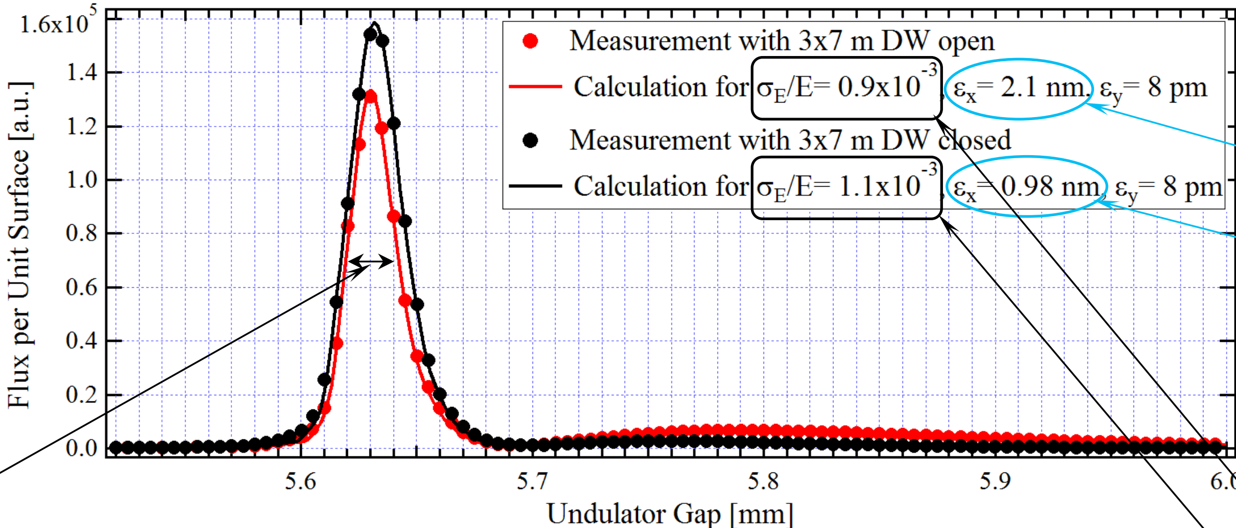

Good Agreement with Accelerator Physics data:
ε_x= 2.1 nm for Bare Lattice,
ε_x= 0.9 nm with 3x7 m DW closed

~Poor Agreement with Accelerator Physics data:
σ_E/E= 0.5x10^{-3} for Bare Lattice,
σ_E/E= 0.9x10^{-3} with 3x7 m DW closed

Harmonic width is sensitive to e-beam Energy Spread (and other factors, e.g. undulator field quality)

Intensity in "Side Lobe" is sensitive to e-beam Horizontal Angular Divergence

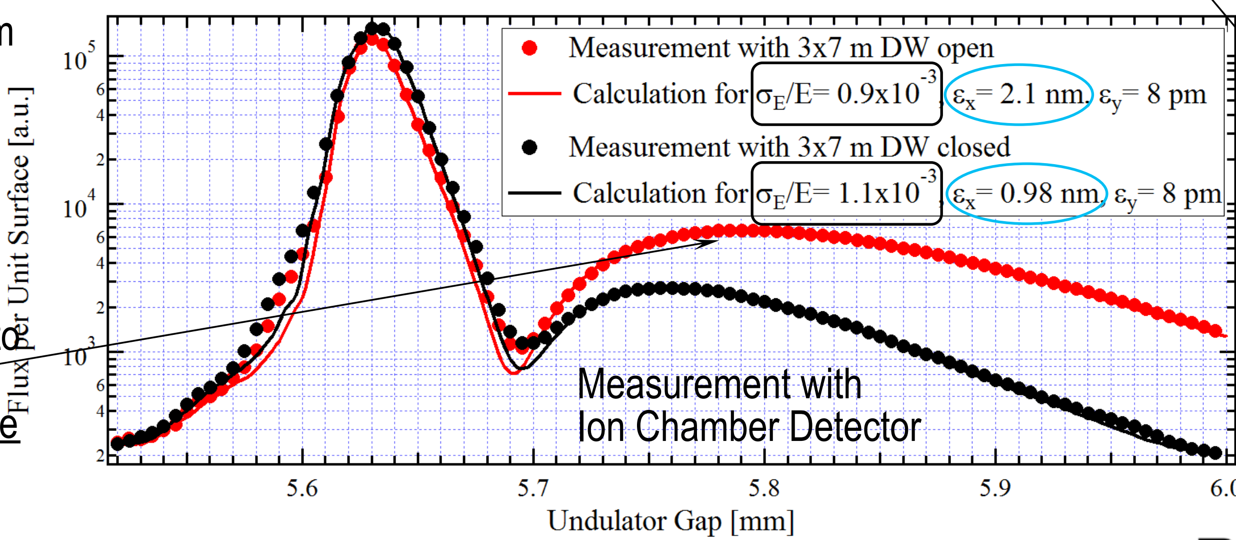

UR based e-beam diagnostics was used at ESRF (P. Elleaume et al.) and at APS (A. Lumpkin, E. Gluskin et al.)

Example of Using High-Accuracy UR Calculation for Advanced Commissioning of SRX Beamline at NSLS-II

Simulation of Taper / Misalignment Effects

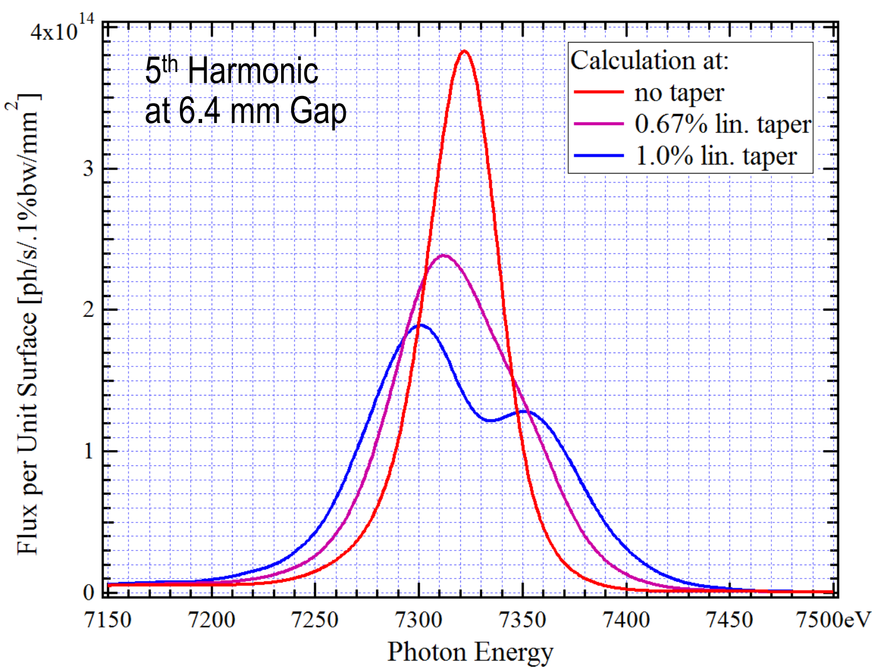

Measurements

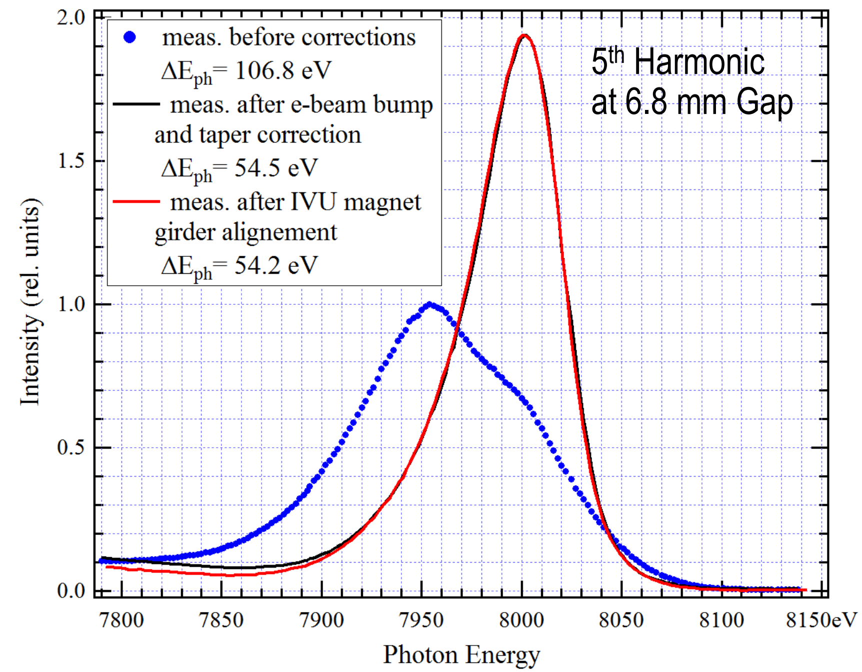

Undulator Radiation Simulations with SRW allowed to:

- Identify case of an under-performing In-Vacuum Undulator;
- Find reason for the reduction of spectral performance (small misalignment of magnet arrays);
- Implement most efficient correction and restore nearly ideal IVU spectrum.

Spectral-Angular Distributions of Emission from NSLS-II 2 x 3.5 m Long Damping Wiggler in "Inline" Configuration

Spectral Flux per Unit Solid Angle

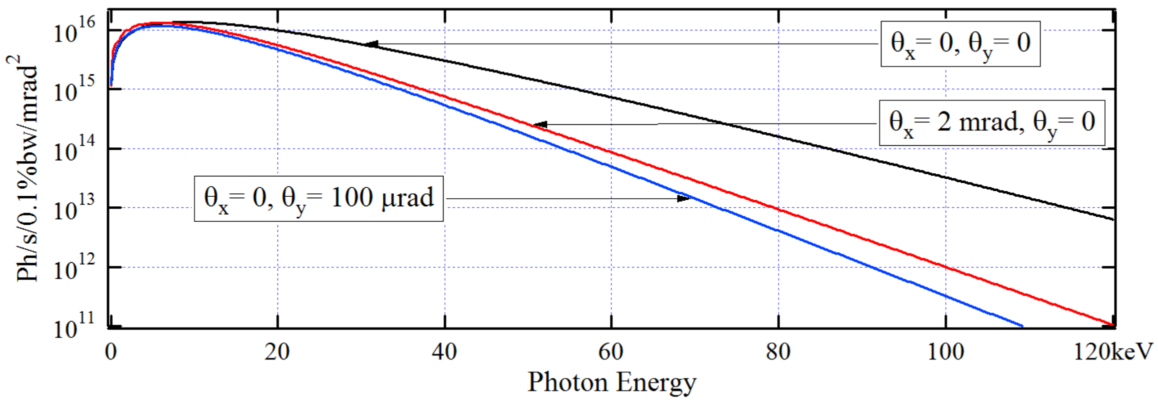

Angular Profiles of DW Emission at Different Photon Energies

Horizontal Profiles

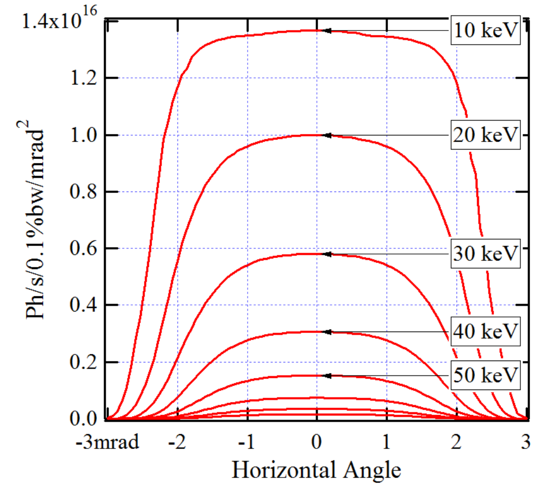

FWHM Angular Divergence of DW Emission

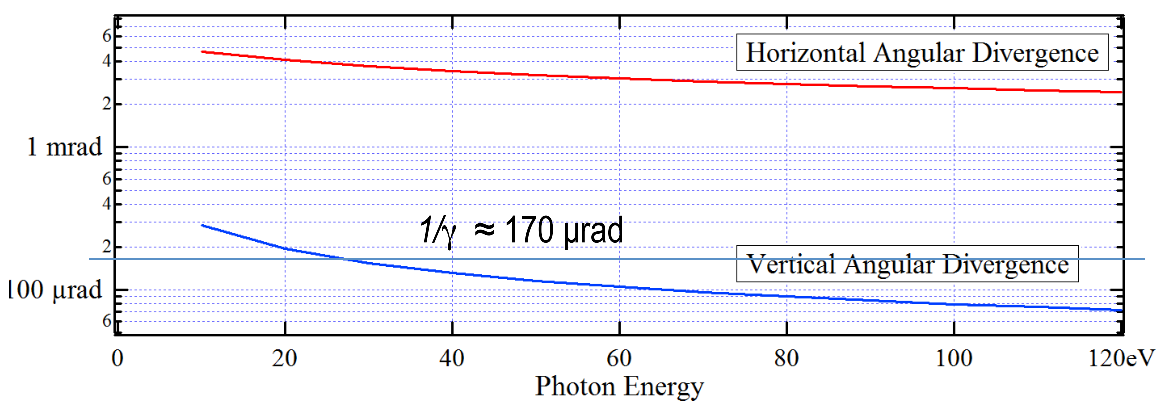

Vertical Profiles

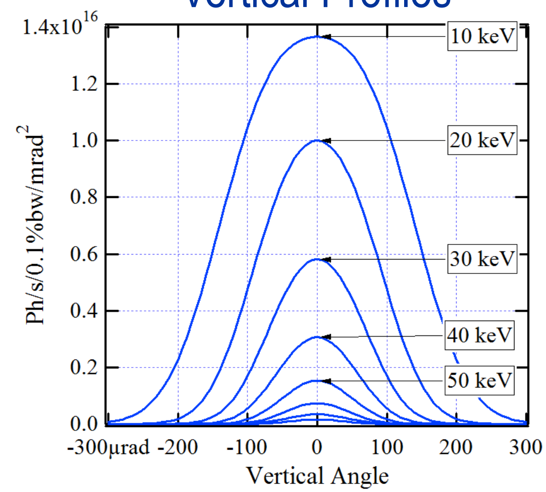

NSLS-II 3PW: Magn. Field, Electron Trajectory, Spectra
(in presence of Bending Magnets)

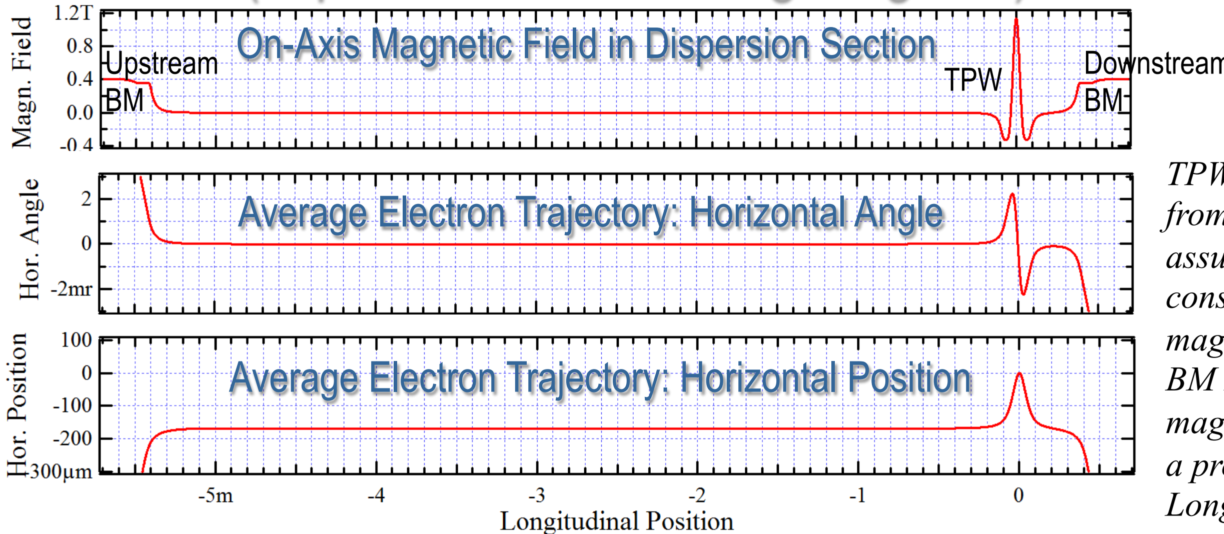

TPW Field taken from magnetic simulations, assuming that TPW will be constructed out of spare DW magnets; BM Field is taken from magnetic measurements on a prototype BM with "nose"; Longitudinal Positions are Approximate (+/- 10 cm)

On-Axis Spectral Flux per Unit Surface at 30 m from TPW

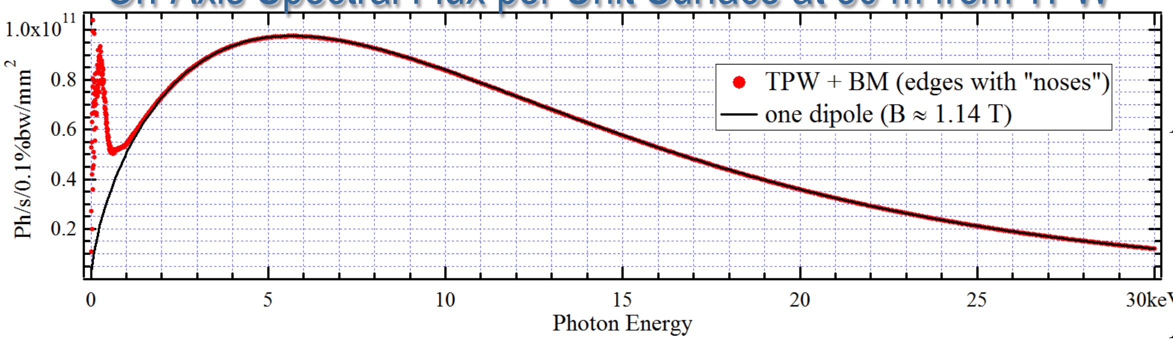

Electron Energy: 3 GeV
Current: 0.5 A
Hor. Emittance: 0.55 nm
Vert. Emittance: 8 pm

Initial Conditions:
<x> = 0, <x'>= 0 in TPW Center

Spectral Flux through 1.75 mrad (H) x 0.1 mrad (V) Aperture
(centered on the axis)

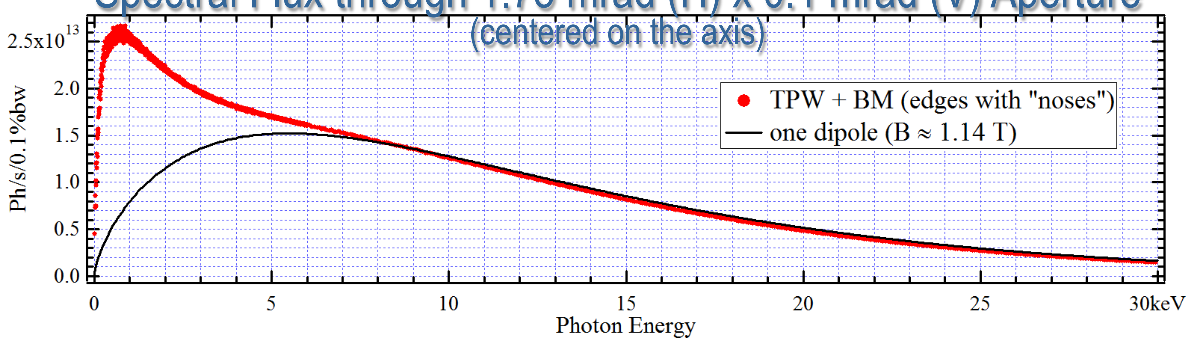

NSLS-II 3PW+BM Radiation Intensity (Hard X-Rays)

Intensity Distributions at Different Photon Energies at 30 m from TPW

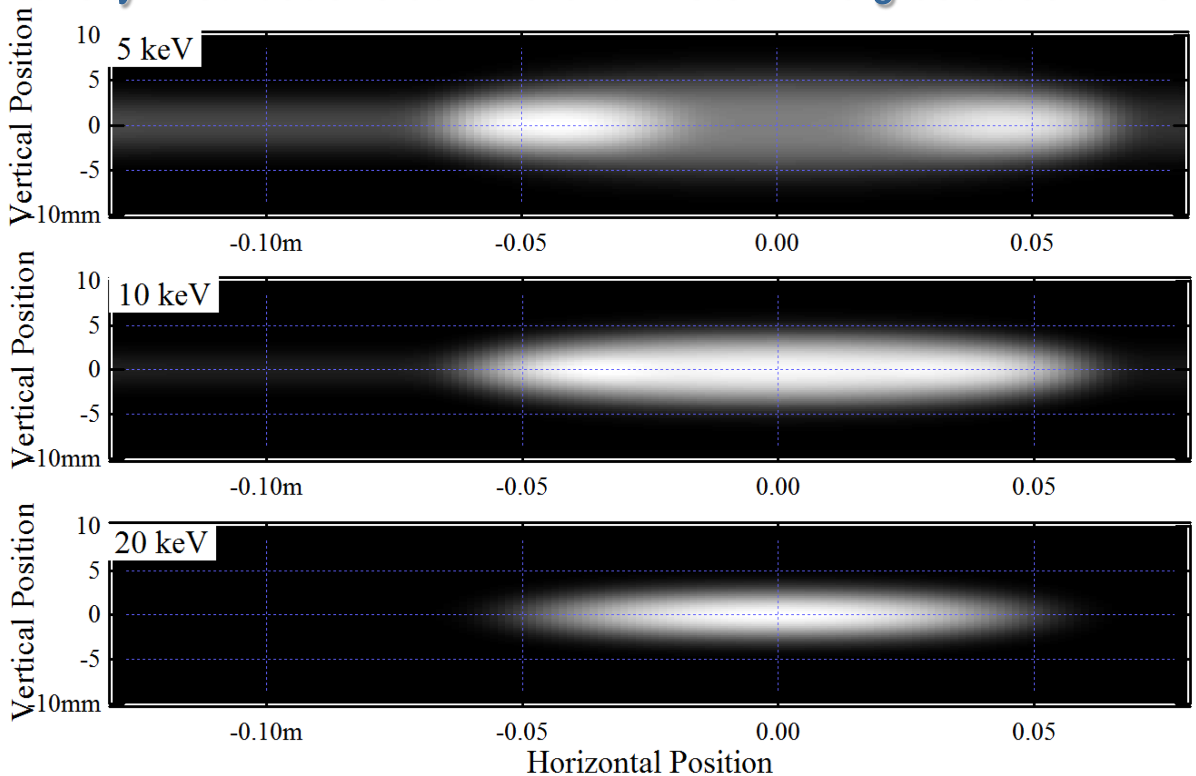

TPW Field taken from magnetic simulations, assuming that TPW will be constructed out of spare DW magnets; BM Field taken from magnetic measurements on a prototype BM with "nose".

Electron Current: 0.5 A

Horizontal Cuts at y = 0

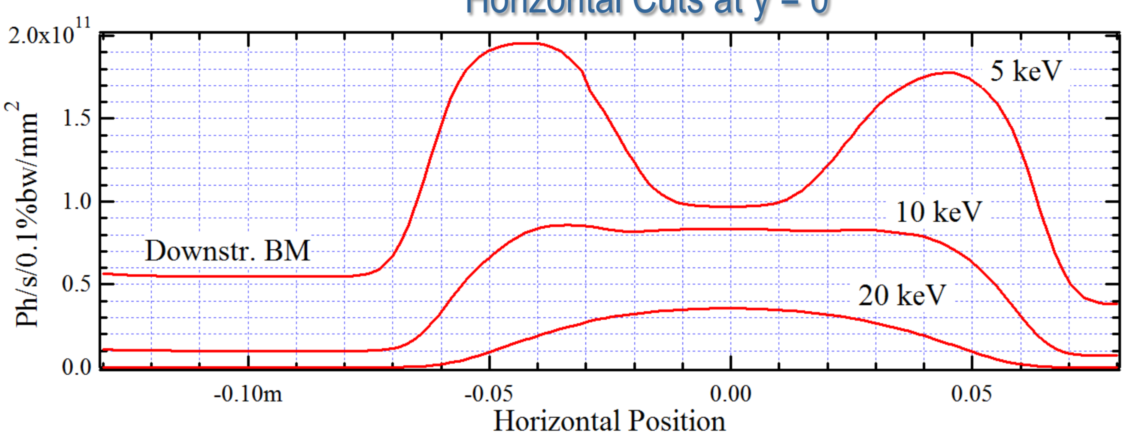

Vertical Cuts at x = 0

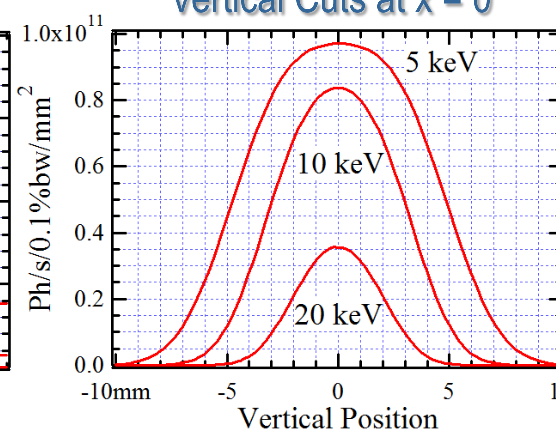

NSLS-II 3PW+BM Radiation Intensity (IR to Soft X-Rays)

Observation Distance: 30 m (from TPW center)

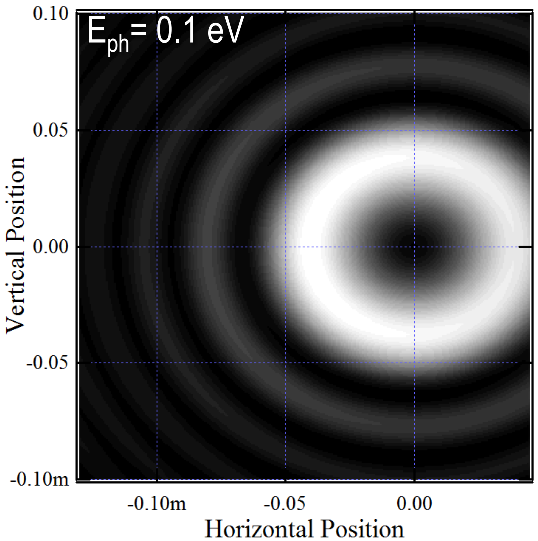

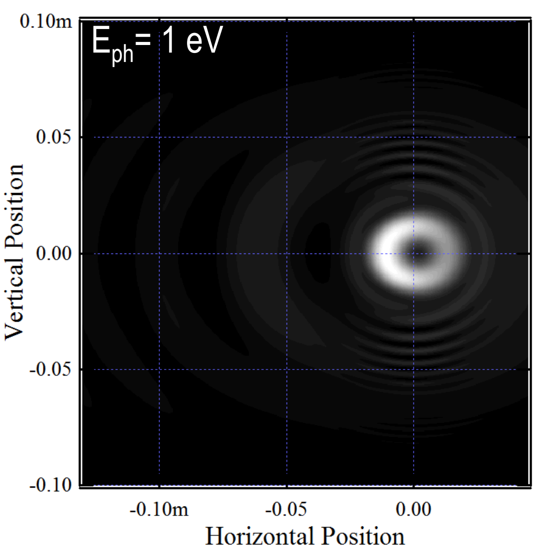

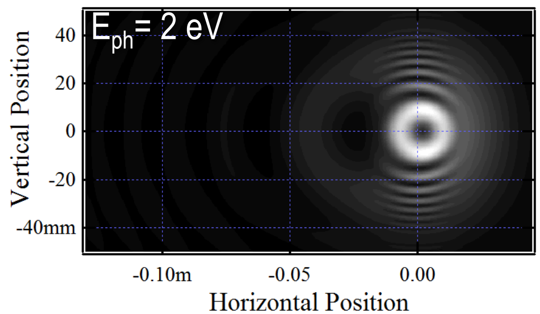

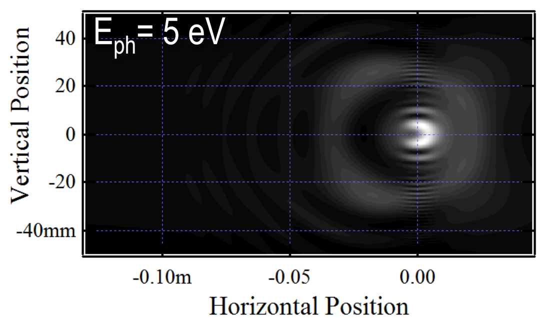

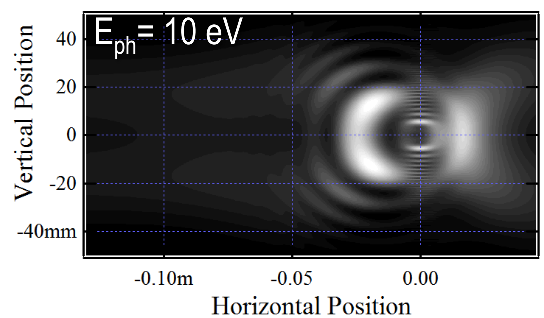

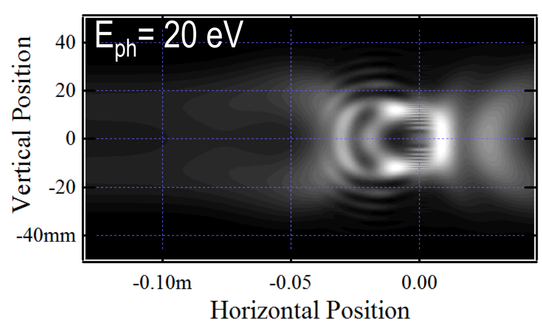

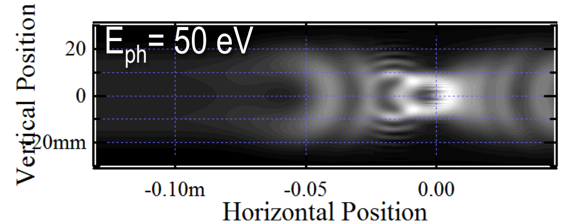

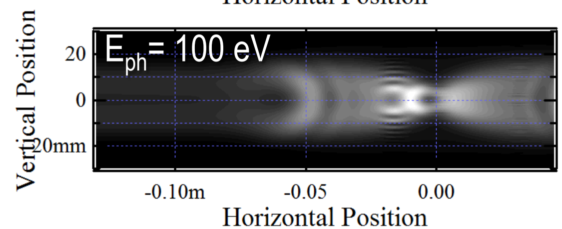

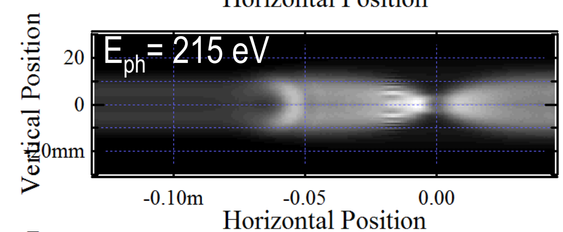

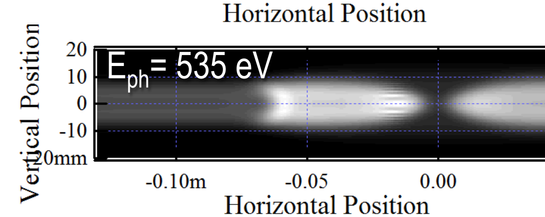

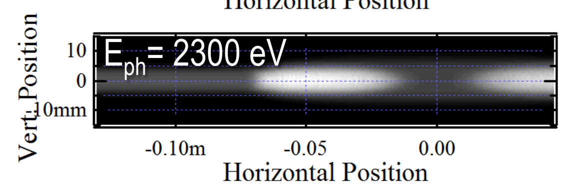

TPW Field taken from magnetic simulations, assuming that TPW will be constructed out of spare DW magnets;
BM Field taken from magnetic measurements on a prototype BM with "nose".

ESRF-U 2PW (option): Magnetic Field and Electron Trajectories

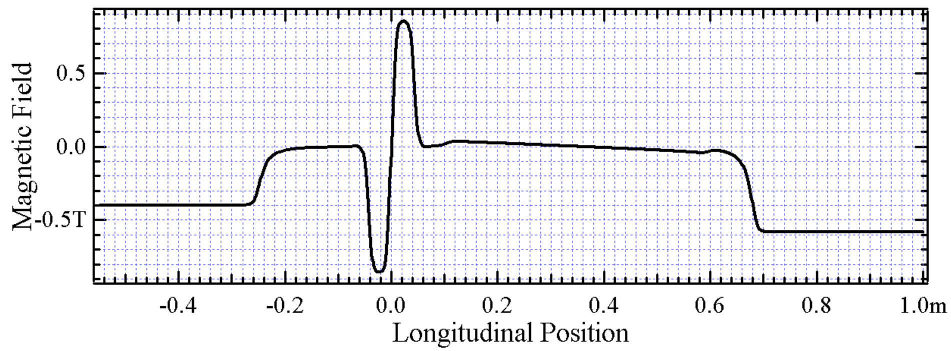

Magnetic design by J. Chavanne

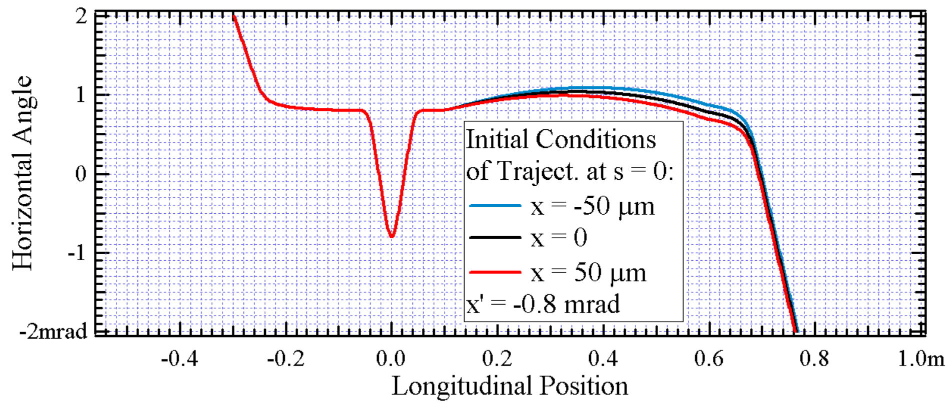

Quadrupole Lens is included into analysis (under testing)

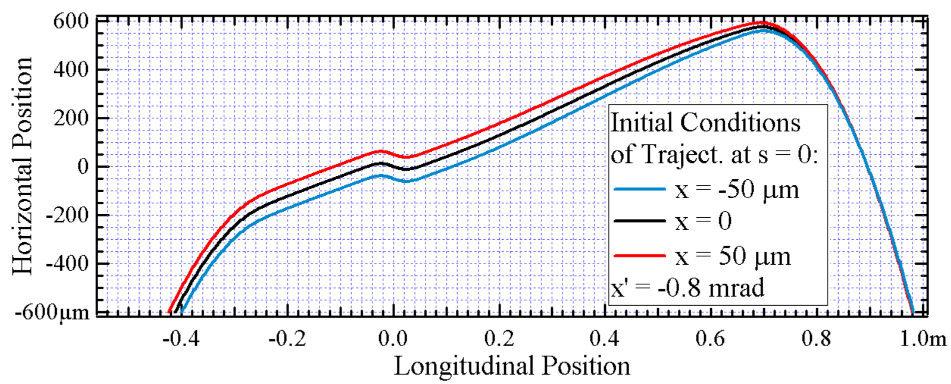

ESRF-U 2PW Radiation Intensity Distributions

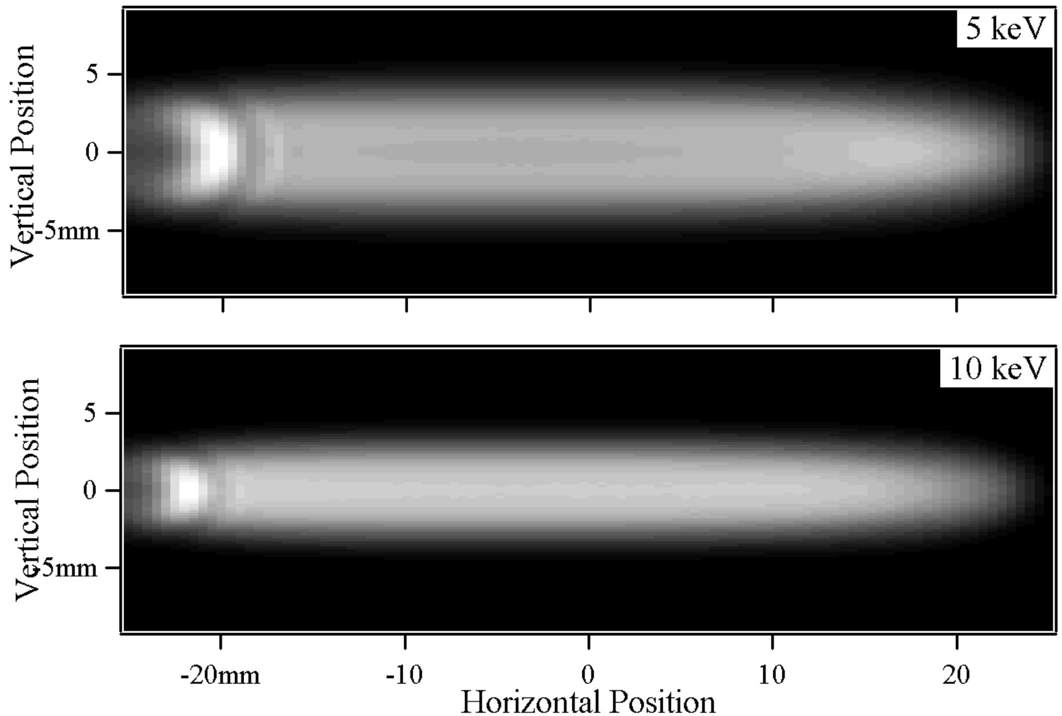

Observation Distance:
R = 30 m

Cuts by Horizontal Median Plane

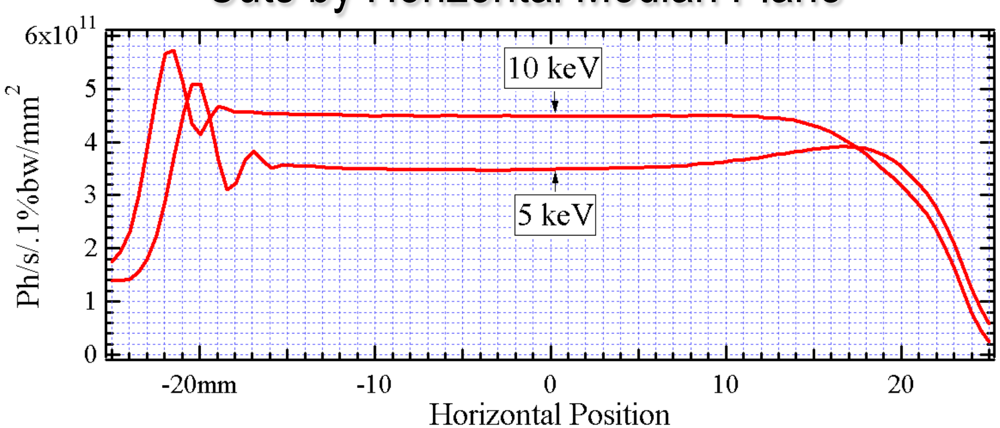

Cuts by Vertical Plane (x = 0)

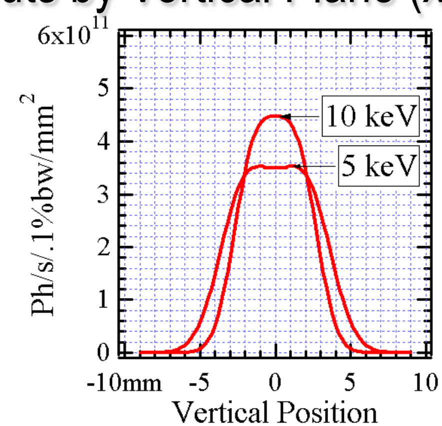

SMIS IR Extraction Scheme at SOLEIL

Fully-Coherent Wavefront Propagation

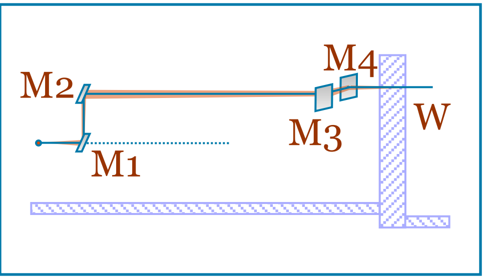

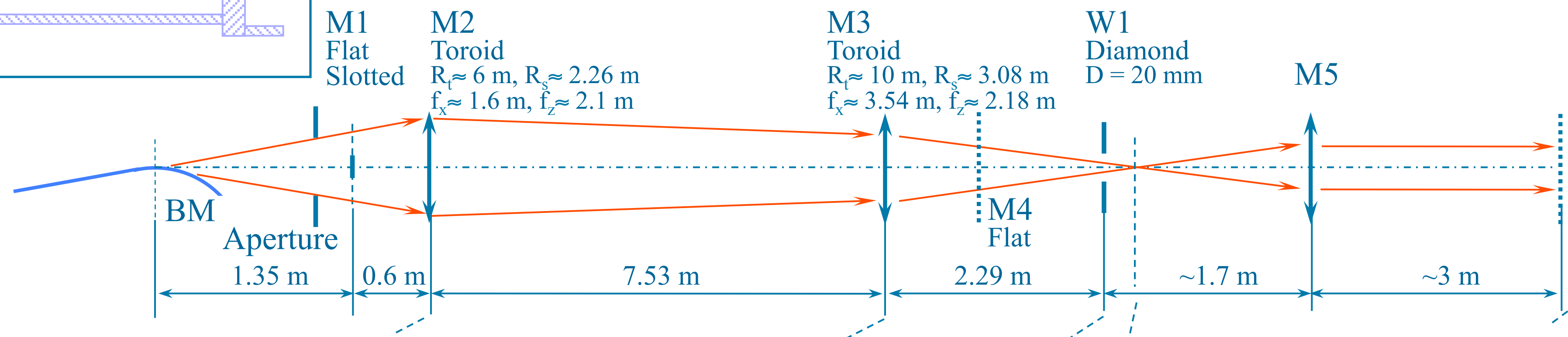

Flux: 1.67 x 10^{14} Phot/s/0.1%bw

Flux: 1.35 x 10^{14} Phot/s/0.1%bw

Intensity Distributions at 10 μm Wavelength

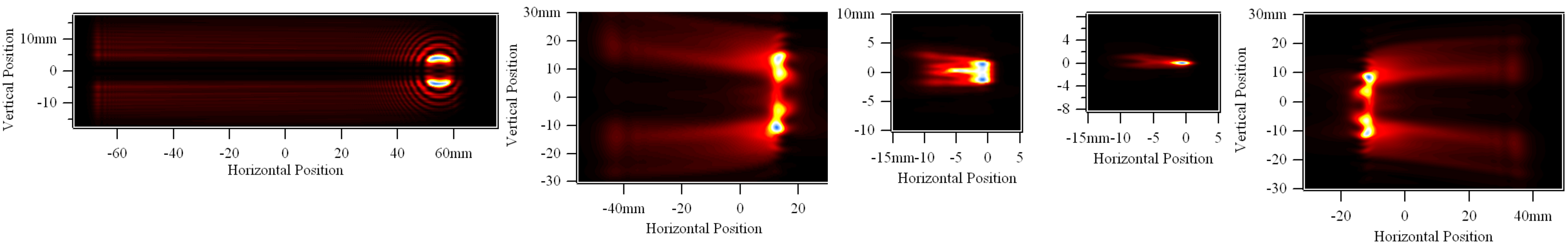

Intensity Profiles

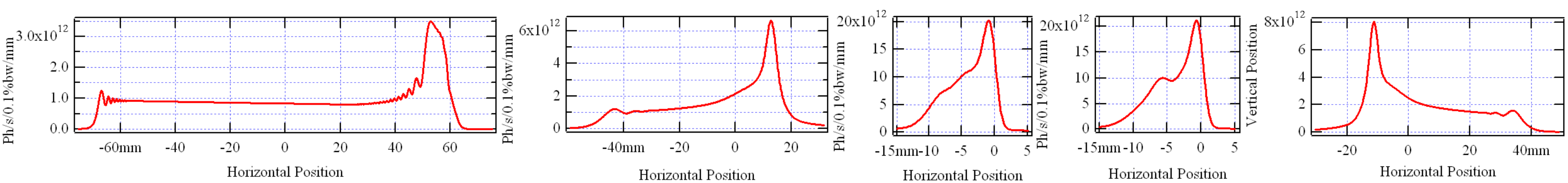

Optical scheme: F. Polack, P. Dumas

Updates of Core Functions in "Synchrotron Radiation Workshop" Code Enabling Physical-Optics Calculations for Beamlines in Low-Emittance Rings and X-FEL

- Accurate partially-coherent emission and wavefront propagation simulations for SR sources are possible with SRW since ~2009:
  O.Chubar, Y.S.Chu, K.Kaznatcheev, H.Yan, AIP Conf. Proc. Vol. 1234, pp.75-78 (2009)
  O.Chubar, Y.S.Chu, K.Kaznatcheev, H.Yan, Nucl. Instr. and Meth., vol. A649, Issue 1, pp.118-122 (2011)

- Parallel calculations of Partially-Coherent Emission and Wavefront Propagation are implemented in SRW for Python (based on MPI / mpi4py). Besides "normal" Intensity, calculation of Mutual Intensity / Degree of Coherence is possible:
  O.Chubar, A.Fluerasu, L.Berman, K.Kaznatcheev, L.Wiegart, J. Phys.: Conf. Ser. 425, 162001 (2013)
  D.Laundy, J.P.Sutter, U.H.Wagner, C.Rau, C.A.Thomas, K.J.S.Sawhney, and O.Chubar, J. Phys.: Conf. Ser. 425, 162002 (2013)

- Increased reliability of Time- / Frequency-Dependent FEL Pulse Propagation simulations:
  S.Roling, H.Zacharias, L.Samoylova, H.Sinn, Th.Tschentscher, O.Chubar, A.Buzmakov, E.Schneidmiller, M.V.Yurkov, F.Siewert, S.Braun, and P.Gawlitza, Phys. Rev. ST Accel. Beams 17, 110705 (2014)

- Physical-optics "propagators" are implemented for:

- Grazing-Incidence Focusing Mirrors, using the stationary phase method / "local ray-tracing":
  N.Canestrari, O.Chubar, R.Reininger, J. Synchrotron Rad. 21, 1110-1121 (2014)

- Perfect Crystals, using the X-ray Dynamical Diffraction methods:
  J.P.Sutter, O.Chubar, A.Suvorov, Proc. SPIE Vol. 9209, 92090L (2014)
  A.Suvorov, Y.Q.Cai, J.P.Sutter, O.Chubar, Proc. SPIE Vol. 9209, 92090H (2014)
  O.Chubar, G.Geloni, V.Kocharyan, A.Madsen, E.Saldin, S.Serkez, Y.Shvyd'ko, J.Sutter, JSR 23, 410-424 (2016)

- Variable Line Spacing Gratings, using the Stationary Phase method:
  N.Canestrari, V.Bisogni, A.Walter, Y.Zhu, J.Dvorak, E.Vescovo, O.Chubar, Proc. SPIE Vol. 9209, 92090I (2014)

NSLS-II Hard X-Ray Nanoprobe (HXN) Beamline Optical Scheme and Partially-Coherent Wavefront Propagation Simulation

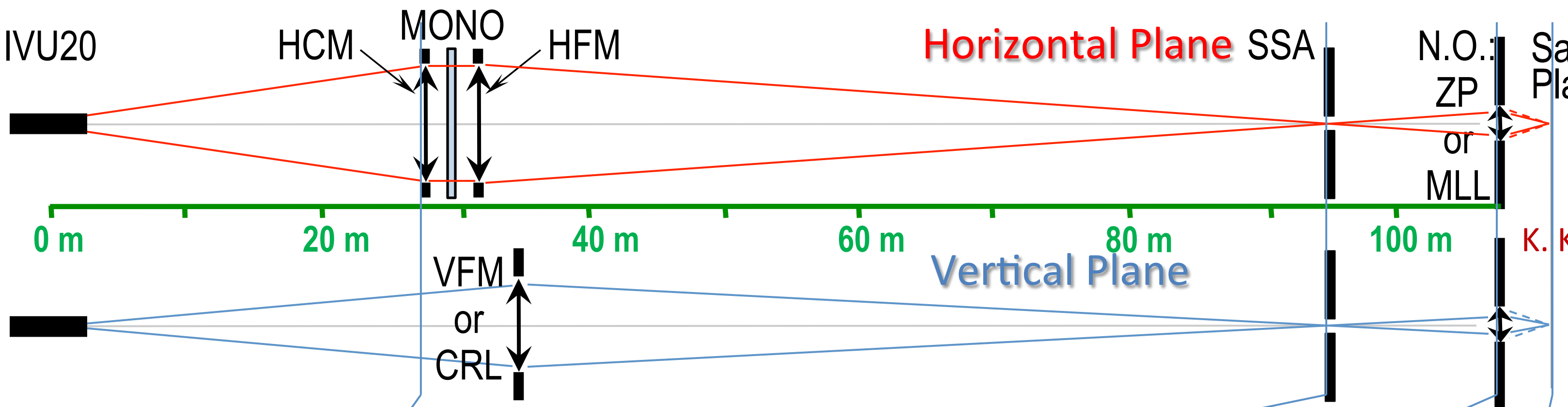

Y. Chu,
H. Yan,
K. Kaznatcheev

Pan-Am SRI-2010

Flux after HCM: **~7.4x10^{14}** ph/s/.1%bw

Intensity Distributions

Flux within N.O. Aperture (d=150 μm): **~3.6 x10^{12}** ph/s/.1%bw

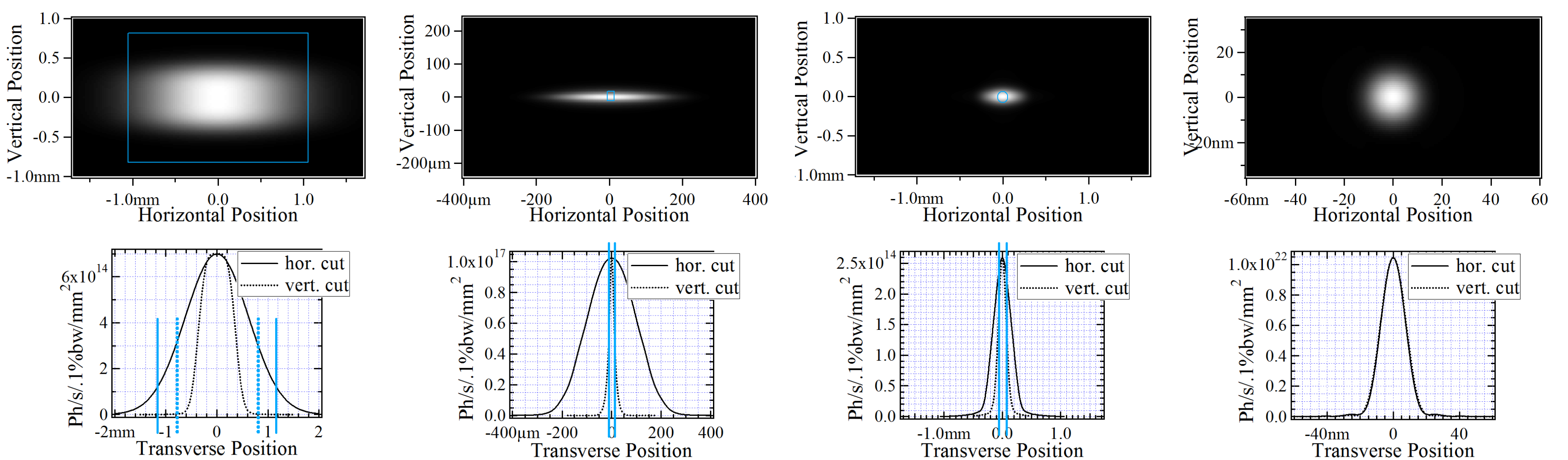

Final Focal Spot Size and Flux at Sample vs Secondary Source Aperture Size (HXN, NSLS-II)

Horizontal Spot Size and Flux
vs Horizontal Secondary Source Aperture Size

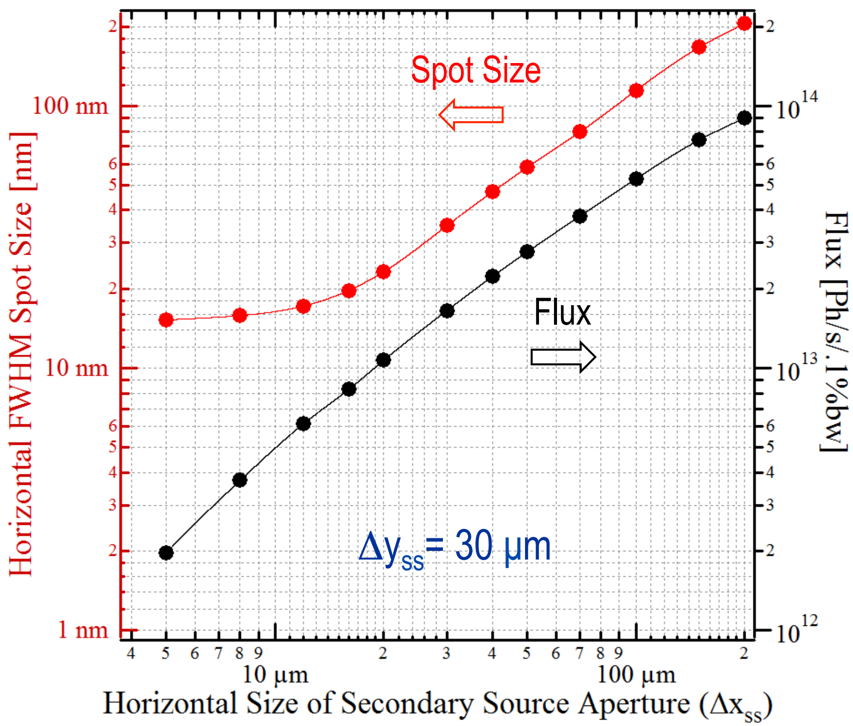

Vertical Spot Size and Flux
vs Vertical Secondary Source Aperture Size

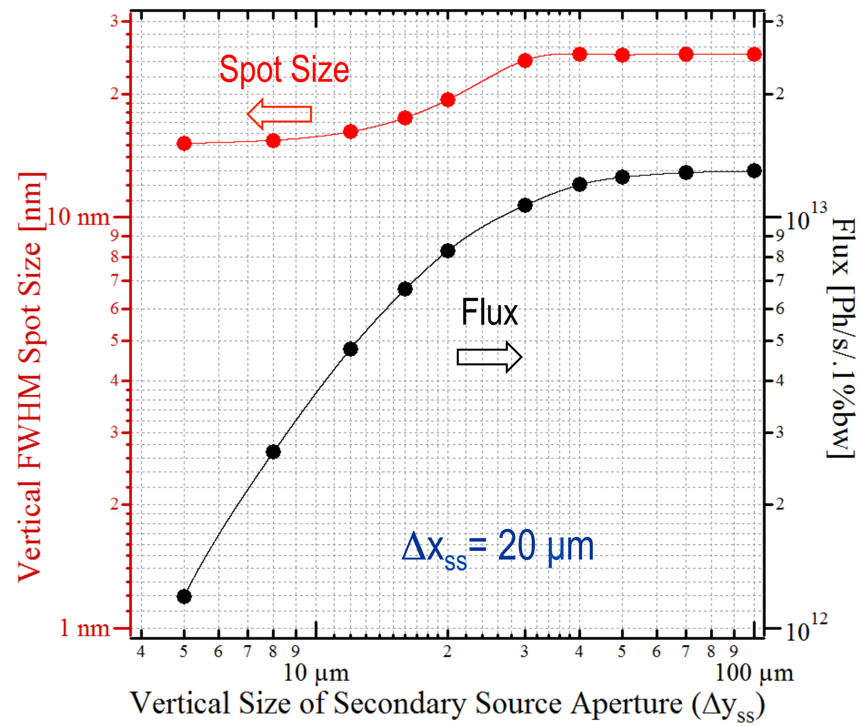

Pan-Am SRI-2010

Secondary Source Aperture located at 94 m from Undulator
Spot Size and Flux calculated for Nanofocusing Optics simulated by Ideal Lens
with F = 18.14 mm, D = 150 μm located at 15 m from Secondary Source (109 m from Undulator)

Intensity Distributions at Sample for Different Secondary Source Aperture Sizes at HXN (NSLS-II)

In Horizontal Median Plane (y = 0)

For Different Horizontal SSA Sizes (Δx_{ss})

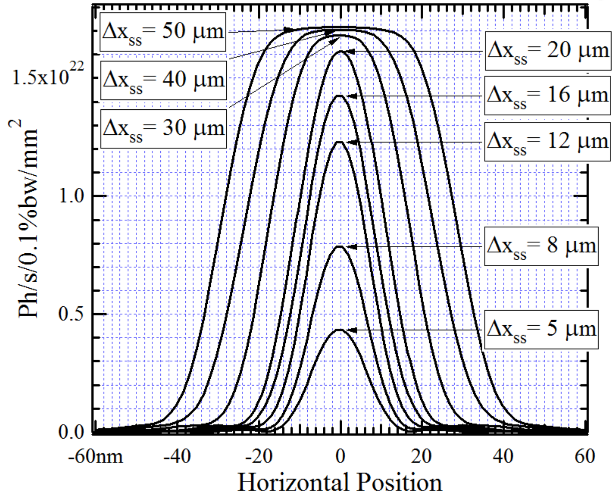

For Different Vertical SSA Sizes (Δy_{ss})

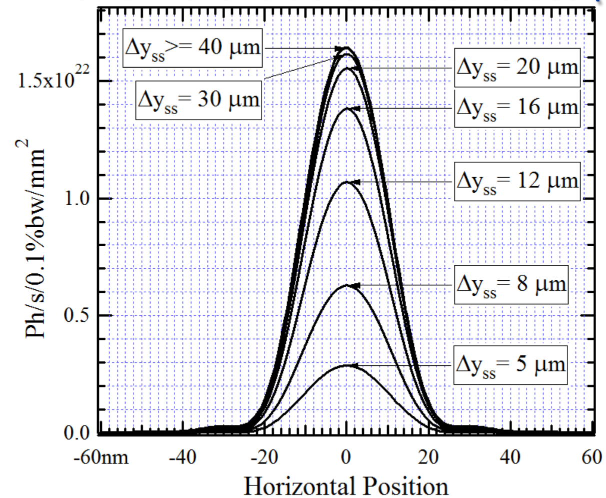

In Vertical Median Plane (x = 0)

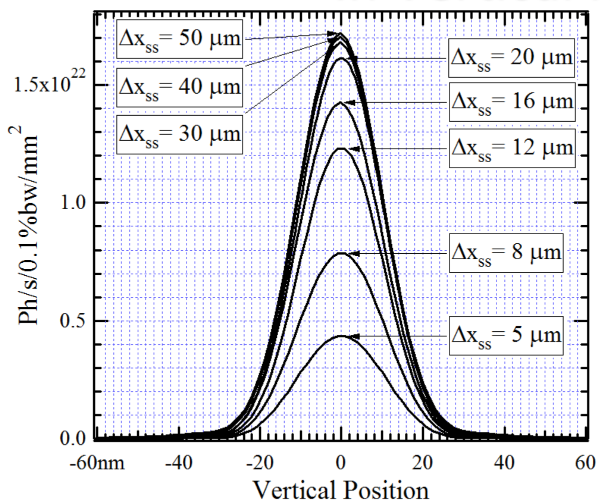

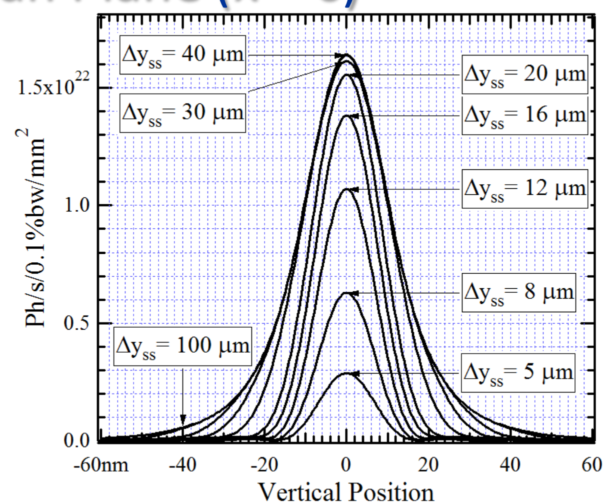

For Nanofocusing Optics with F = 18.14 mm, D = 150 μm ($\Delta r \approx$ 15 nm; $E_{ph} \approx$ 10 keV)
SSA located at 94 m, Nanofocusing Optics at 109 m from Undulator

Partially-Coherent Wavefront Propagation Simulations for a Beamline with Grazing-Incidence Focusing Mirrors, Taking Into Account Their Imperfections (FMX @ NSLS-II)

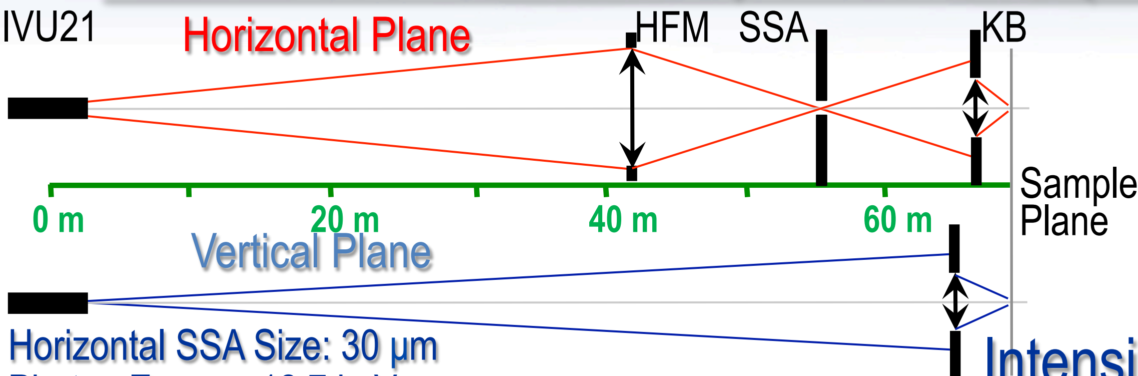

KB simulated using Grazing-Incidence "Thick Optical Element" Propagator based on "Local Ray-Tracing".
KB Surface Height Error simulated by corresponding Phase Shifts ("Masks") in Transverse Plane at Mirror Locations.

Horizontal SSA Size: 30 μm
Photon Energy: 12.7 keV
Flux at Sample: ~5.4x10^{13} ph/s/.1%bw

Mirror Slope Error

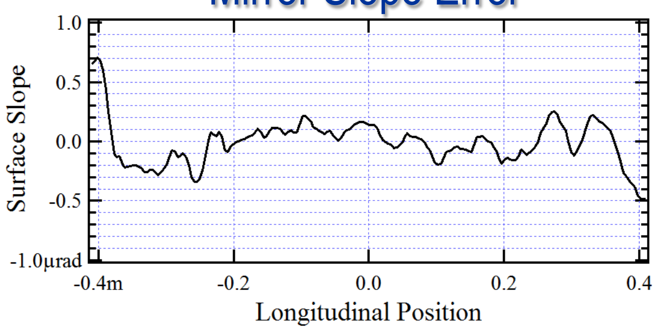

Mirror Height Profile Error

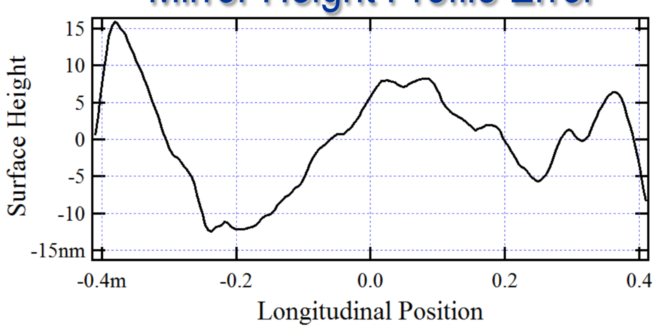

Intensity Distributions at Sample

Without Mirror Errors

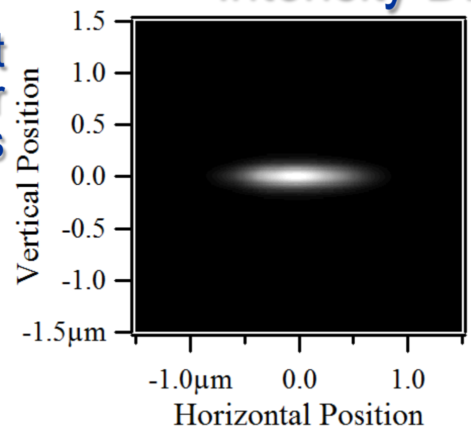

With Mirror Errors

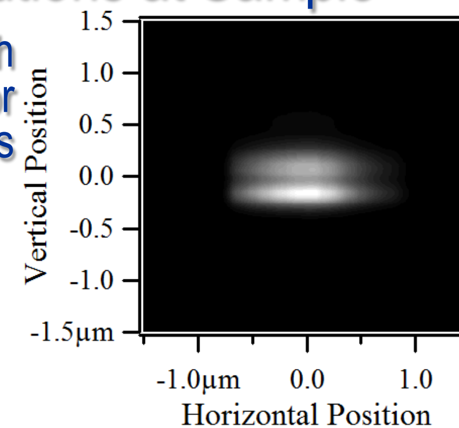

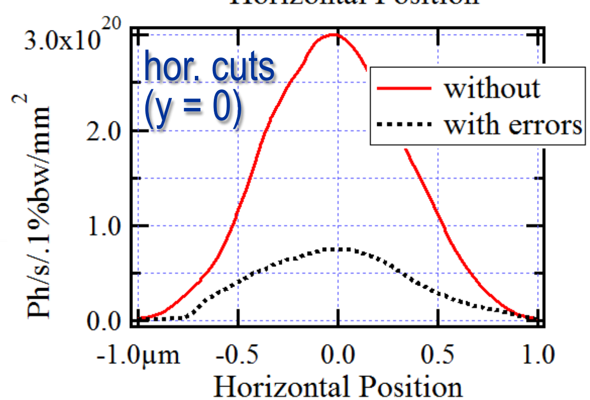

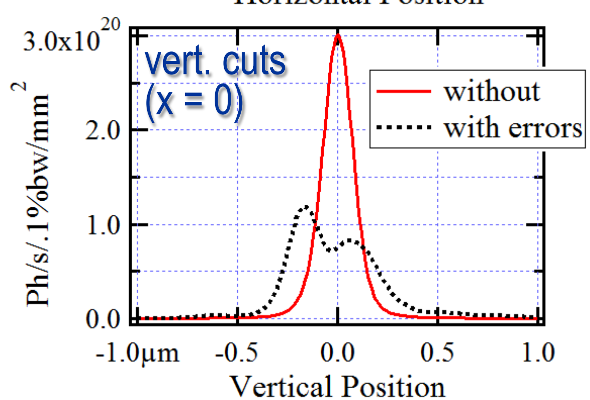

Using CRL for Producing "Large Spot" at Sample of FMX Beamline @ NSLS-II

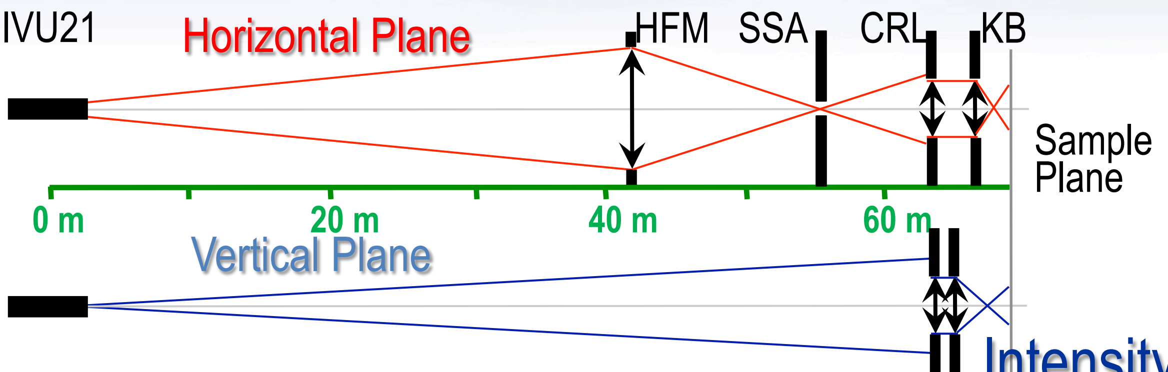

Source:

Electron Current: 0.5 A
Horizontal Emittance: 0.55 nm ("ultimate")
Vertical Emittance: 8 pm
Undulator: IVU21-1.5 m centered at +1.25 m from Low-Beta Straight Section Center

Horizontal SSA Size: 30 μm
Photon Energy: 12.7 keV

CRL "Transfocator":

8 Horizontally + 3 Vertically-Focusing Be Lenses
R_{min} = 200 μm
$F_h \approx$ 5.9 m, $F_v \approx$ 15.8 m
Geom. Ap.: 1 mm x 1 mm

Located at 0.75 m before VKB edge (10 m after SSA)

Flux Losses at CRL: ~1.6 times

Intensity Distributions at Sample

Without Mirror Errors

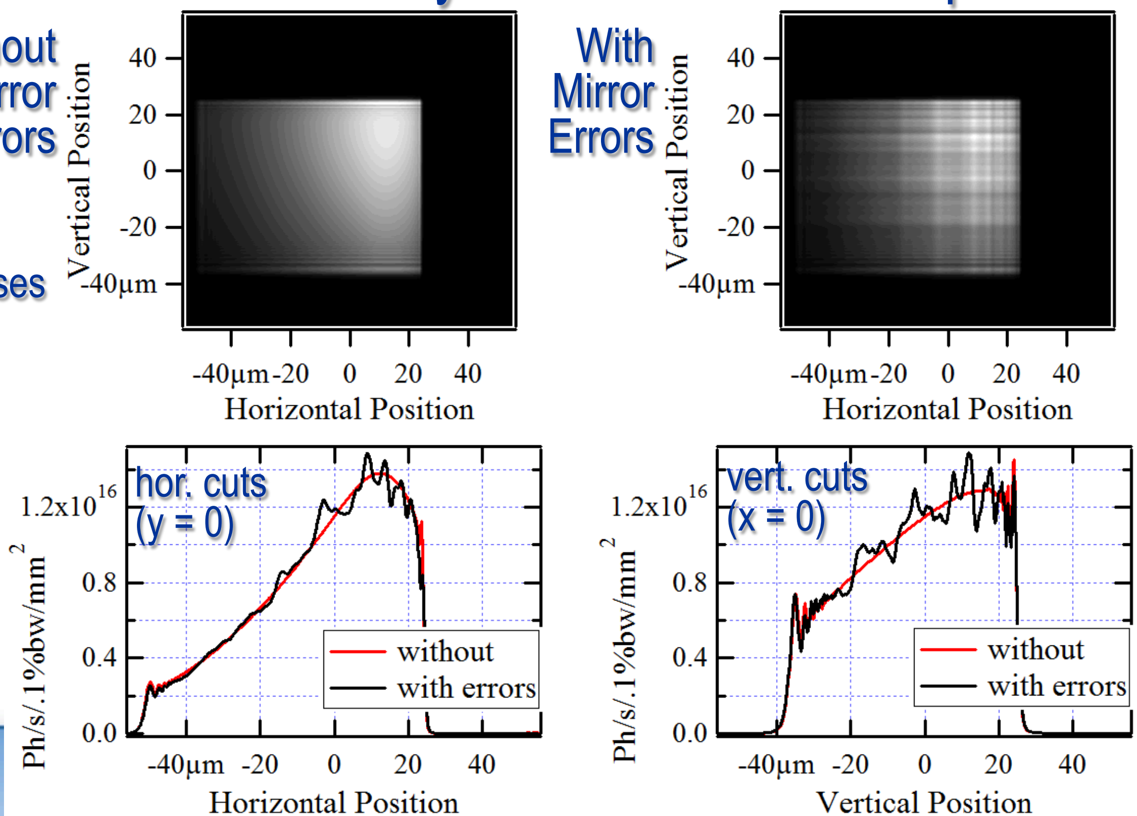

Partially-Coherent Wavefront Propagation Simulations for CHX Beamline @ NSLS-II

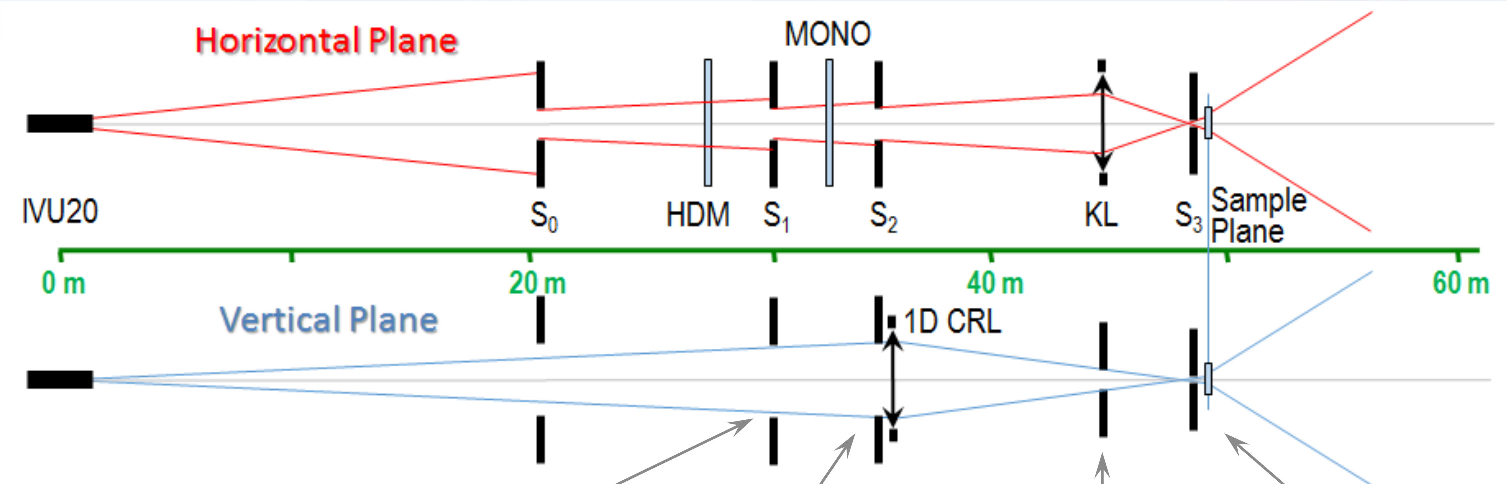

Intensity Distributions

for E = 10 keV
ΔS_{1x}= 44 µm
ΔS_{1y}= 1 mm

Before SS1 (@33.5 m)

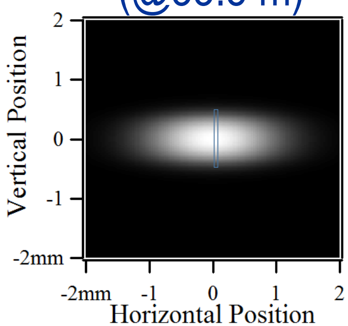

Before CRL (@35.8 m)

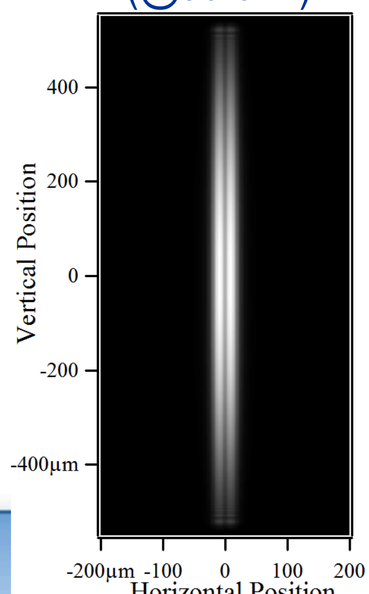

Before KL (@44 m)

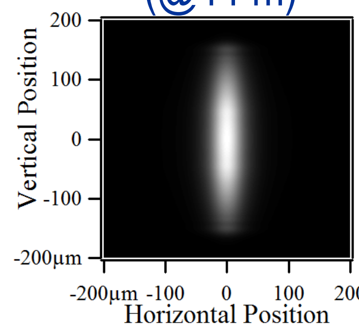

At Sample (@48.5 m)

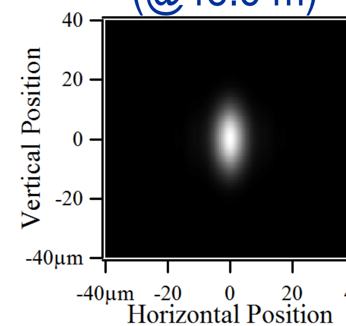

Flux: 10^{13} ph/s/.1%bw

Estimating Degree of Coherence of Radiation from U20 Installed in Low-Beta Straight Section of NSLS-II

Intensity Distribution at 30 m from Undulator

Intensity Distributions at 30 from Young's 2 Slits

Visibility of Fringes in Young's 2-Slit Interference Scheme

Vertical Slits (to estimate coherence in horizontal direction)

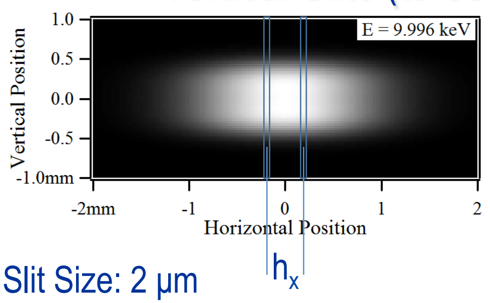

Slit Size: 2 µm

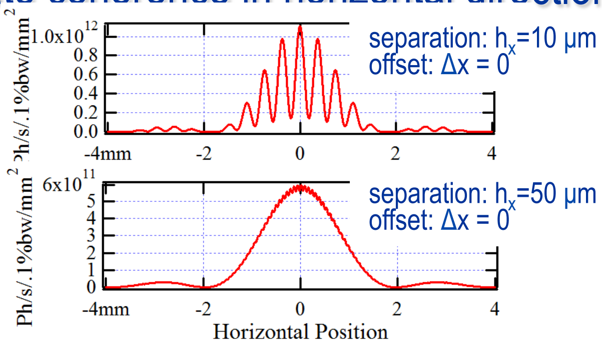

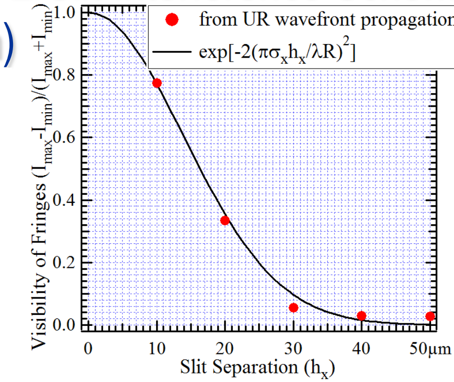

$E_{ph} \approx$ 10 keV

σ_x= 42.6 µm

Horizontal Slits (to estimate coherence in vertical direction)

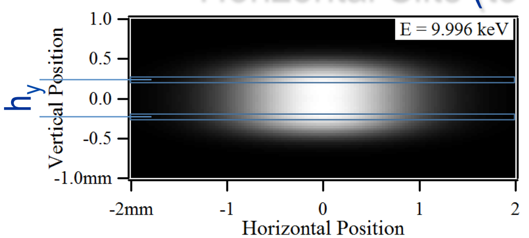

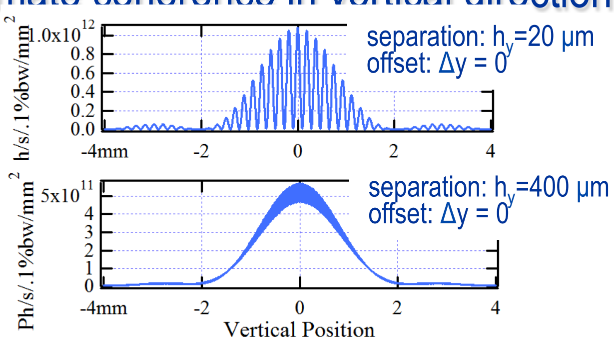

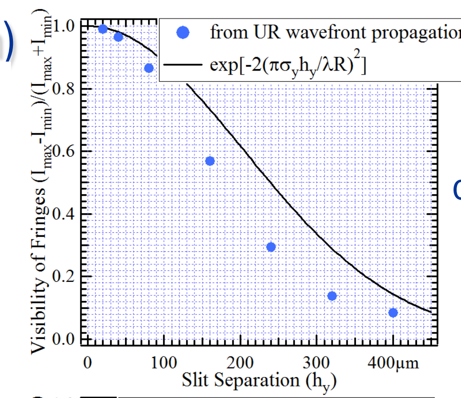

σ_y= 2.9 µm

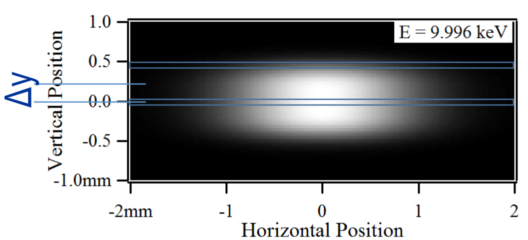

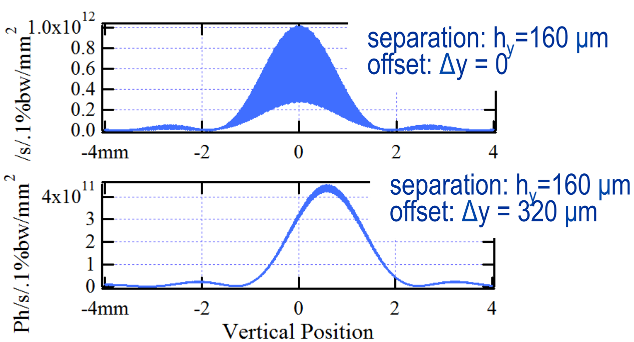

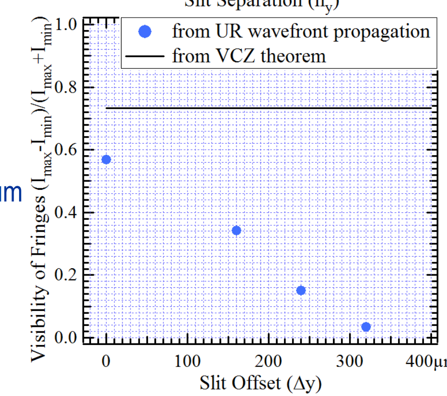

Tracking Intensity and Degree of Transverse Coherence at a Sample (CHX @ NSLS-II)

Intensity Distribution

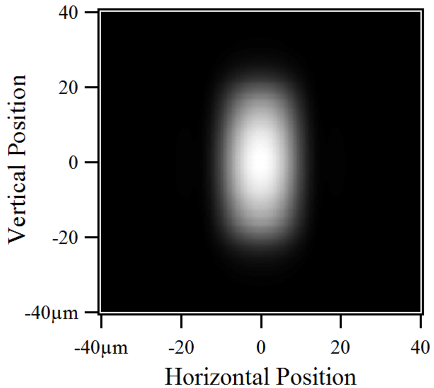

Degree of Transverse Coherence

In Horizontal Mid-Plane

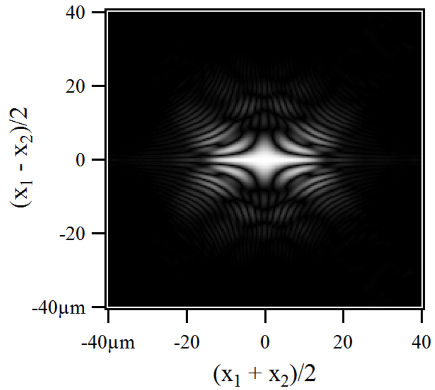

In Vertical Mid-Plane

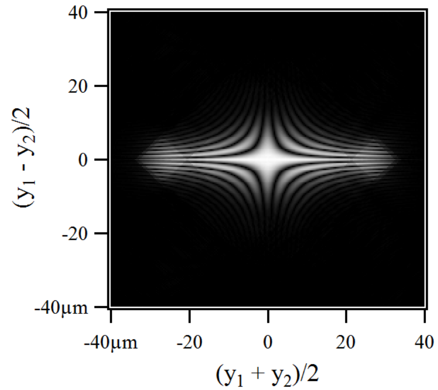

$$\mu(\mathbf{r}_1,\mathbf{r}_2,\omega) = |W(\mathbf{r}_1,\mathbf{r}_2,\omega)|/[W(\mathbf{r}_1,\mathbf{r}_1,\omega)W(\mathbf{r}_2,\mathbf{r}_2,\omega)]^{1/2}$$

$$W(\mathbf{r}_1,\mathbf{r}_2,\omega) \sim \langle E(\mathbf{r}_1,\omega)E^*(\mathbf{r}_2,\omega)\rangle$$

Angular Intensity (far field) after Two Slits separated by 10 µm

In Horizontal Plane (after vertical slits)

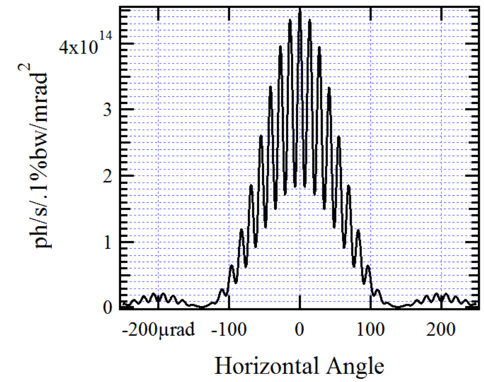

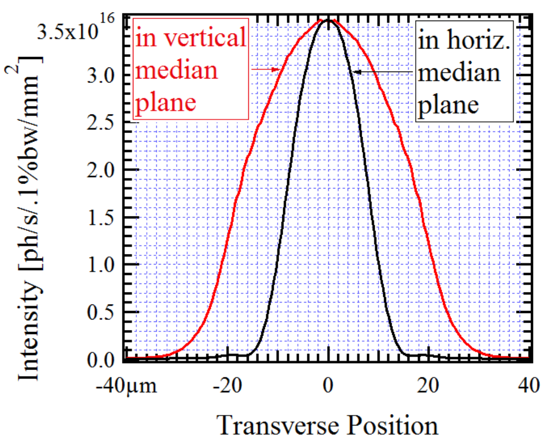

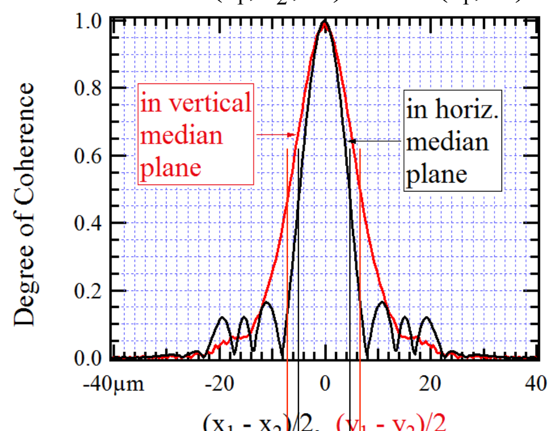

In Vertical Plane (after horizontal slits)

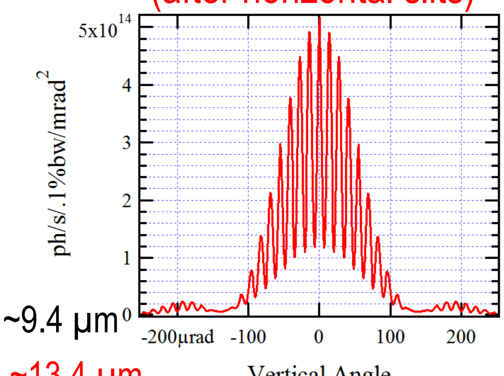

hor. coherence length: ~9.4 µm

vert. coherence length: ~13.4 µm

Good agreement with 2-slit interference simulation results

Partially-Coherent Wavefront Propagation Simulations for Inelastic X-ray Scattering Beamline with Advanced High-Resolution Crystal Optics (IXS @ NSLS-II)

A.Suvorov, Y.Q.Cai, J.P.Sutter, O.Chubar, Proc. of SPIE Vol. 9209, 92090H (2014)

Extended testing of new physical optics propagator for crystals

IXS Monochromators contain:
- DCM: 2 Crystals
- HRM: 4 Crystals of HRM

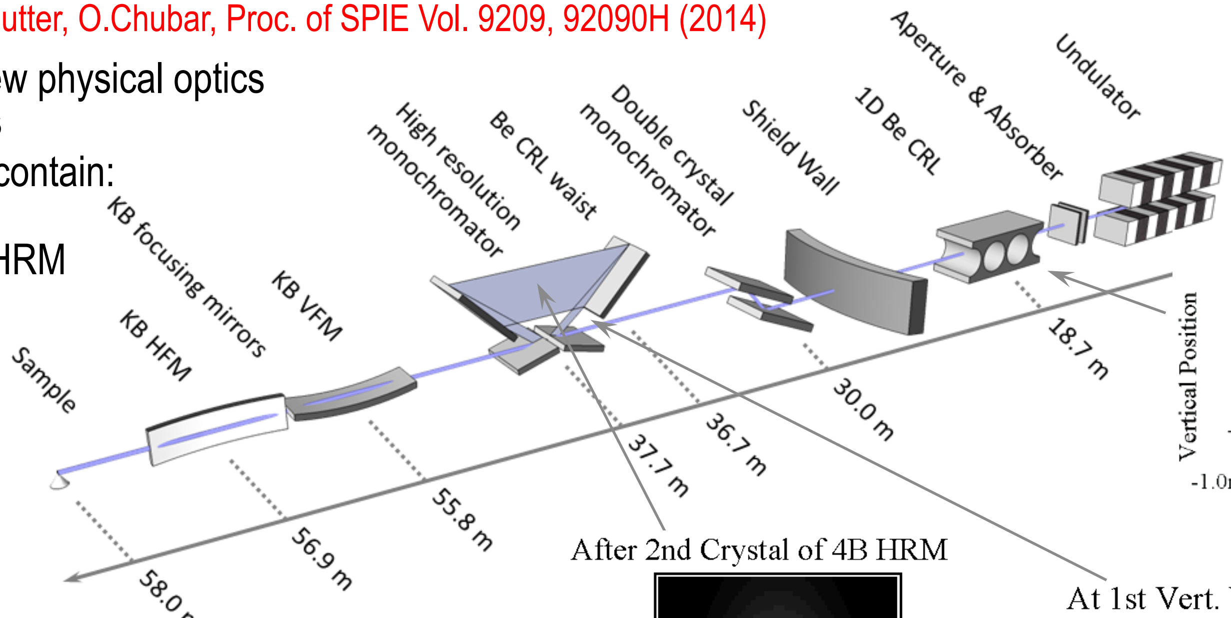

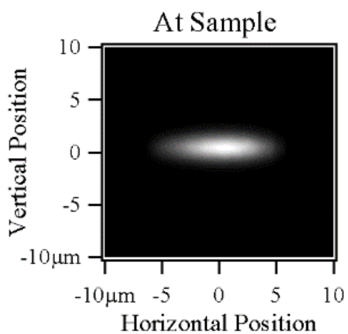

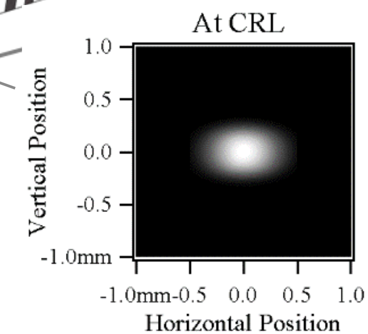

Mirror Surface Error is not taken into account

$E_0 \approx 9131.7$ eV

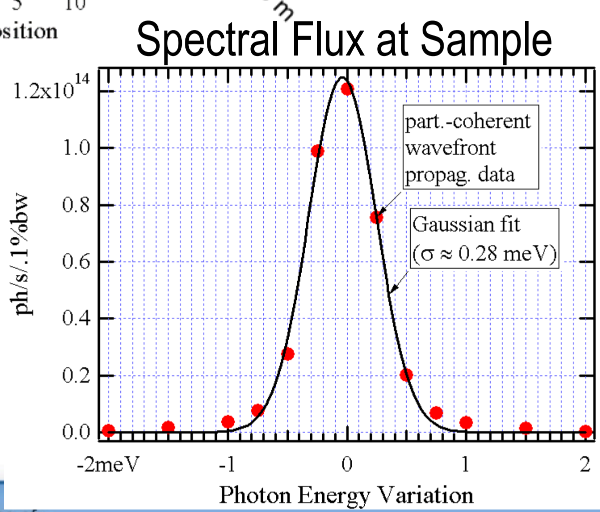

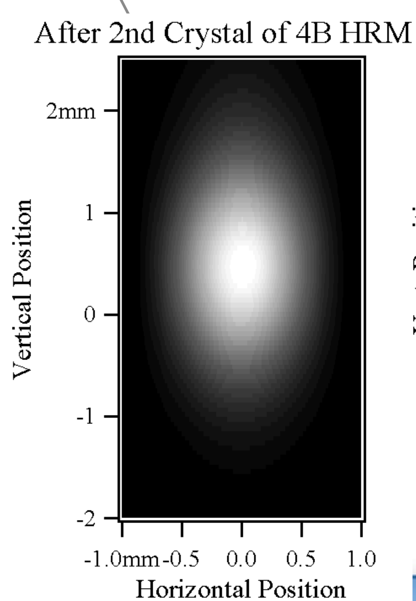

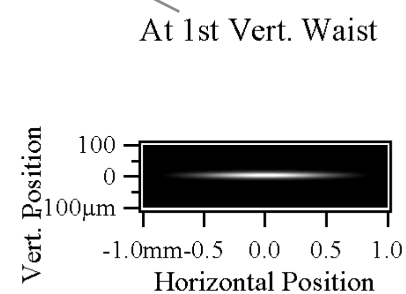

NSLS-II Soft Matter Interfaces beamline modelling

Courtesy of M. Zhernenkov and M. Rakitin

SRW modelling with:

- ✓ actual measured SMI mirrors' profiles
- ✓ FEA heat load on 1st DCM crystal

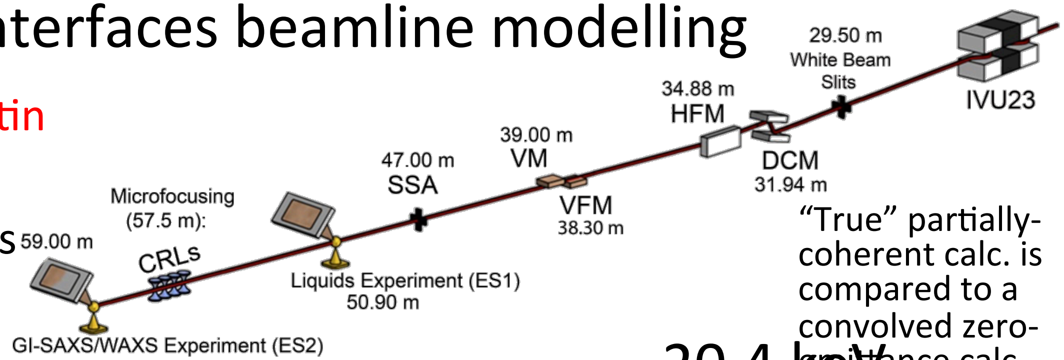

"True" partially-coherent calc. is compared to a convolved zero-emittance calc. (obtained in 30 s)

2.1 keV

ES2 focus with CRLs

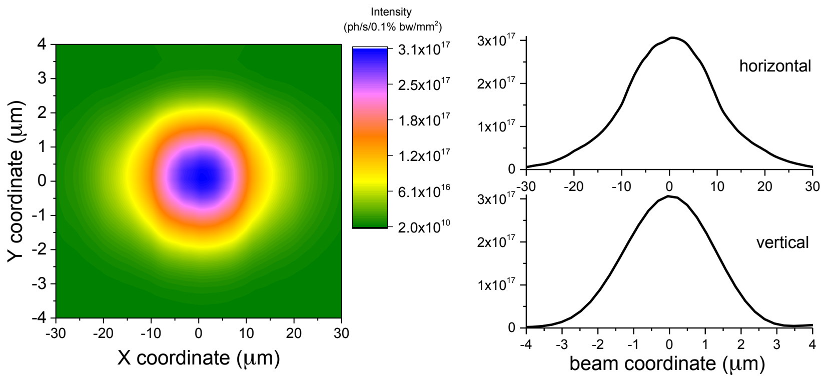

ES2 focus no CRLs

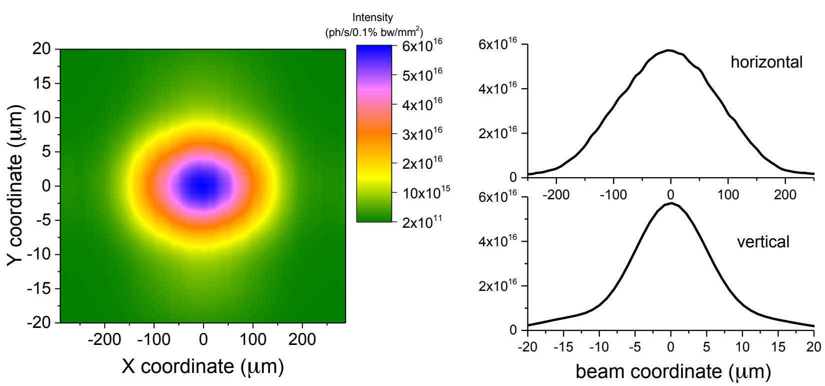

20.4 keV

ES1 focus

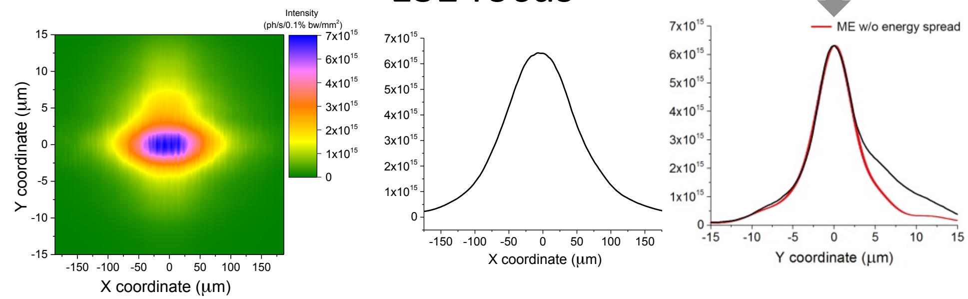

ES2 focus with CRLs

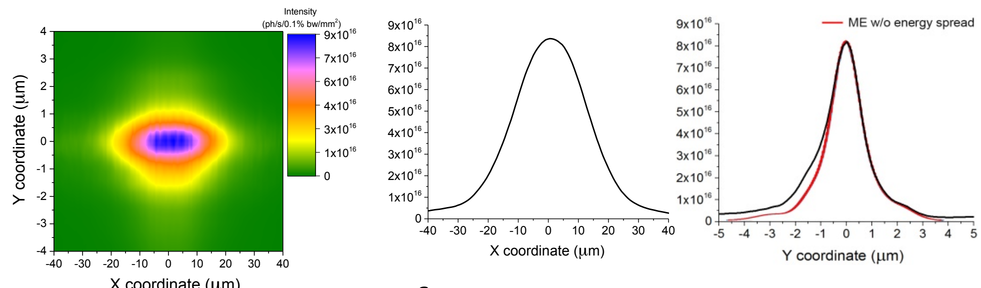

ES2 focus no CRLs

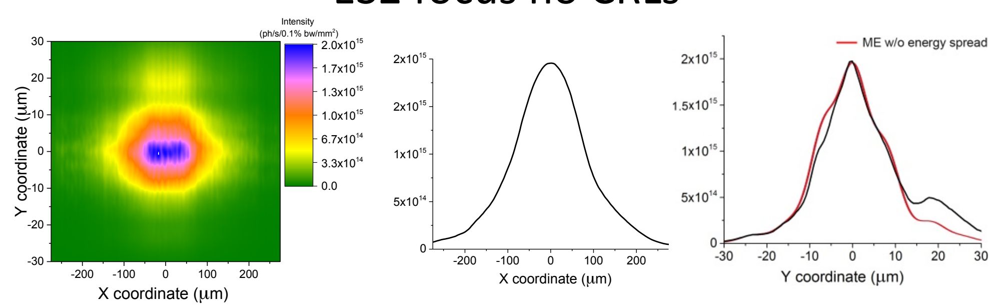

Partially-Coherent Wavefront Propagation Simulations for a Soft X-ray Beamline with VLS grating (ESM @ NSLS-II)

Beamline Design:

R.Reininger, S.L.Hulbert, P.D.Johnson, J.T.Sadowski, D.E.Starr, O.Chubar, T.Valla, E.Vescovo, Rev. Sci. Instrum. 83, 023102 (2012)

Partially-Coherent Wavefront Propagation Simulations:

N.Canestrari, V.Bisogni, A.Walter, Y.Zhu, J.Dvorak, E.Vescovo, O.Chubar, Proc. of SPIE Vol. 9209, 92090I (2014)

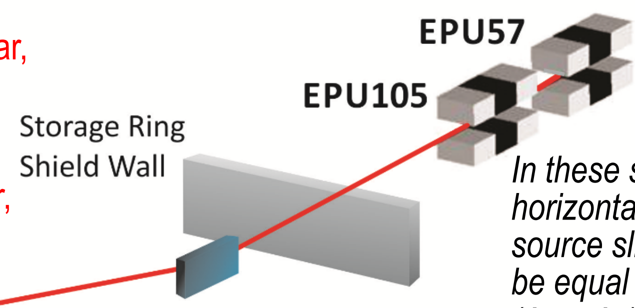

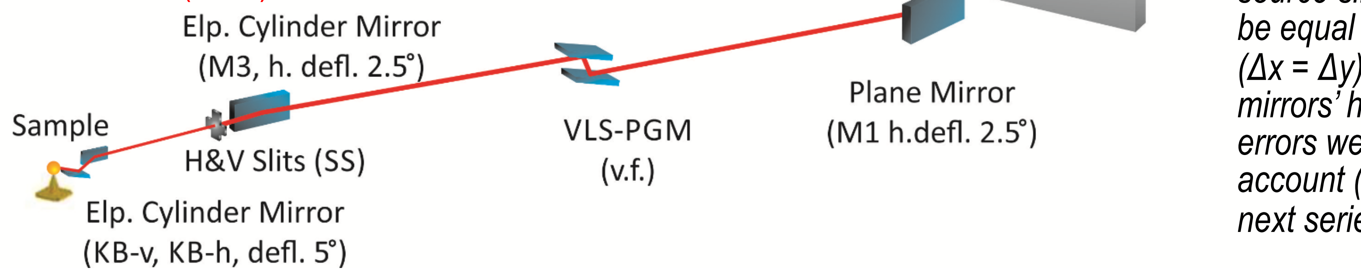

In these simulations, the horizontal secondary source slit size was set to be equal to the vertical size (Δx = Δy); mirrors' height / slope errors were not taken into account (to be included in next series of simulations).

Energy Resolution Spatial Resolution Flux (finite-bandwidth) at Sample
as functions of the Secondary Source (Monochromator Exit) Slits

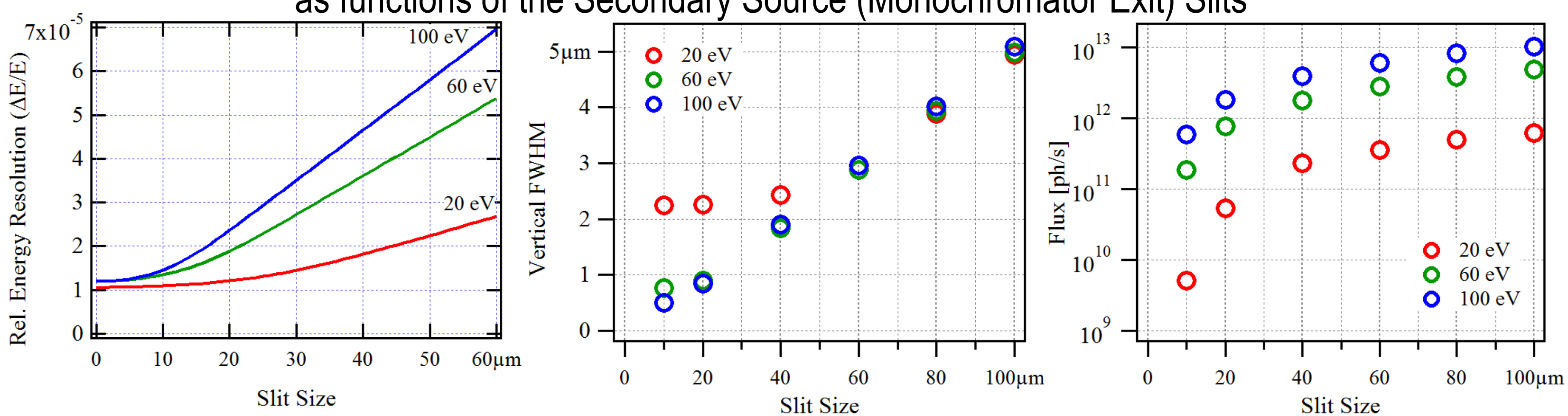

$\Delta E/E > (mN)^{-1}$

Two different VLS Gratings (160 mm long) were used:
a_0 = 800 lines/mm for E = 20 eV; a_0 = 600 lines/mm for E = 60, 100 eV

NSLS-II Emittance Reduction by DWs Observed after Imperfect Optics at “Secondary Source” of HXN

Intensity Distributions at 8.0 keV (5^{th} UR Harmonic) at “Secondary Source”

in Intermediate Hatch (Optical Magnification: ~0.93)

Measured | **Calculated** | For perfect optical elements

At Damping Wiggler Gaps “Open” ($\varepsilon_x \approx 2.1$ nm, $\sigma_x \approx 61$ μm)

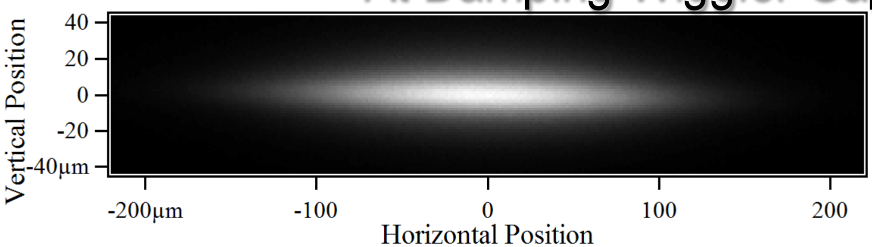

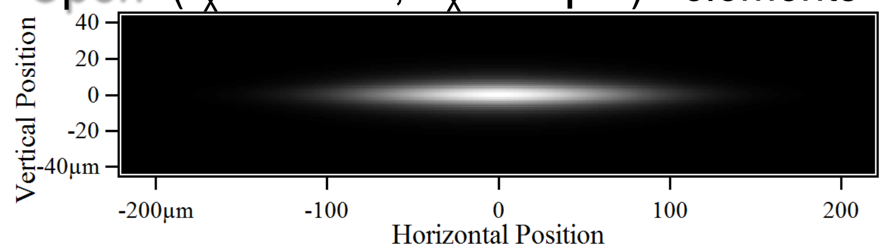

At Damping Wiggler Gaps “Closed” ($\varepsilon_x \approx 0.9$ nm, $\sigma_x \approx 40$ μm)

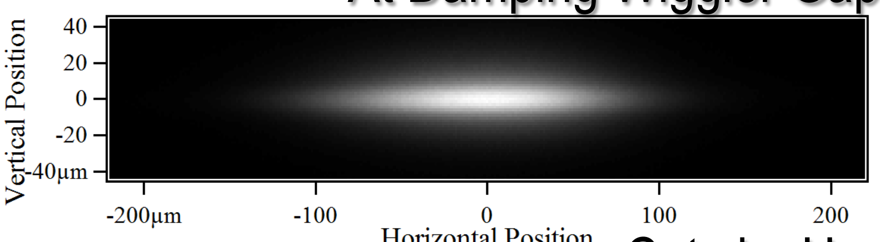

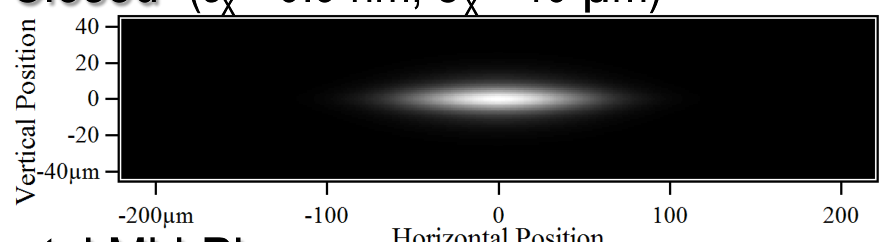

Cuts by Horizontal Mid-Plane

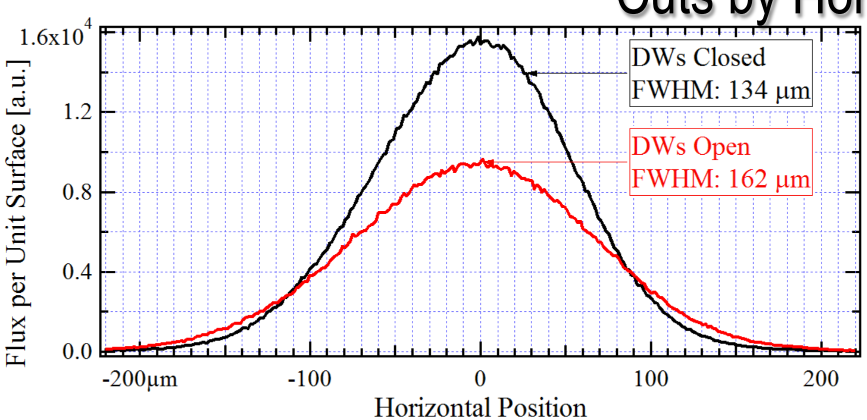

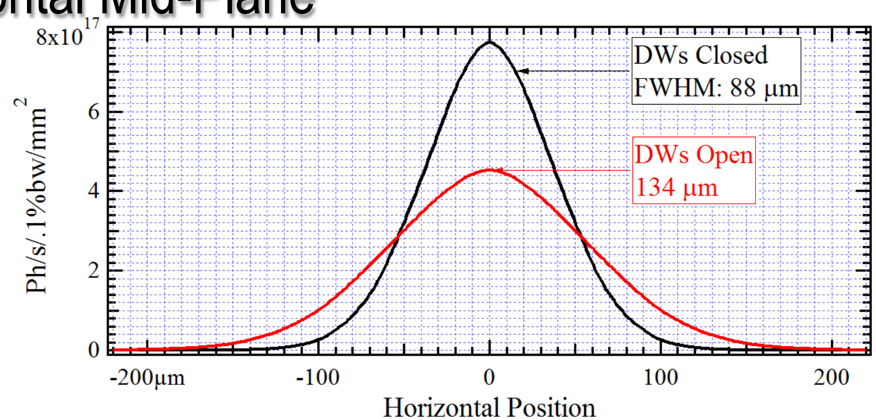

NSLS-II Brightness: Nominal and Estimated from Measurements at HXN Beamline

Approximate Spectral Brightness of IVU20 in Low-Beta Straight Section of NSLS-II

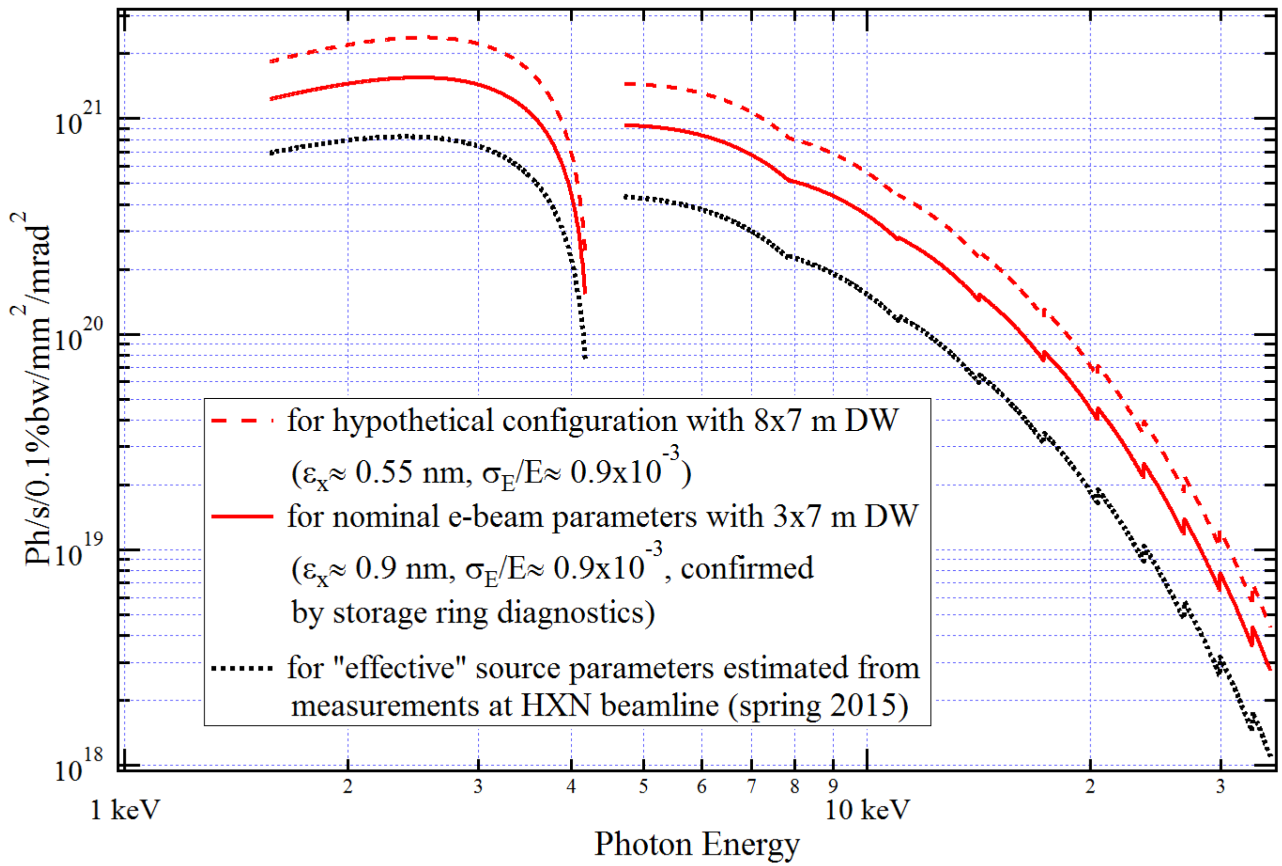

All curves are scaled for 0.5 A e-beam current.

Note: absolute values of spectral brightness may not be very accurate, however, relative "locations" of the curves are credible.

The reduction of brightness "observed" at the beamline is attributed to imperfections of X-ray optics (horizontally-focusing bendable mirrors, monochromator, vertically-focusing CRL) and undulator magnetic field.

It will be possible to "restore" this "effective" brightness in the future (by further fine-tuning / processing / replacing of individual beamline components, identified from simulations and dedicated measurements).

Approach to Coherence Preservation Diagnostics Assisted by Simulations (Illustration)

V.Kohn, I.Snigireva and A.Snigirev, Phys. Rev. Lett., vol.85(13), p.2745 (2000)

A.Snigirev, V.Kohn, I.Snigireva, B.Lengeler, Nature, vol.384, p.49 (1996)

O.Chubar, A.Fluerasu, Y.S.Chu, L.Berman, L.Wiegart, W.-K.Lee, J.Baltser, J. Phys.: Conf. Ser. 425, 052028 (2013)

Optical scheme of test experiments with CRL and a Boron fiber probe

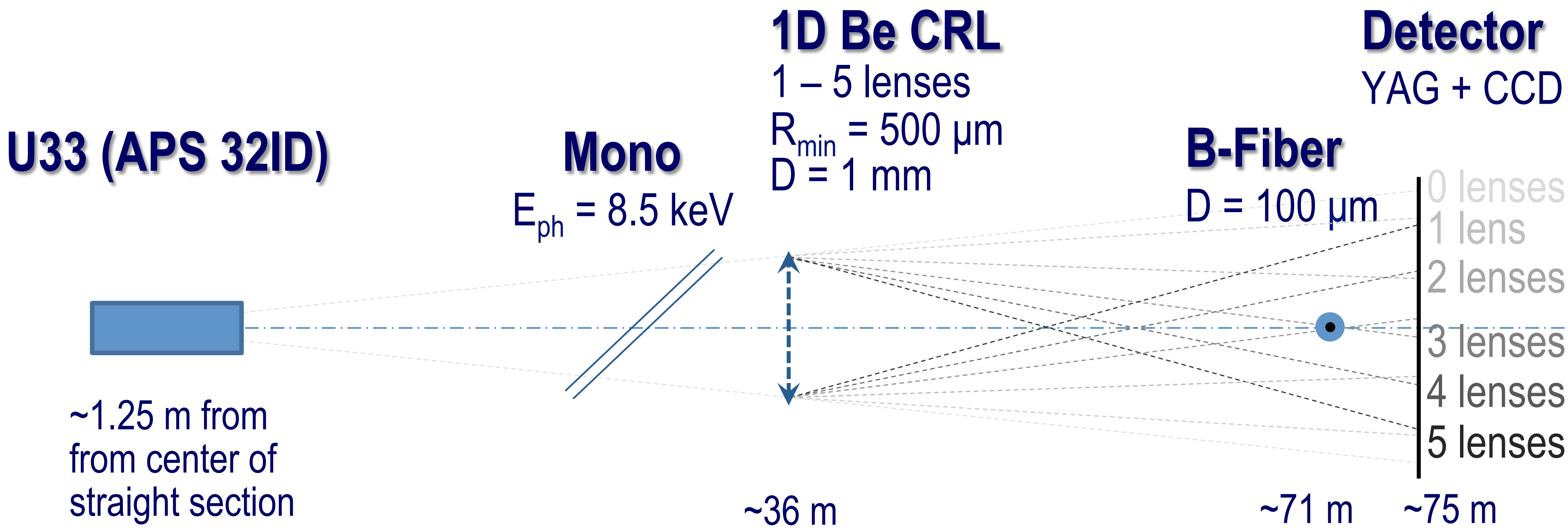

Intensity Distributions in the B-fiber Based Interference Scheme for Different Numbers of CRL in Optical Path

Simulations allow to conclude about coherence preservation in presence of any beamline optics!

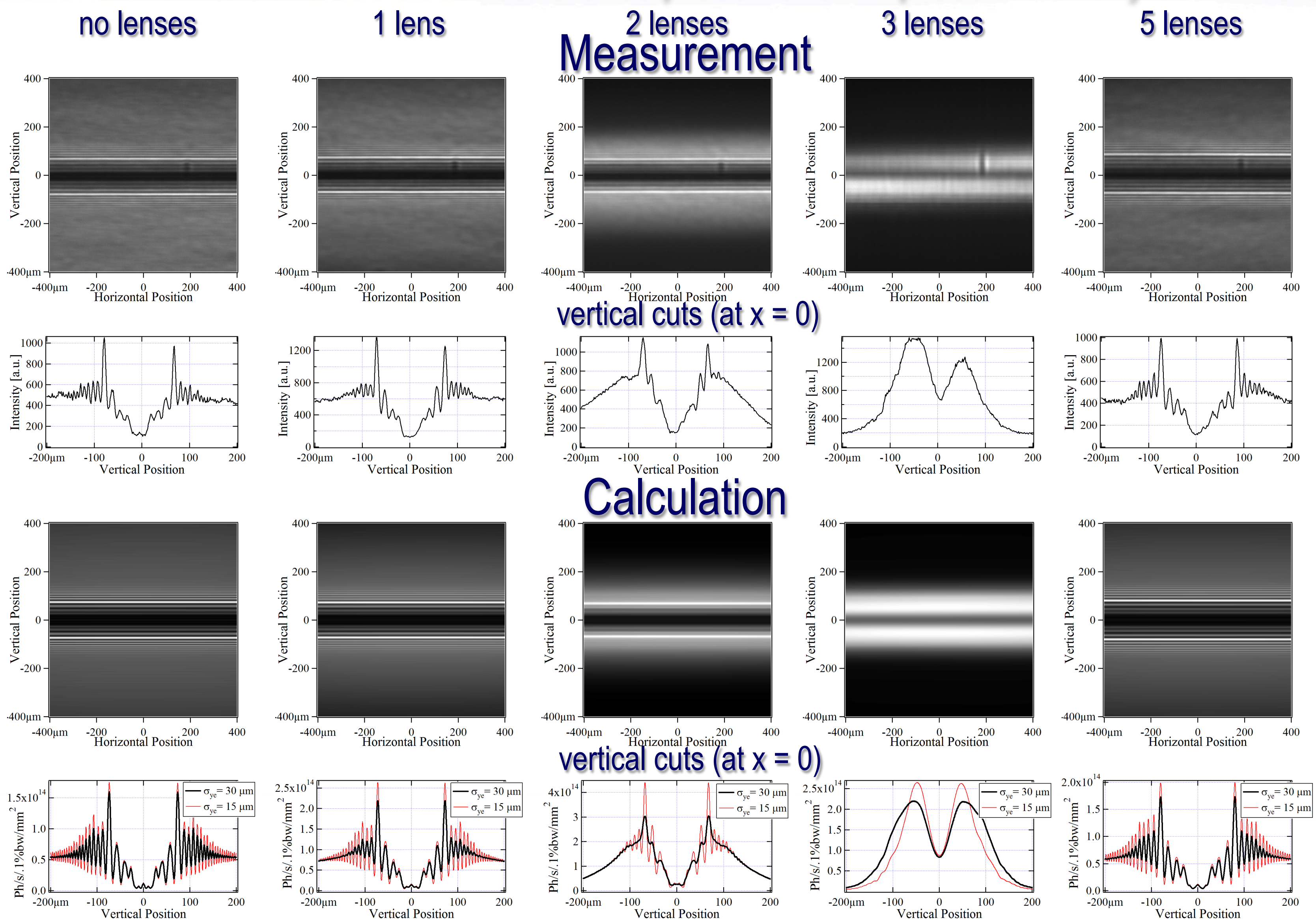

Intensity Distributions of Focused Wiggler Radiation from Partially-Coherent Wavefront Propagation Calculations

On-Axis Collection: $\theta_{x0} = 0$, $\theta_{y0} = 0$
$|\theta_x - \theta_{x0}| < 0.1$ mrad
$|\theta_y - \theta_{y0}| < 0.1$ mrad

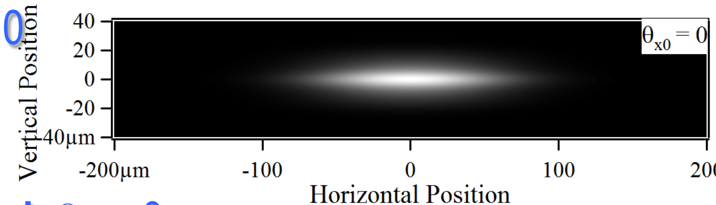

1 : 1 Imaging Scheme with "Ideal Lens"

Off-Axis Collection: $\theta_{x0} = 0.5$ mrad, $\theta_{y0} = 0$

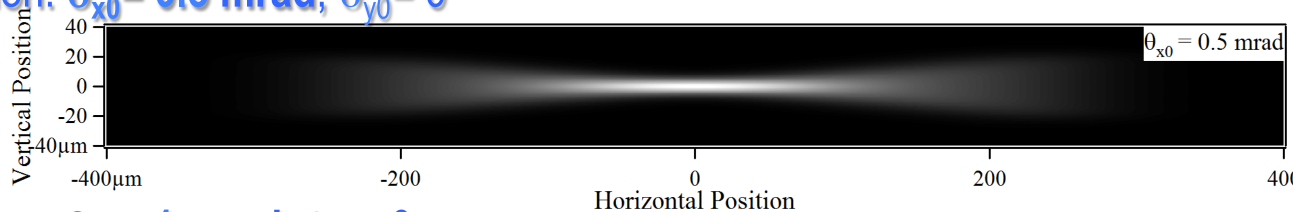

$\theta_{x0} = 1$ mrad, $\theta_{y0} = 0$

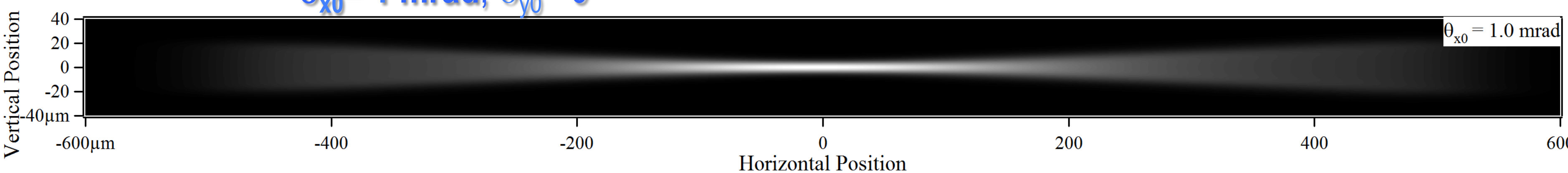

Horizontal Cuts (y = 0)

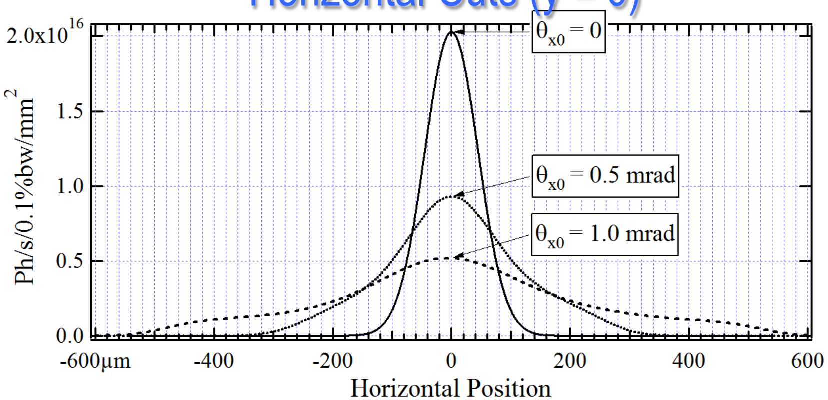

Vertical Cuts (x = 0)

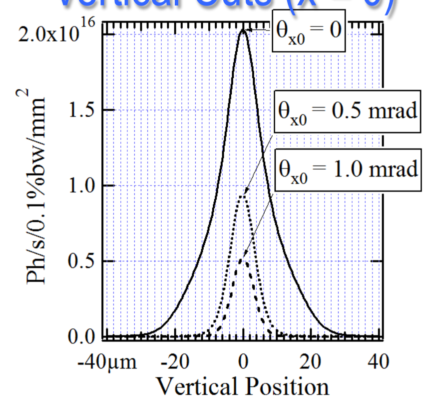

NSLS-II Low-Beta Straight Section
$I = 0.5$ A, $\varepsilon_x = 0.9$ nm, $\varepsilon_y = 8$ pm

SCW40: $\lambda_u = 40$ mm, $B_{max} = 3$ T, $L = 1$ m
Photon Energy: $E_{ph} = 10$ keV

Wavefront Propagation Calculations for ROBL at ESRF

Figure courtesy A. Scheinost

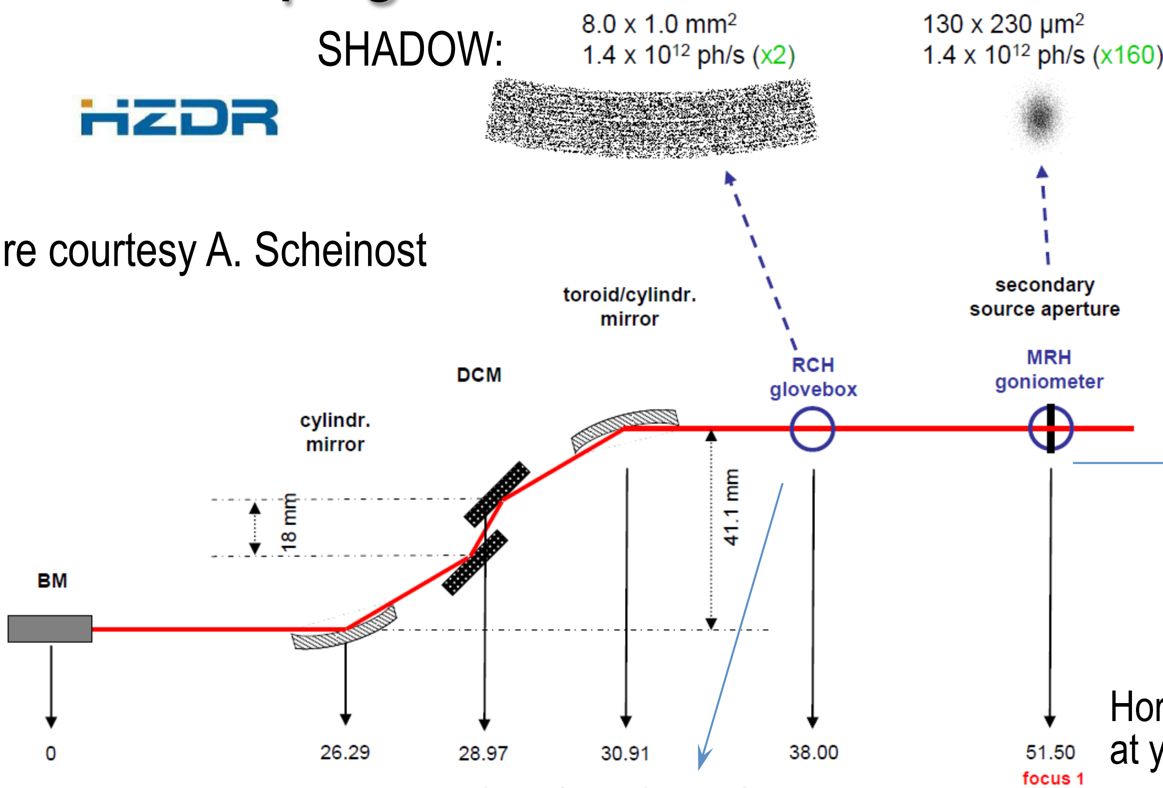

E = 18 keV

Intensity Distribution at MRH / focus (by SRW)

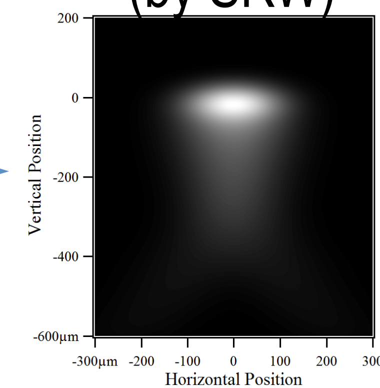

Hor. cut at y = 0

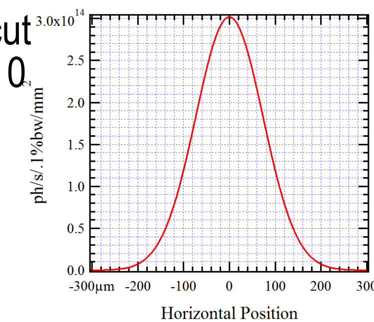

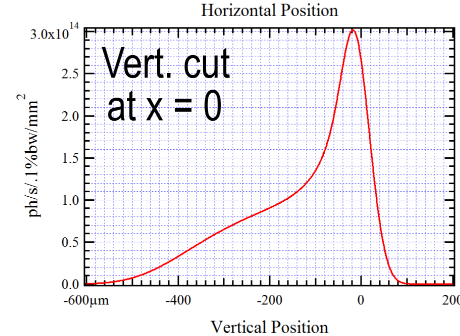

Intensity Distribution at RCH (by SRW)

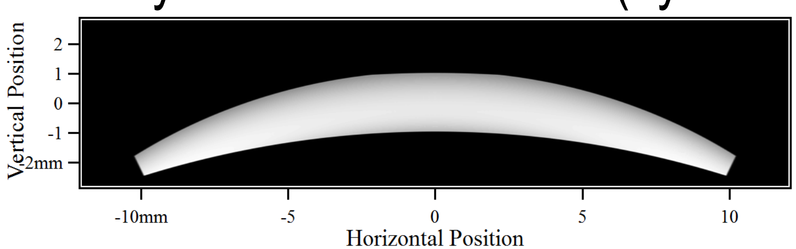

Hor. cut at y = 0

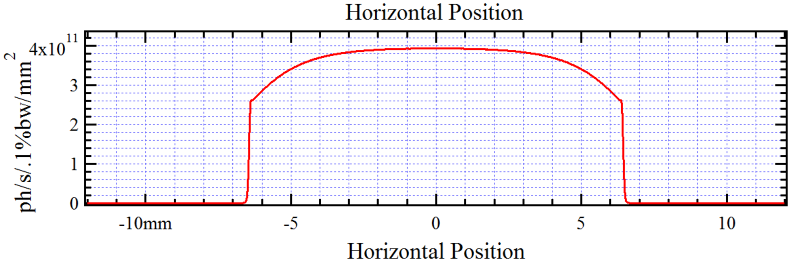

Vert. cut at x = 0

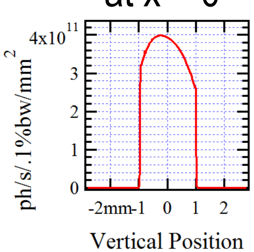

2PW-B Option for ROBL after ESRF Upgrade

Intensity Distribution at 18 keV at ~29.3 m from Source (assuming no apertures upstream)

In this case, since the initial wavefront is very "spiky" (because of interference of several sources), the simulation was done in steps:
- first, intensity in transverse plane before 1st aperture was calculated;
- second, electric field was instantiated from this intensity, assuming spher. wave, and propagated to final observation plane;
- finite e-beam size was taken into account by convolution.

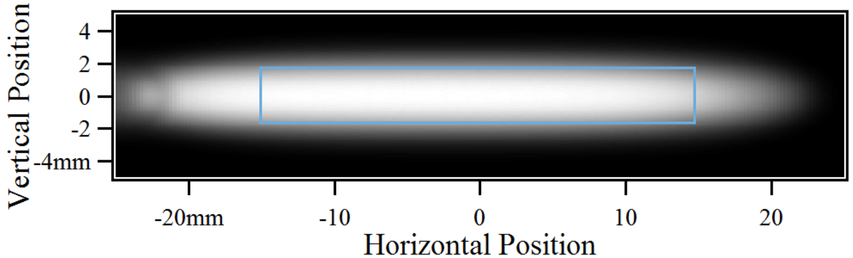

Spectral Flux

within |x| < 14.65 mm, |y| < 1.625 mm:
~4.0 x 10^{13} ph/s/.1%bw

Horizontal Cut at y = 0

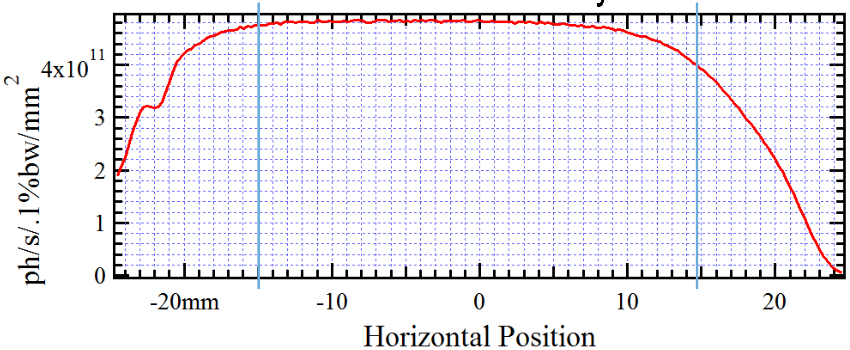

Vertical Cut at x = 0

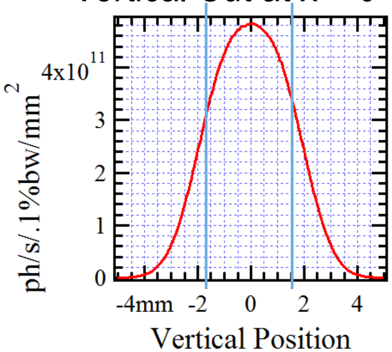

Optical Scheme Parameters

Longitudinal Positions:
- VCM: 29.3 m
- TFM: 34.3 m
- SSA: 54.5 m

Mirror Radii:
- VCM: R = 20 km
- TFM: R_s = 61.8 mm
- R_t = 18.0 km

Incident Angles:
- VCM: 2.5 mrad
- TFM: 2.42 mrad

e-Beam Parameters:

E = 6 GeV, I_e = 200 mA
ε_x= 130 pm, ε_y= 5 pm
β_x= 1.81 m, β_y= 2.57 m

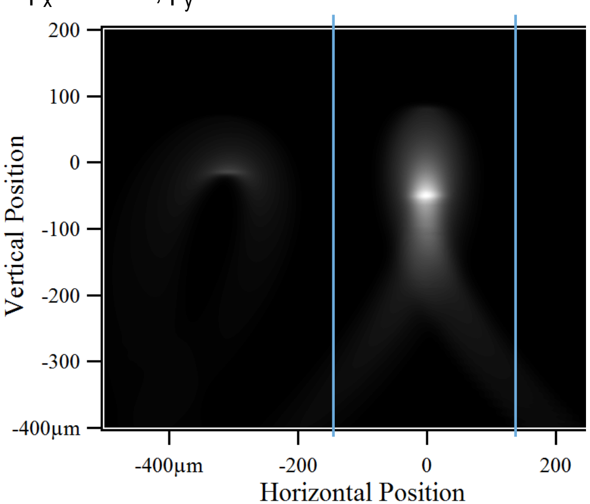

Intensity Distribution at SSA

Horizontal Cut through Max.

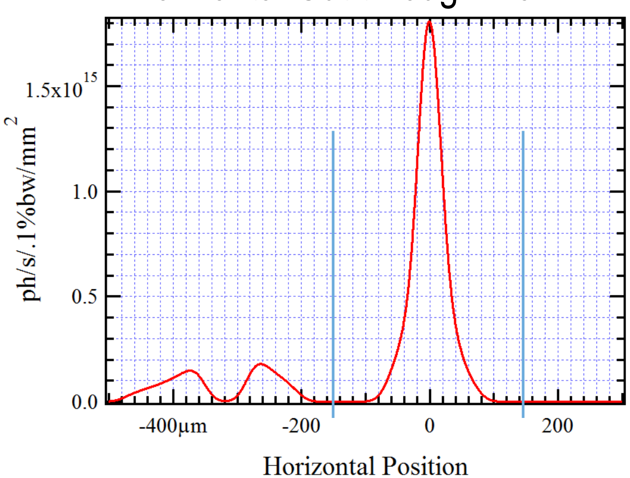

Vertical Cut through Max.

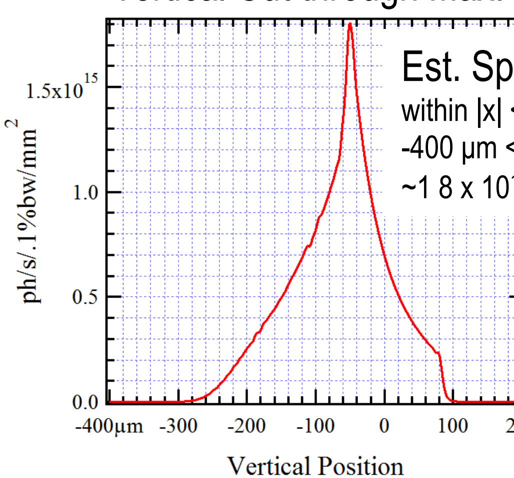

Est. Spec. Flux

within |x| < 150 µm,
-400 µm < y < 200 µm:
~1 8 x 10^{13} ph/s/.1%bw

Estimating Degree of Coherence (/ Transverse Coherence Lengths) of Radiation from ESRF-U 2PW by Simulating Young's 2-Slit Interference Schemes

Far-Field Interference Patterns from 2 Vertical Slits Separated by Horizontal Distance h

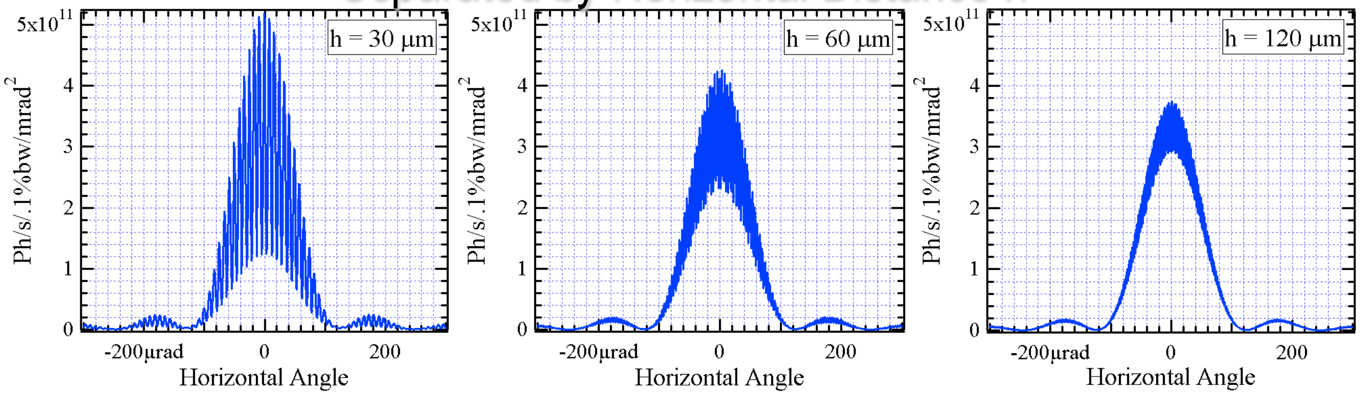

Vertical Aperture: 1 mm; Slit Size: 2 µm

Horizontal Coherence Length: ~40 µm
For a BM-like Source should be ~60 µm

Fringe Visibility vs h in Horizontal Plane

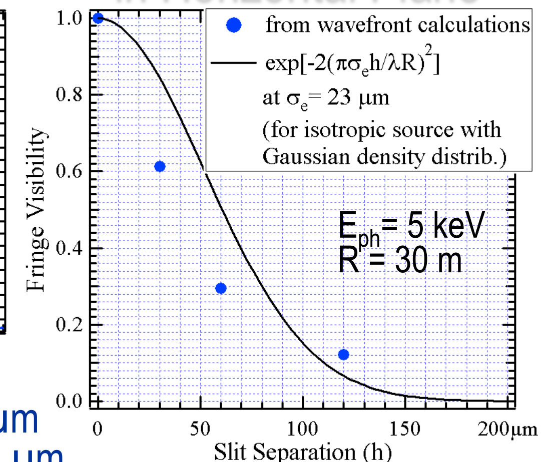

Far-Field Interference Patterns from 2 Horizontal Slits Separated by Vertical Distance h

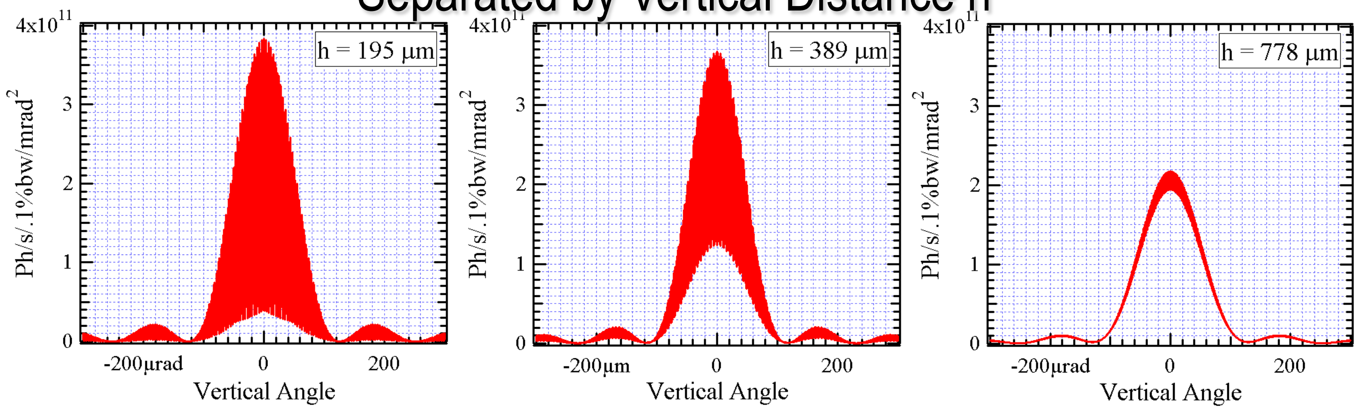

Horizontal Aperture: 1 mm; Slit Size: 2 µm

Vertical Coherence Length: ~390 µm
For a BM-like Source should be ~390 µm

Fringe Visibility vs h in Vertical Plane

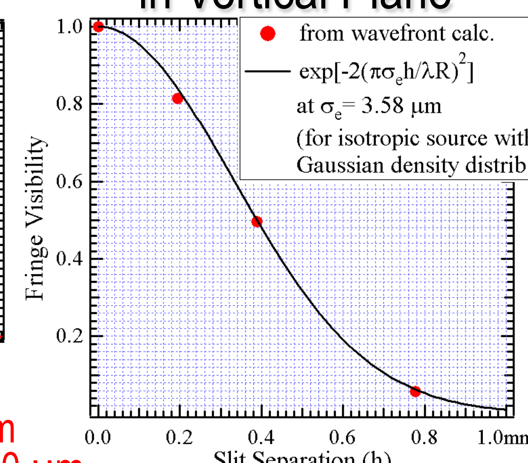

Testing Untra-High Resolution Inelastic X-ray Scattering Scheme at High-Rep-Rate Self-Seeded X-FEL

O.Chubar, G.Geloni, V.Kocharyan, A.Madsen, E.Saldin, S.Serkez, Y.Shvyd'ko, J.Sutter, J. Synchrotron Rad. 23, 410-424 (2016)

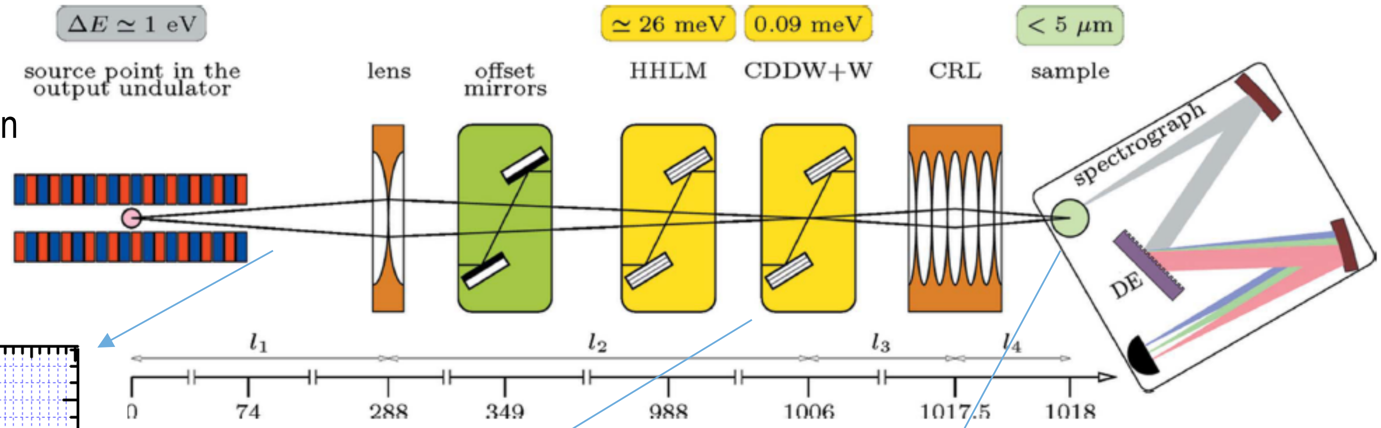

At FEL Exit

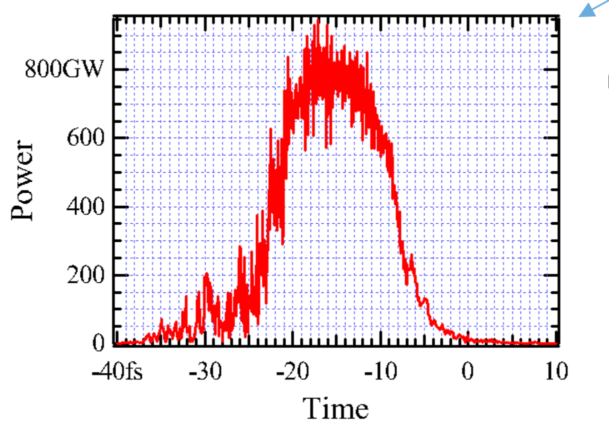

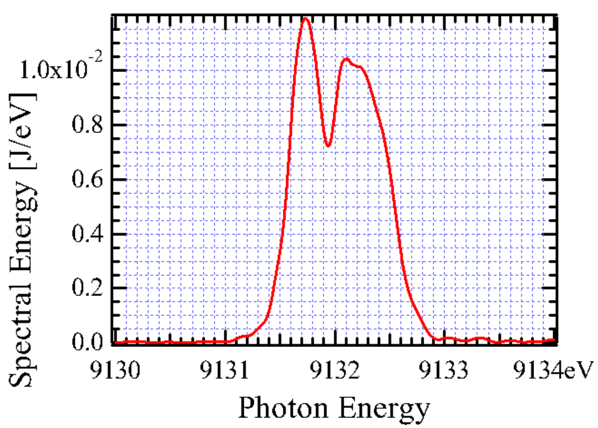

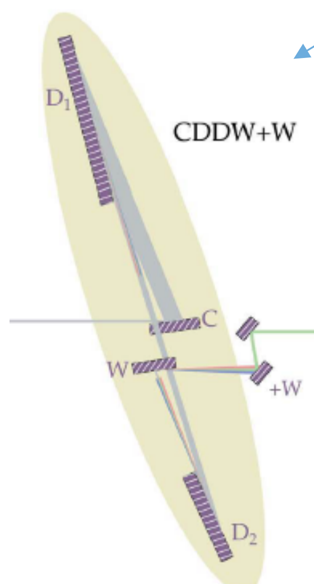

E_0 = 9131.850 eV

Photon flux on Sample: ~6x10[12] ph/s (at ~27000 pulse/s) i.e. ~1000 more than in a storage ring.

At Sample

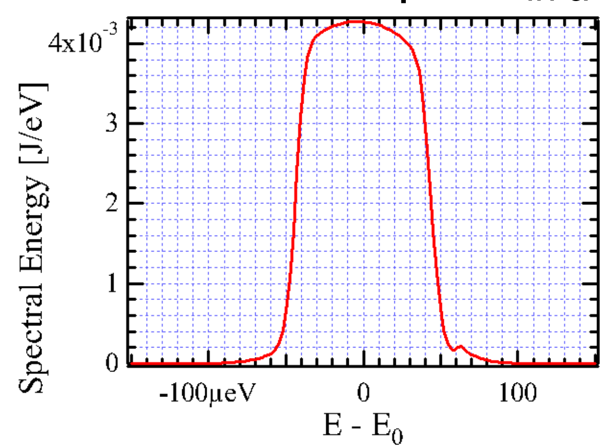

Pulse Energy at FEL Exit: ~12 mJ; at Sample: ~0.37 μJ

IXS at X-FEL: Radiation Pulse Characteristics Near Sample

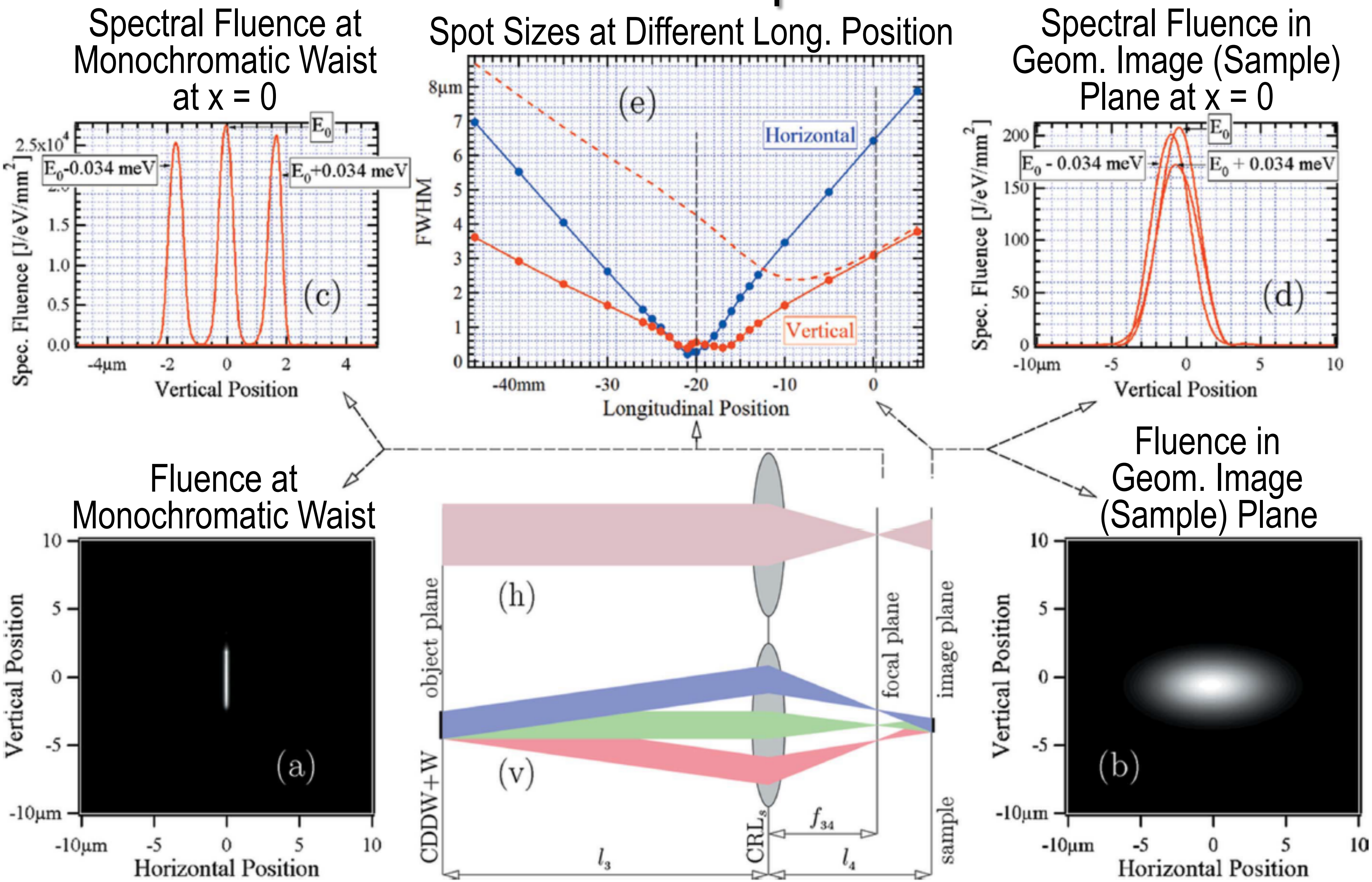

Summary and Comments

- High-accuracy fully- and partially-coherent synchrotron emission and wavefront propagation calculations for sources and beamline optics are currently done routinely for beamlines at new storage rings and FEL (though performance can still be an issue in cases of low coherence).
- An advantage of high-accuracy wavefront calculations is very broad range of applications (because of their general electrodynamics basement): design of new sources and optics (maximizing performance of both), commissioning, diagnostics, simulation of user experiments, addressing misc. inverse problems of data processing, etc. Some interesting potential applications are not fully explored yet.
- Main disadvantage of these calculations is currently a ~low CPU performance in low-coherence cases compared to geometrical ray-tracing; however, it can be mitigated by parallelization, coherent mode decomposition and other methods.
  Note: the higher is the degree of coherence in a beamline, the easier is the treatment of partial coherence, which is very good for applications in FEL and MBA storage rings.
  Another "disadvantage" is higher complexity of these calculations compared to ray-tracing. It can be mitigated by programming more robust "propagators", propagation "drivers", as well as developing better user interfaces and writing better help.

Acknowledgments

- Pascal Elleaume, Jean-Louis Laclare
- Colleagues contributed to development of SRW: J. Sutter (DLS), D. Laundy (DLS), A. Suvorov (BNL), N. Canestrari (ESRF-BNL), R. Reininger (ANL), X. Shi (ANL), R. Lindberg (ANL), L. Samoylova (E-XFEL), A. Buzmakov (E-XFEL), D. Bruhwiler (RadiaSoft LLC), R. Nagler (RadiaSoft LLC), M. Rakitin (BNL)
- Management and colleagues who helped in transition to Open Source: G. Materlik (DLS, London Centre for Nanotechnology), K. Sawhney (DLS), J. Susini (ESRF), M. S. del Rio (ESRF), S. Dierker (BNL), Q. Shen (BNL), P. Zschack (BNL), S. Hulbert (BNL), H. Sinn (E-XFEL)
- NSLS-II scientists: A. Fluerasu, L. Wiegart, K. Kaznatcheev, E. Vescovo, V. Bisogni, M. Zhernenkov, E. DiMasi, Y. Cai, Y. Chu, I. Jarrige, D. Schneider, M. Fuchs, J. Thieme, L. Yang, T. Shaftan
- Many thanks to Luca and Manuel – the S.O.S. Workshop Organizers!